

**UNIVERSITY OF WEST BOHEMIA IN PILSEN
FACULTY OF ELECTRICAL ENGINEERING
DEPARTMENT OF TECHNOLOGY AND MEASUREMENT**

BACHELOR THESIS

**Organic materials based on carbon allotropes for
sensorics**

ZÁPADOČESKÁ UNIVERZITA V PLZNI

Fakulta elektrotechnická

Akademický rok: 2020/2021

ZADÁNÍ BAKALÁŘSKÉ PRÁCE

(projektu, uměleckého díla, uměleckého výkonu)

Jméno a příjmení: **Malinga TEMBO**
Osobní číslo: **E17B0176P**
Studijní program: **B2612 Elektrotechnika a informatika**
Studijní obor: **Komerční elektrotechnika**
Téma práce: **Organické materiály na bázi alotropů uhlíku pro sensoriku**
Zadávající katedra: **Katedra materiálů a technologií**

Zásady pro vypracování

1. Zpracujte přehled vhodných organických materiálů na bázi alotropů uhlíku, používaných v oblasti sensoriky.
2. Proveďte rešerši vhodných technologií depozice materiálů na bázi alotropů uhlíku.
3. Prakticky ověřte teplotní závislost u vybraných materiálů na bázi alotropů uhlíku.
4. Zhodnoťte a porovnejte získané výsledky.

Seznam doporučené literatury:

1. Organic Electronics: Materials, Manufacturing, and Applications ISBN: 978-3-527-31264-1
2. TrAC Trends in Analytical Chemistry Volume 68, May 2015, Pages 37-47 Graphene-based hybrids for chemiresistive gas sensors
3. Chemical Society Reviews Recent developments in carbon nanomaterial sensors

Vedoucí bakalářské práce:

Ing. Josef Šlauf

Katedra materiálů a technologií

Oponent bakalářské práce:

Ing. Jiří Štulík, Ph.D.

Katedra materiálů a technologií

Datum zadání bakalářské práce:

30. června 2021

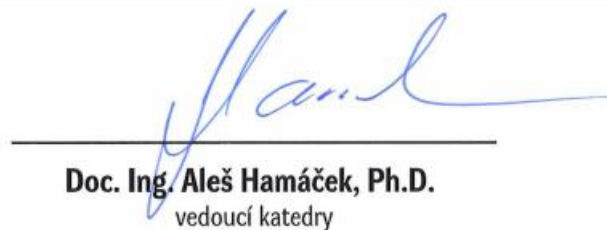
Termín odevzdání bakalářské práce:

20. srpna 2021



L.S.

Prof. Ing. Zdeněk Peroutka, Ph.D.
děkan



Doc. Ing. Aleš Hamáček, Ph.D.
vedoucí katedry

V Plzni dne 30. června 2021

Abstract

The presented bachelor thesis is focused on the description of carbon allotropes for sensor applications and subsequent verification of temperature dependencies of selected carbon allotrope materials. The first two chapters of the work are theoretical whereas section three and four are concerned with the thesis experiment. Section one is an overview of some carbon allotropes used in sensor technology with a particular focus on carbon nanotubes. Section two reviews some suitable technologies for carbon deposition onto substrates in the fabrication of carbon-based sensors. Section three describes an experiment to practically verify the temperature dependence of SWCNT, SWCNT-COOH, MWCNT and MWCNT-COOH deposited on BI2 interdigital substrate by airbrush spray deposition. An evaluation and comparison of obtain results is presented in the last section.

Keywords

Carbon allotrope, carbon nanotube, BI2 sensor platform, temperature dependence.

Declaration

I Declare that I have prepared this bachelor's thesis independently, using the professional literature and sources listed in the list that is part of this diploma thesis.

.....

Signature

In Pilsen on: 23/8/2021

Malinga Tembo.

Acknowledgment

My deep gratitude goes to my supervisor Ing. Josef Šlauf for his unflinching support and guidance throughout the duration of this work.

Table of contents

Introduction.....	10
List of Symbols and Abbreviations.....	13
1. Overview of suitable organic materials based on Carbon.....	14
1.1 Fullerene.....	15
1.1.1 <i>Fullerene C60</i>	16
1.2 Carbon nanotubes.....	18
1.2.1 <i>SWCNT</i>	19
1.2.2 <i>MWCNT</i>	20
1.3 CNT synthesis methods.....	20
1.3.1 <i>Carbon arc discharge</i>	21
1.3.2 <i>Laser Ablation</i>	22
1.3.3 <i>Chemical vapour deposition</i>	23
1.4 CNT functionalization.....	24
2. Overview of some deposition technologies for carbon-based allotrope materials.....	26
2.1 Wet deposition techniques.....	26
2.1.1 <i>Langmuir-Blodgett depositing technique</i>	26
2.1.2 <i>Drop Casting</i>	27

2.1.3 Electrophoretic depositions.....	28
2.1.4 Dip coating.....	28
2.1.5 Spin Coating.....	29
2.1.6 Air brush spray deposition.....	29
2.2 Dry deposition techniques.....	30
2.2.1 chemical vapour deposition.....	30
3. Experiment.....	32
3.1 List of materials and apparatus used in the experiment.....	32
3.2 Procedure.....	33
3.2.1 Preparation of CNT materials (dispersion).....	33
3.2.2 Sensor assembly.....	33
3.2.2.1 Interdigital sensor platform.....	33
3.2.2.2 CNT thin-layer deposition by airbrush spray.....	35
3.2.3 Measurement of sensor parameters.....	36
3.2.3.1 Measurement set-up.....	36
3.2.3.2 Climatic chamber temperature profile.....	37
3.2.3.3 Measurement channels.....	38
Data analysis.....	39

Discussion.....	46
Conclusion.....	47
References.....	48

Introduction

Carbon is a non-metallic chemical element listed sixth on the periodic table and represented by the letter C. The name carbon is derived from the Latin word for coal, “carbo” [1]. Carbon occurs naturally in three isotopes: ^{12}C , ^{13}C , and the radioactive isotope ^{14}C . It is a tetravalent element and forms covalent bonds with itself as well as with other elements. It is considered to be the fourth most common element in the earth’s crust with relative abundance assessed to be 180 - 270 ppm [2].

People have used carbon in technology and in everyday life for many centuries. Carbon black, charcoal and graphite are some of the many materials known to have been used in prehistoric times. In those times, carbon-based materials were used as writing and drawing materials, among other uses. Today, carbon lends itself to contemporary science and technology as an invaluable elemental asset, revolutionising the nanotechnology industry [3].

Nanotechnology is defined as the understanding and control of matter at dimensions between 1 and 100 nm where unique phenomena enable novel applications [4]. The last 100 years have seen rapid growth in the nanotechnology industry. The increased interest in nanotechnology research and development has consequently led to the development of outstanding industrial applications. Nanotechnology has attracted so much popularity chiefly because its domain of operation is at the very foundation of matter, at the most fundamental level of organization of atoms and molecules in both living and anthropogenic systems. Experiments with particles at the nanoscale reveal that these particles exhibit exceptional tuneable physical properties as well as outstanding solvent interactions [5], [6]. Manipulation of materials at atomic level has brought to light the possibility to synthesize very small structures or devices from atomic or molecular building blocks using the so-called “bottom-up” approach [7], making possible the design and assembly of nanoscale functional gadgets through the emergence of technologies such as micro-electromechanical system (MEMS), to name but a few [8].

These concepts of nanotechnology were first formally introduced by the 1965 Nobel Prize Laureate in Physics [9], Richard Feynman in 1959. However, it wasn’t until the

1980s that the golden era of nanotechnology launched. In 1985 Kroto, Drexler, Curl, and Smalley discovered fullerene using principles first laid out by Feynman and other pioneers in the field. Great interest in nanotechnology was further enhanced when Iijima discovered carbon nanotubes in 1991 [10]. The revolutionary discoveries of fullerene and carbon nanotubes have since placed carbon nanotechnology squarely at the helm of the nanotechnology industry.

Nanomaterials are generally classified as zero-dimensional if all three dimensions of the material are less than 100 nm; one-dimensional if the material has two of its dimensions less than 100 nm; two-dimensional if the material has one dimension less than 100 nm. Three-dimensional nanomaterials are usually bulky structures composed of nano-sized building block structures. Functionalization of nanoparticles, permits construction of composite nanostructures of higher dimensions. Functionalization technologies also serve to alter the properties of nanomaterials [8].

Carbon presents itself in many different natural and artificial allotrope forms [8]. The eight allotropes of carbon are, 1) graphite, 2) diamond, 3) C₆₀ (buckminster fullerene or bucky ball), 4) C₇₀, 5) C₅₄₀, 6) lonsdaleite, 7) carbon nanotubes (buckytube), 8) amorphous carbons [1]. In contrast to other nanomaterials such as metal oxide nanowires and transitional metal nanomaterials, carbon-based nanomaterials possess exceptional chemical, physical, mechanical and electronic properties [11]. These brilliant properties of carbon include, but are not limited to; wide specific area, biocompatibility, high electro-chemical stability, ease of manipulation, good electrical and thermal conductivity, high mechanical resistance, low cost, suitable surface chemistry for a wide range of oxidation-reduction reactions, and environmentally friendly qualities [2]. Structure and size play a huge role in determining the carbon allotropes' properties [12].

The past 25 years have seen a rise in the use of conjugated carbon materials [3]. Many novel carbon allotropes have been discovered since Krato *et al.*'s 1985 [13] discovery of fullerene. Furthermore, carbon nanotubes (CNTs), a tubular shaped member of the fullerene family was first presented by Iijima in 1991 [14]. This discovery facilitated an increase in the works on CNTs [15]. Graphene, the first two-dimensional atomic crystal discovered, was discovered in 2004 by Novoselov *et al.* [16]. This discovery was

rewarded with the 2010 Nobel prize in physics, a testament to the importance of carbon in today's development of science and technology.

It is therefore no surprise that carbon has attracted substantial attention owing to its direct application in the generation of new materials with exclusive properties [3]. Carbon is thus one of the most studied and used materials in the field of nanotechnology. This is mainly because of the many advantages that carbon holds over conventionally used materials. Its manufacturing process is simple and efficient with low densification defects. In addition, materials based on carbon can be considered as cheaper alternative materials to some of the current electronic materials in use. Carbon allotrope structures are also considered to be environmentally friendly [15].

It is thanks to the properties mentioned above that carbon nanostructures are continually investigated for their deployment in sensor technology. A sensor is defined to be a device that responds to stimulus, generating a signal that can be analysed. It is required of good quality sensors to have fast response to external stimulus, low recovery time, and the ability to detect an analyte in proportion as low as possible. A sensor must also be easy to operate. These high-quality sensing properties are a direct result of carbon's superior chemical and physical qualities [15].

Part one of this thesis gives an overview highlighting the unique properties of some carbon allotropes suitable for use in sensor technology. An overview of a representative 0- and 1-dimensional carbon allotropes is given. Chapter two outlines some suitable carbon thin-film deposition technologies used in sensorics. The third chapter is concerned with experimentally verifying the temperature dependence of pristine as well as carboxyl functionalized single- and multi-walled CNT. Data analysis and interpretation of the results obtained from the measurements in chapter three is given in the fourth and final chapter.

List of Symbols and abbreviations

CNM.....	carbon nanomaterials
CNT.....	carbon nanotube
SWCNT.....	single walled carbon nanotube
MWCNT	multi walled carbon nanotube
C ₆₀	Buckminsterfullerene
COOH	Carboxyl group
CVD	Chemical vapour deposition
PVD.....	Physical vapour deposition
LB.....	Langmuir-Blodgett
EPD	Electrophoretic deposition
LB.....	Langmuir-Blodgett
EPD	Electrophoretic deposition
DMAc.....	N, N dimethylacetamide polar solvent
IPA.....	Isopropyl alcohol
IDE	Interdigital electrode
R	Resistance
R _{Ts}	Average resistance at a given step temperature value of climatic chamber
T _n	n th climatic chamber time period

1. Overview of some suitable organic material based on carbon suitable for sensorics

Carbon, a group 14 (IV A) element, is the most versatile of all known elements, presenting many bonding possibilities [17], [18]. Its extent of catenation is unrivalled by any other element. Carbon not only bonds with nearly all other elements of the periodic table, but also with itself in almost limitless variations. It also has the ability to form long chains of atoms, thus displaying polymerization. Further still, carbon bonds with both electropositive and electronegative elements. Carbon atoms are capable of forming single, double and triple carbon-carbon bonds where the average bond energies are reported to be approximately 350 kJ mol^{-1} , 610 kJ mol^{-1} , 840 kJ mol^{-1} between single, double and triple bonds, respectively [19].

Even though chemically speaking, graphite and diamond are similar, they manifest completely different physical parameters [3] [20]. Graphite and diamond, are two physically different substances but composed entirely of the same atom, carbon. Graphite and diamond are thus said to be allotropes of carbon. Allotropes occur when the atoms of a substance that has only one kind of atom arrange differently [3]. Carbon nanomaterials (CNMs) can be classified with respect to the number of dimensions, which are not confined to the nanoscale range ($<100 \text{ nm}$) [21]. Some allotropes of carbon can be classified yet still with respect to their shape, size, and the orientation of their carbon bonds [1]. More accurately, allotropes are classified on the basis of the hybridisation of their carbon atoms. Based on this classification scheme, each one of the three main carbon valence states is characterised by a unique and specific allotrope form. For instance, single bond sp^3 hybridisation as is observed in the bulk 3D structure of diamond, double bonds in sp^2 hybridisation of the 2D layers of graphene structure and the sp hybrid state of the linear chain 1D carbene structure. Buckyball fullerenes are considered quasi-zero-dimensional and nanotubes quasi-one-dimensional allotrope [15]. Both buckyball fullerenes and carbon nanotubes manifest quasi sp^2 hybridisation [18]. Valence atoms of some carbon allotrope such as amorphous carbons, diamond like carbon and nanocrystalline diamond aren't always in the sp , sp^2 or sp^3 hybridization states. They maybe in the so-called mixed and intermediate states, sp^n where $1 < n < 3$ [22].

The energy level distribution of the 2s and 2p electronic shells are responsible for the many structures carbon has to offer. The 4 valence electrons, with atomic configuration $2s^2 2p^2$, are able to transition energy states at minimal energy cost. These electrons can be involved in sp, sp^2 and sp^3 hybridisation due to carbon having energy bands that are so close in energy, consequently enabling carbon to occur in numerous allotropic forms [23].

Research and development in the field of carbon nanotechnology is actively investigating the synthesis and applicability of novel as well as known CNMs [24]. CNM surfaces, however, need functionalization before deployment for use in most technologies. Furthermore, CNTs can be modified by conjugation with organic or metallic nanoparticles [25]. Modification and functionalization is not only essential to remedy their insolubility and tendency to aggregate, but also to ultimately enhance their properties (e.g., mechanical, chemical, optical properties, electrical, physical etc) [25]. The broad structural dimensionality and ease of functionalization enables the adaptation of these brilliant electromechanical properties possessed by CNTs at nanoscale, via composite materials, for use at microscopic scales [26]. Carbon based organic materials have reportedly been used in different sensing applications for targets such as temperature, pressure, biomolecules, environmental pollution to mention but a few [2], [8], [27], [28]. Physicochemical properties of an allotrope depend strongly on the allotropes' structure and size [12]. In this section, an overview of the properties of the 0D CNM C_{60} fullerene, 1D carbon nanotubes (CNTs), and 2D graphene and its derivatives, is given. Their surface properties, rather than bulk properties, are presented as they play a significant role in sensor applications.

1.1 Fullerene

Fullerenes are a family of carbon allotropes that generally exist in two distinct categories based on their shape, displaying distinct chemical-physical properties. Closed, ellipsoidal or hollow spherical shaped fullerenes are called buckyballs while the tubular fullerenes are called carbon nanotubes (CNTs) or buckytubes. Carbon nanofibers and carbon nanobuds are some of the other fullerenes synthesised for scientific research and use [29]. Fullerenes can be thought of as rolled up graphene sheets [12].

1.1.1 Fullerene C₆₀

Discovery and some basic properties

The presence of the fullerene C₆₀ had been predicted as far back as 1970 by Eiji Osawa [30] of Japan in his paper on superaromaticity. However, it wasn't until 1985 when during an experiment to simulate the conditions under which the formation of red stars occurs, that Kroto et al. [13] discovered fullerene C₆₀. The experiment involved vaporisation of the surface of a solid block of graphite by irradiation into a plasma of atoms and free ions. Upon cooling the plasma, mass spectrometry analysis of the resulting clusters showed a sharp spike commensurate with 60 atoms of carbon and in second place another spike consistent with 70 atoms of carbon. The more stable molecule C₆₀ was observed to assume the shape of a soccer ball whereas the C₇₀ was more ellipsoidal. This discovery marked the start of intense research into CNMs [31] and was later awarded the 1996 Nobel Prize in Chemistry.

Kroto et al. [13] named the newly discovered molecule C₆₀, "buckminsterfullerene" in honour of the architect, Richard Buckminster Fuller, who had designed geodesic domes of similar structure. Despite being closed caged, all buckyball fullerenes are 5-fold symmetrical and have so far been shown to comprise an even count of carbon atoms, C_{2n}. C₆₀ fullerene, for instance, exhibits spheroidal geodesic geometry with a diameter of 7.1 Å or approximately 0.7 nm. Buckyball fullerenes are thus generally taken to be 0D CNMs as all of their three spatial dimensions are below 100 nm. Buckyball fullerenes can be considered to be the smallest stable CNM structures and are right at the molecule-nanomaterial boundary. These structures have been shown to be consistent with Euler's polyhedron formula and the isolated pentagon rule. It is by Euler's polyhedron formula and isolated pentagon rule that it can be understood why C₆₀ fullerene is observed to be the most stable buckyball fullerene.

Natural occurrences of fullerene have been reported in several scientific papers [32]–[35]. Geological sources were identified as far back as 1992 when Buseck et al. identified fullerene (C₆₀ and C₇₀) in Precambrian rock from Russia. Meteoritic as well as geological sources have been the main sources of natural occurring fullerenes, although at really low concentrations. Localised energetic events such as lightning, soot from wildfires and

impacts of extra-terrestrial bodies are thought to be the responsible for these occurrences [36]. Buseck offers a comprehensive review on natural occurrence of fullerenes [36].

Before fullerenes could be widely studied, fullerene production technologies of sufficient yield had to be sought. Kroto et al.'s [13] initial laser ablation (figure 1.1.2) of graphite experiment produced an insufficient yield to attract meaningful research as fullerenes could only be detected through mass spectroscopy analysis [37]. It wasn't until 5 years later, in 1990, that Huffman and Krätschmer [38] produced sufficient macroscopic quantities of fullerene, that the era of scientific fullerene exploration launched [37]. The "Krätschmer–Huffman method" is essentially synthesis of fullerene by electric arc heating of graphite. It involves the vaporisation of graphite electrodes by means of resistive heating in inert (helium) environment. An electric arc is generated between the electrodes producing a soot. Benzene solvent was used to extract the fullerene contained in the resultant soot. Mass spectral analysis revealed the presence of C₆₀ and C₇₀ in the final yield in proportions of 10:1, respectively [37]. In the same year, 1990, Smalley and co-workers reported the design of another fullerene production mechanism they called "C₆₀ generator" [39]. They synthesised fullerene by resistive arc heating of graphite by generating an electric arc between graphite electrodes completely enclosed in a reaction chamber in an inert environment. Organic solvents were used to extract fullerenes from the soot produced in the C₆₀ generator. One of the modern methods of fullerene production is the synthesis by laser irradiation of polycyclic hydrocarbons (PAHs). PAHs have shown to be better at the synthesis of new fullerene homologues as compared to graphite vaporisation methods. Through the use of flash vacuum pyrolysis, PAHs of a desired carbon structure can be "rolled up" by laser irradiation [40]. Other production methods include sputtering, electron beam evaporation, soot combustion of hydrocarbons and electron beam ablation. Arc plasma or radio-frequency-plasma methods are usually the most used commercial methods [1]. Sorting and purification methods such as column chromatography, selective chemistry and high performance chromatography are some of the procedures after fullerene production to isolate monodisperse fullerenes [41]. The demand for low-cost, high-quality fullerene production of sufficient yield is a challenge synthetic production methods seek to accomplish [42]. Readers are referred to Alonso et al.'s [42] detailed review on the synthesis of fullerenes. The relatively high-cost and low yield of available commercial production methods of buckyball fullerene is a major practical hinderance.

Physically, fullerene- C_{60} shows elasticity when compressed up to 75% its size. Mathematical models indicate that it has a bulk modulus of 668 GPa making it harder than diamond whose bulk modulus is 160 GPa [43], [44]. Generally fullerenes can withstand pressure of up to 3000 atmospheres [44]. Fullerene is the only soluble allotrope of carbon under ambient conditions and thus can be used to prepare carbon films in solution. However, elemental fullerene is hydrophobic and is insoluble in many solvents, such as polar solvents. It is soluble in non-polar solvents such as carbon disulphide o-dichlorobenzene, toluene and xylene. Solutions of fullerene C_{60} are deep-purple/violet whereas those of C_{70} are brick red in colour [40], [45], [46]. Fullerene size and morphology are responsible for its unique optical properties such as the large indices of refraction, broad absorption of light in the UV-VIS region [26], [47]. When exposed to light fullerene- C_{60} produces singlet oxygen [46], a trait not least suitable *in vivo* biosensing application. fullerene- C_{60} also polymerise when exposed to ultra-violet light [48].

1.2 Carbon nanotubes

Carbon nanotubes (CNTs) are a 1D allotrope of carbon. They are one atom thick rolled-up graphene sheets, of cylindrical tubular shape CNTs are often capped with buckyball fullerene hemispheres at both ends during their formation[31]. They exist either as multiple-walled CNTs (MWCNTs) or single-walled CNTs (SWCNTs), both of which were discovered by Iijima et al. in 1991 [14] and 1993 [49], respectively [50]. Iijima first discovered MWCNTs as a by-product during the synthesis of fullerene, by the arc discharge method [51]. SWCNTs are a single rolled-up layer of graphene sheet and MWCNTs consist of more than two concentric rolled-up layers. Two concentric rolled-up layers are known as double-walled CNTs. The diameter range of CNTs varies from about 0.4 nm to about 70 nm and can have variable lengths in the order of micros [52], [53].

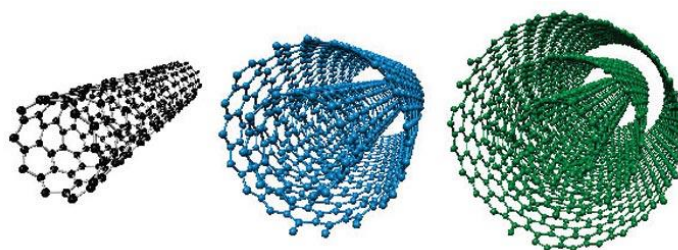


Figure 1. SWCNT, DWCNT and MWCNT

1.2.1 SWCNT

SWCNTs are rolled up single graphene sheets that have a typical diameters about 1nm [54]. Structurally, all the carbon atoms on the cylinder surface are placed in equivalent positions in hexagonal rings. Buckyball fullerene hemispheres which may be present, during formation, on both ends of the SWCNT contain pentagonal rings favouring chemical reactivity [55]. SWCNT atoms in the hexagonal rings are not planar due to the presence of sp^3 hybridisation component. This has the overall effect of making the surface SWCNTs more reactive than planar graphene sheet [55].

To form a SWCNTs, a graphene sheet can be rolled in a number of different ways with respect to lengths along graphene crystal lattice unit vectors (in the honey comb structure) as shown in figure 1.6 [54]. Therefore, the structure of any type of SWCNT can be described in terms of chirality (hexagon orientation with respect to the tube axis [54]) with the aid of the chiral vector index, (n, m) , where n and m are integers. Chirality is determined by the rolling angle or rather orientation of carbon atoms around the circumference [51]. Chirality, c_h , not only indicates the angle between the hexagons and the CNT axis [26] but also the alignment of the π -orbitals. Figure 1.2.1.1 illustrates chirality. To roll-up a sheet of graphene along a vector $c_h = na_1 + ma_2$, the first and the last carbon atom on c_h must be overlaid [53]. The electrical properties are a function of the CNTs chirality depending on the value of the chiral vector index (n, m) . Chiral vector indexes (n, n) and $(n, 0)$ result in arm-chair and zigzag configurations, respectively. Any other configuration is considered helical also known as chiral. Figure 1.2.1.1 shows these configurations. Chirality can be rolled up in different ways to make the CNTs either semiconducting or conducting. A SWCNT, (n, m) , is considered metallic if $m=n$ or $(n-m)$ is a multiple of 3; otherwise, the CNT is a semiconductor. Arm-chair SWCNTs even display higher values of electrical conductivity than that of copper [54]. Electrical conductivity is also a function of SWCNT's diameter and helicity. The emission wavelengths of CNTs vary based on the diameter and chirality. SWCNT diameters may vary from nanometers to micrometres.

Table 1 Some remarkable mechanical, physical and electronic properties

Specific surface area	200-900m ² J ⁻¹
Specific gravity	0.8-2g-1cm-2
Electrical conductivity	2 x 10 ⁻² -0.25Scm ⁻¹
Thermal conductivity	6600Wm ⁻¹ K ⁻¹
Elastic Modulus	>1TPA
Tensile strenght	>100GPa

1.2.2 MWCNT

MWCNTs are intrinsically more complex than SWCNTs. They may house from two to unlimited number of graphene sheets [55]. They have typical diameters of between 5 to 25 nm, and variable lengths from nm to 10 μ m [54], [55]. They consist of more than one SWCNT is arranged coaxially such that the diameter of the innermost SWCNT is the smallest and that of the outermost SWCNT has the greatest diameter.

The carbon layers that make up MWCNTs have inconsistent chirality and thus don't display electric properties as extraordinary as SWCNT. However, MWCNT show extraordinary mechanical properties far superior to those of SWCNTs as reported by Hyung et al. [56], rendering them more useful in strain sensor technology [51], [57]. Thermally, the properties of MWCNTs have been observed to be extremely similar to that of graphene, but quite different to those of SWCNTs [58]. Even though MWCNT do not have qualities as varied and high as SWCNTs, they are easier to process owing to their larger size. MWCNTs contain range from 20 to 40nm and have lengths in the range of 1 to 50 [55].

Apart from the commonly studied SWCNT and MWCNT, other CNTs of varied shapes such as ropes, stripes, springs, bamboo structures, hollow-tube, herringbone etc have been reported [31].

1.3 CNT synthesis methods

The three most common bulk production methods of CNTs are arc discharge, laser ablation, and chemical vapour deposition.

1.3.1 Carbon arc discharge

Carbon arc discharge method involves the growth of CNTs on graphite electrodes by vaporisation of the graphite using direct current (D.C). The synthesis occurs in a vacuum chamber filled with an inert gas such as helium or argon at low pressure (50 - 700 mbar) [52]. An inert environment speeds up reaction (carbon deposition [59]) because of its high ionisation potential [51]. Upon stabilization of chamber pressure, a D.C potential difference is set up between the electrodes. The anode is slowly moved towards the cathode to strike the electric arc [59]. When the graphite anode and cathode are about less than a millimetre apart, a 100 A current flows through the electrodes conveying a large amount of heat through the discharge, creating a plasma arc [60]. The temperature generated in the plasma exceeds 3000 K and vaporises the carbon atoms on the anode, depositing them on the cathode. As the anode depletes, during the course of the production, its position relative to the cathode should be adjusted so as to maintain optimal inter electrode separation for plasma arc uniformity. Once the required length of synthesised CNTs is collected, at the cathode, the D.C power supply source is disconnected and the electrodes are water cooled.

Both SWCNTs and MWCNTs of high quality can be synthesised via carbon arc discharge. Diameters of MWCNTs produced by this method vary from 10 to 200 nm while those of SWCNTs vary from 0.7 to nm. CNT length is dependent on time of synthesis. MWCNTs are produced without the aid of a catalyst whereas SWCNTs are produced with the aid of a metal catalysts on the cathode or electrode. Yield quality of the SWCNTs is greatly affected by parameters such as metal concentration at the electrodes, inert gas pressure etc [61], [62].

The major drawbacks of arc discharge method of CNT production are the labour-intensive recovery and purification required to isolate pure CNTs from the residue by products such as amorphous carbons and non-tubular fullerenes. These processes in part compromise the structural integrity of the produced CNTs. Furthermore, the evaporation of carbon at very high temperature tends to promote the formation of bundled CNTs of limited use. This method requires large amounts of graphite and also consumes a lot of energy.

1.3.2 Laser Ablation

Smalley and co-workers [63] first outlined the use of laser ablation for CNT production in 1995. They reported the production of SWCNTs of diameters between 5 and 20 nm as was observed by X-ray diffraction and transmission electron microscopy analysis.

The laser ablation method setup is very similar to that of the carbon arc discharge except that laser ablation uses a laser beam to evaporate a graphite pellet target containing cobalt or nickel catalyst. The vaporisation is conducted in an inert (He or Ar) gas environment where a pulsed or continuous laser beam is aimed at the target in a furnace at over 1000 °C and 67 kPa. The cloud of carbon and catalyst metal vapour produced is accumulated on a water-cooled copper collector in another section of the reactor. The catalyst in, vapour form, prevent the closing of the CNTs in formation as it condenses slowly. Production ceases when the chamber is cooled or the catalyst structures become too large. The by products are amorphous carbons, fullerenes and carbon polyhedrons with enclosed metal particles.

The SWCNT yield produced by this method show a high degree of structural perfection [64]. The typical SWCNT yield is roughly 70% [65]. Increasing laser force has been observed to increase yield diameter of the SWCNT product [60]. Other factors like wavelength and power of the laser, chemical constituents of target material, chamber pressure, distance between laser source and target material, fluid dynamics near the carbon target etc, have been observed to affect the amount and quality of the SWCNTs produced [61].

Good quality CNTs with yields of up to 70% can be obtained via laser ablation [51]. However, researchers are constantly seeking ways to improve the classic version of this setup to so as to improve upon the pitfalls and thus increase production efficiency. One example is given in ref [66].

Regardless of the advantages of carbon arc discharge and laser ablation, these procedures require vast amounts of graphene and energy and are thus costly. In addition, the yield needs further refinement in order sort-out unwanted carbons and catalysts [58]. Laser ablation has not, so far, been reported to produce MWCNTs

1.3.3 Chemical vapour deposition

To overcome the major pitfalls (high-cost, high energy consumption and yield purities) inherent in the classic carbon arc discharge and laser ablation methods, chemical vapour deposition (CVD) was developed rather modified to synthesis CNTs [51]. CVD was first used in the synthesis of CNTs by Yacaman [67] and co-workers in 1993.

CVD is basically the decomposition of volatile precursor over a catalyst in a chamber containing an inert gas. In the case of CNTs production, the volatile precursor is a hydrocarbon such as CO, acetylene, ethylene, methane etc. The production involves imparting the precursor hydrocarbon with thermal energy at temperatures between 550 and 750°C in order to decompose it into reactive radical species (carbons) over a heated wafer substrate coated with Ni, Co or Fe nanomaterial catalysts. Upon hydrocarbon decomposition, the carbon is dissolves into the molten nano catalyst until a certain saturation point is reached. The catalyst serves as a nucleation site to initiate the growth of CNTs. At this point a semi fullerene cap forms before carbon atoms with honeycomb structure appear to begin CNT precipitation. The growth of the CNT continues as long as the reaction chamber is supplied precursor hydrocarbons. Further purification and filtration is required to separate the CNTs from the catalysts and hydrocarbons. An exhaustive review of sorting and purification techniques is given in citation [68].

CVD's ability to control diameter-size for desired CNTs is made possible by adjusting the size of the metal catalyst nanoparticles, effectively altering CNT properties. Diameters of 0.5 - 5nm for SWCNTs and 8 – 10 nm for MWCNTs are possible [69]. Methane hydrocarbon is used in the synthesis of SWCNTs whereas acetylene or ethylene for MWCNTs. Well separated large quantities of direction controlled CNTs can be produced by CVD.

The nature of the chosen precursor hydrocarbon and chosen nanoparticle catalyst material are the main parameters that influence the production of CNTs by CVD. Length of produced CNTs is dependent on time taken to grow them.

1.4 CNT functionalization

Covalent and non-covalent methods are the most commonly used functionalization methods for CNTs.

Covalent functionalization involves modification of the CNT sidewalls defect sites or at the caps. It deals with the formation of a chemical bond between the carbon skeleton of CNTs and a functional group [70]. This effectively disrupts the pure CNT properties like luminescence and Raman detection shift plots which are reportedly lessened, making covalently bonded CNTs less favourable for use in photothermal or imaging application [71]. The loss in qualities is caused by alterations in the conjugated π -grid of pristine CNTs. Despite these losses, functionalization such as oxidation by a strong acid presents new possibilities for further modification of the CNTs with amines, amino acids etc. Oxidation has the effect of imparting physical strain upon the sp^2 hybridised carbon atoms due to tension in the curvature, converting the sp^2 hybridised carbon atoms to sp^3 making the CNT more susceptible to further reactions [70]. Functionalization with strong acids also has the effect of reducing CNT length, opening the CNT ends and creation of carboxyl groups there [72].

Addition reactions with hydrophilic groups can be used to improve solubility and avoid some of the side effects of acid functionalization [72].

Covalent functionalization can also be used to improve dispersion of CNTs in aqueous solutions by covalently bonding them to surfactants, peptides and proteins on their surface [72].

Unlike covalent functionalization, non-covalent functionalization is non-evasive, in that it can be done without altering the sp^2 hybridised carbon network of the CNT wall [71]. From this it follows that non-covalently functionalised CNTs preserve their electronic structure, inevitably leaving the physical electronic and optical properties unaltered [53], [55]. This surface functionalization procedure is based on adsorption and weak interaction forces such as π - π stacking, Van der Waals force, hydrophobic interaction, electrostatic, charge transfer or hydrogen bonds. It is therefore not surprising that the load that non-covalently functionalised CNTs can take on might be low. This functionalization happens by

the adsorption of surfactant molecules on the outer walls of CNTs or the wrapping of polymer chains around the nanotubes [71].

2. Overview of some deposition technologies for carbon-based allotrope materials

The large surface area presented by CNTs is one of the qualities that is essential in their application as sensor platform active layers. This quality enhances the sensor active-layer with analyte interaction. However, to achieve the desired sensor performance, a suitable CNT deposition technique must be sought. A suitable deposition technique is important because overall sensor quality is heavily dependent on the quality of the deposited active layer. Methods that are able to yield homogeneous and thin layers are more desirable [73].

Deposition techniques are generally divided into wet and dry techniques. Some selected wet techniques are presented in section 2.1 whereas section 2.2 highlights a few dry deposition techniques. Wet techniques involve the creation of thin-film deposition from the liquid phase of CNMs whereas dry techniques seek to create films directly from CNM assemblies [51].

2.1 Wet deposition techniques

2.1.1 Langmuir-Blodgett depositing technique

The Langmuir-Blodgett (LB) depositing technique was first introduced by Irving Langmuir and Katharine Blodgett after whom it is named. This method involves the deposition of amphiphilic monolayers of particles trapped at the air/water interface onto a solid substrate by means of a vertically dipping the substrate immersed at the sub-phase [74], [75]. The amphiphilic materials used often are those with hydrophobic tails and hydrophilic heads[50].

The deposition procedure is conducted in two main steps. The first involves dissolving the amphiphilic material in a volatile solvent, ideally one with positive spreading coefficient and insoluble in the subphase. The solution is then spread onto the air/water surface followed by solvent evaporation which enables the formation of the amphiphilic material monolayer. Upon the attainment of thermodynamic equilibrium, the monolayer-thick film is isothermally compressed in order to form a stable monolayer film. The compression has the effect of altering its shape all the while altering its phase states. The second stage involves

transfer of the film onto the solid substrate. To attain this, the solid substrate is dipped into the sub-phase and is then raised out subsequently depositing the monolayer film onto the substrate. During this stage, surface pressure is monitored via isobars and is kept constant by adjusting the moveable barrier to achieve the target pressure. Surface pressure is an important parameter in determining the quality of the coating. More monolayers may be coated onto the substrate by repeating the transfer process.

A similar mono-layer deposition technique called Langmuir-Schaefer method involves horizontal deposition of a thin film onto a substrate as opposed to the vertical deposition of LB technique.

2.1.2 Drop Casting

This is a cheap, easy and tuneable deposition procedure most suitable for small areas of about 1cm². This method involves dispersing a specific quantity of suitable CNM into a volatile solvent and then literally dropping it on a prepared substrate, using a pipette for instance. The drop is then left to evaporate off the substrate, under controlled conditions of temperature and pressure, leaving a CNM deposition onto the substrate. Varying the CNM concentration or volume of dispersion or indeed repeating the procedure could be done to vary the thickness of the coating. Complete wetting and hydrophobic properties of the substrate must be taken into account to determine solvent properties for the chosen CNM [50], [76], [77].

It is very difficult to obtain a uniformly thick coating across the substrate using this procedure. This is due to differences in the rates of evaporation on different substrate points under a given drop. Fluctuations in CNT concentration within a droplet also negatively impacts uniform CNT deposition onto a substrate. There is also always a chance for void formation on the substrate upon solvent evaporation. These reasons make drop casting unsuitable for use across large areas [78].

2.1.3 Electrophoretic depositions

Electrophoretic deposition (EPD) is a two-step wet approach method. The two main steps are, electrophoresis followed by deposition. In the first stage, electrophoresis, colloidal

charged particles or molecules are dispersed in a suitable solvent (or aqueous solution). They then migrate towards an electrode under the influence of an electric field. Deposition occurs at the target electrode surface by particle accumulation and coagulation, forming a coherent homogeneous deposit [79], [80]. Deposition can either be set up to occur at the cathode (cathodic electrophoretic deposition) or at the anode (anodic electrophoretic deposition) depending on the polarity of the particles in the suspension [81].

Deposition uniformity and the ability to control deposition thickness on the surfaces of irregular and regularly shaped substrates alike, achieving microstructural homogeneity, are some of the main advantages of EPD. In addition, EDP has the potential to infiltrate porous substrates. It is also a simple and inexpensive deposition procedure [79].

2.1.4 Dip coating

Dip coating is a well-known thin film coating procedure. It is conducted in three main steps. The first step involves immersion of the substrate, at constant speed, into a solution containing the coating material where it is left for a predetermined time. Deposition occurs as the substrate is retrieved from the solution at constant speed to ensure homogeneous coating. The coat thickness is directly proportional to the speed at which the substrate is being retrieved from the solution. This is followed by drainage of excess solution off the surface of the substrate by baking or forced air drying. Excess solvent is left to evaporate off the surface and a thin film is deposited onto the substrate [82]–[84]. Number of dipping cycles, rate of solvent evaporation, solution contents, viscosity, concentrations, temperature, etc. also affect film properties and thickness [82], [85].

Though similar to most wet deposition techniques, dip coating is remarkably faster. It is also simple and cheap and thus may not be suitable for use in situations requiring high quality substrate deposits. Nonuniformity in coating thickness is the main disadvantage of dip coating. It is however suitable for use in laboratory set up and for large scale requirements for which low quality depositions are sufficient [82], [83].

2.1.5 Spin Coating

Spin coating utilises centrifugal force for its operation. It is well known for depositing thin films of even thickness on flat substrates. The procedure involves placing a small puddle of CNT based solution, of known concentration, on a substrate. The substrate is then spun at high, predetermined speeds, in order to spread the solvent evenly over the entire substrate by centrifugal force. Film properties, such as thickness, are mainly determined by the nature of the solvent and spin parameters [85].

Spin coating is ideal for preparation of CNT polymer composite films. However, it is an impractical procedure for large area film depositions. It is also very cumbersome to use for multi-layer deposition purposes. Worse still the material efficiency of spin coating is low as a substantial amount of raw material is lost by not landing on the substrate. Spray Coating

2.1.6 Air brush spray deposition

This wet film deposition makes use of a nebuliser to spray a CNM suspension onto a preheated substrate. The CNM dispersion is first introduced into the input chamber of the spray gun. Nebuliser air pressure, distance of substrate from nozzle and the spray quantity adjustment settings on the gun are some of the variables that help set spray quantity per spray. The substrate is paced onto a heater set to the boiling point temperature of the dispersion solvent. This temperature is important to ensure the dispersion solvent evaporates off the substrate evenly upon deposition, leaving behind an evenly thick CNT layer. Deposited layer thickness can be varied by continually making more short sprays onto the substrate. Short spray pulses often lead to higher quality depositions.

2.2 Dry deposition techniques

2.2.1 Chemical vapour deposition

Chemical vapour deposition (CVD) is a popular dry approach materials processing technology. In materials science, CVD denotes various techniques that deposit solid material, in gaseous phase, onto a solid substrate. In addition to thin film deposition onto

substrates, CVD is also used to produce powders, composite and high-purity bulk materials. [86].

CVD involves the deposition of a solid thin film produced from the chemical reaction of a gas phase precursor, over a heated substrate. CVD differs from physical vapour deposition (PVD) in that PVD uses a solid precursor material which is vapourised right before deposition. Tunability of the CVD processes renders it more superior to PVD processes like sputtering and evaporation procedures [87].

The first stage in CVD involves feeding the reactor chamber, at roughly ambient temperature, with a reactant precursor gas which may be diluted in a volatile carrier gas. Upon entering the reaction chamber, the reactant may undergo gas-phase reactions or diffuse into the substrate right away through the substrate boundary layer. Gas-phase reaction requires, a high temperature and this may be supplied by various sources such as resistive, radiation or radio frequency induction heaters etc. Plasma energy and laser sources may also be used. The gas-phase reaction leads to the formation of intermediate reactants as well as volatile gaseous by-products which are removed via the reaction chamber exhaust system. Alternatively, the reactant precursor gas could diffuse into the substrate via the boundary layer. At this stage, in both gas-phase reaction and direct diffusion, the intermediate reactants or reactant gas adsorb onto the heated substrate. Following reactions at the gas-solid interface, the deposition of a film on the substrate surface through nucleation, coalescence and growth is initiated. Unreacted reactants and reaction by-products are discarded via the exhaust [87].

At industrial scale, CVD is the most widely used deposition technology for CNMs considering the controllable deposition sizes and structure [88]. The general CVD method was tailored to CNMs in order to overcome most of the shortcomings of other methods like laser ablation, arc discharge that lack high efficiencies, suffer low yield purity, and have high energy consumption costs [51].

CNT deposition by CVD enables the production of highly tenable CNTs. CNT properties can be tuned by varying the CVD parameters such as choice of catalyst, substrate, precursor concentration and flow rate, deposition time etc. A metallic substrate and gaseous carbon precursor are used in the presence of a catalyst. When the precursor decomposes onto

the substrate, CNTs growth may occur by two mechanisms, tip-growth or base-growth. Heterogeneous reactions and diffusion of the carbon atoms through the metal particles leads to the formation of the CNT structure [89].

The main advantages of CVD over other deposition technologies are the high purity deposits, conformal coating and high efficiency. However, it requires expensive raw materials and it produces toxic by-products [86].

3. Experiment

This part of the thesis is concerned with practically verifying the temperature dependence of carbon-based organic materials, carbon nanotubes. The experiment was done in three main steps. In the first step, CNT materials were prepared for deposition by means of dispersion. Thereafter, CNT thin film deposition onto a sensor substrate was done. The third and final procedure was measurement of the sensor parameters. The aforementioned steps are described in detail in the appropriate sub-sections below.

3.1 List of materials and apparatus used in the experiment

CNT materials used.

- SWCNT
- MWCNT
- SWCNT-COOH
- MWCNT-COOH

Sensor substrate.

- BI2 interdigital sensor platform

Auxiliary materials used.

- N, N dimethylacetamide polar solvent (DMAc)
- Isopropyl alcohol (IPA).

Main apparatus used.

- Climatic chamber
- Interdigital electrode (IDE) contact box
- RLC meter
- Computer (data logger)
- Airbrush deposition apparatus
- Digital ultrasonic cleaner
- Bench-top centrifuge machine
- Multimeter

- Analytical balance
- Vials (Headspace and Eppendorf)

3.2 Procedure

3.2.1 Preparation of CNT materials (dispersion)

The CNT materials, initially in powder form, were first mixed with a polar solvent N, N-dimethylacetamide (DMAc). Each material was mixed in the ratio, 1mg CNT: 15ml DMAc solvent. CNTs, however, tend to bundle-up and form complex structural morphologies mainly due to the van der Waals interactions among individual tubes [90]. These van der Waals interactions are in part responsible for the poor solubility and dispersion of CNTs in aqueous as well as organic solvents [91]. In order to ensure stable and homogeneous CNT dispersion, two mechanical treatment procedures were conducted on the mixtures. Sonication of the mixtures in a water-cooled ultrasonic cleaner at an output power of 700W for 24 hours was first administered. This was done in order to break up CNT agglomerations and thus reduce tube entanglements [92]. Centrifugation at 10000 rpm for 45 minutes then followed. Centrifugation was necessary in order to separate the residual solid particles and aggregates, left over from sonication, from the rest of the homogeneous dispersions [90]. Mechanical dispersion was chosen over chemical dispersion as it ensures, with greater probability, that the resultant CNTs contain the least contaminants which may otherwise interfere with physical properties of the CNTs [93].

3.2.2 Sensor assembly

3.2.2.1 Interdigital sensor platform

An interdigital, also called interdigitated, sensor platform consists of parallel in-plane periodic microstrip electrode structures that form a “comb-like” or “grating” pattern. The electrode structure serves as mediator between the sensitive layer (thin or thick film) and relevant electronics circuitry. Gold and platinum electrodes are usually employed for use as sensor electrodes thanks to their inert and flexible nature. Silver (Ag) and nickel-chromium (NiCr) are also used as electrodes. By a suitably chosen technique, the

periodic microstrip electrodes are deposited onto a substrate. Flexible or rigid substrates can be used depending on sensor application and requirements [94].

In this experiment, the Interdigital electrode BI2 sensor substrate was used. This substrate is a two-electrode ceramic-base sensor platform. The properties of the BI2 IDE sensor platform used are shown in table 2 below. BI2 IDEs of line/gap $100\mu\text{m}/100\mu\text{m}$ were used for the deposition of SWCNT, SWCNT-COOH and MWCNT. MWCNT-COOH was deposited on IDEs of line/gap $50\mu\text{m}/50\mu\text{m}$.

Table 2 Sensor Platform BI2 (data sheet) Characteristics.

BI2 sensor substrate.	
Interdigitated electrodes (IDE): line / gap	$100\mu\text{m} / 100\mu\text{m}$
	$50\mu\text{m} / 50\mu\text{m}$
Structure of IDE multilayer	NiCr/Ni/Au
Connection	Ag wire $\varnothing 0.25\text{ mm}$
Temperature range	$-30\text{ }^{\circ}\text{C}$ to $+200\text{ }^{\circ}\text{C}$
Dimensions	$5.5 \times 8.8 \times 0.6\text{ mm}$

Before the BI2 IDE sensor substrates could be used for thin film deposition, they were cleaned with isopropyl alcohol (IPA) to ensure that the substrate surfaces were clean and free of contaminants that could potentially interfere with the test results.

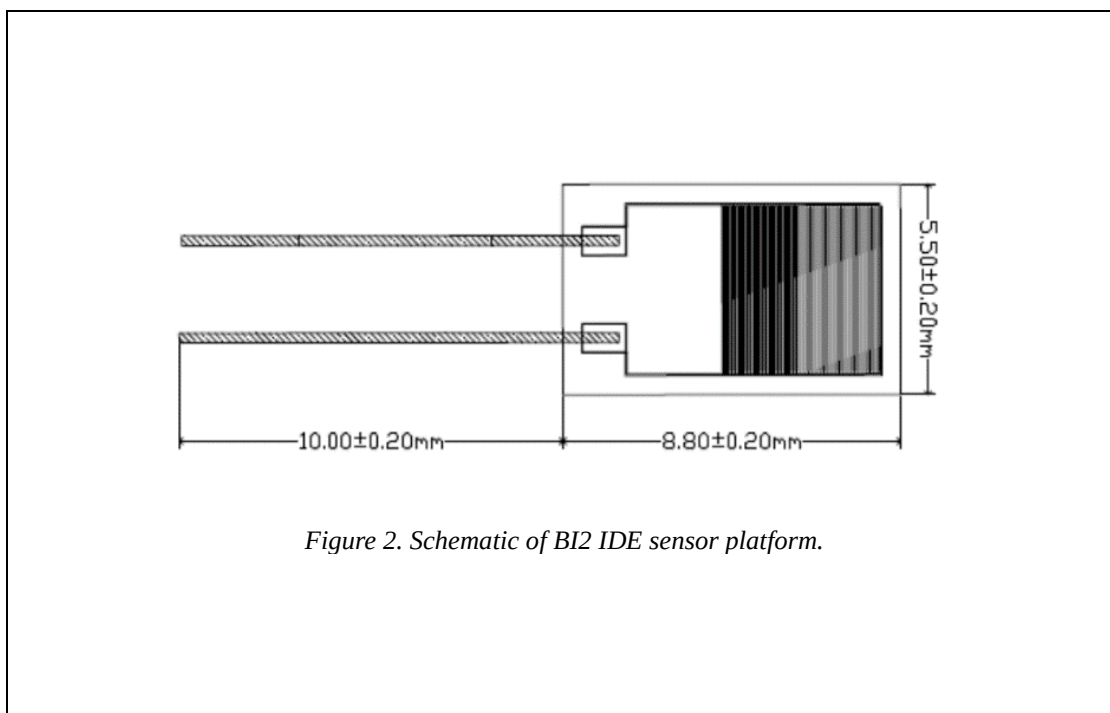


Figure 2. Schematic of BI2 IDE sensor platform.

3.2.2.2 CNT thin-layer deposition by airbrush spray

When the BI2 IDE sensor substrates were cleaned, thin-layer deposition of the sample CNT materials was done by airbrush spray coating. For each of the dispersed CNT materials, five BI2 IDE substrates were thin-film coated by airbrush spray method.

To deposit a CNT thin-film onto a BI2 IDE sensor substrate, the substrate had to be first placed on a preheated plate at a temperature of 165°C. At this plate temperature all the IPA that may have remained on the BI2 substrate, from the cleaning process, would have evaporated off before the start of CNT thin-film deposition. Secondly, 165°C plate temperature was necessary because it is the boiling point of the dispersion solvent, DMAc. This temperature ensured sufficiently quick evaporation of the dispersion solvent, DMAc, leaving behind a CNT thin-film deposition with the least chance of coffee ring formation, thus avoiding CNT agglomeration.

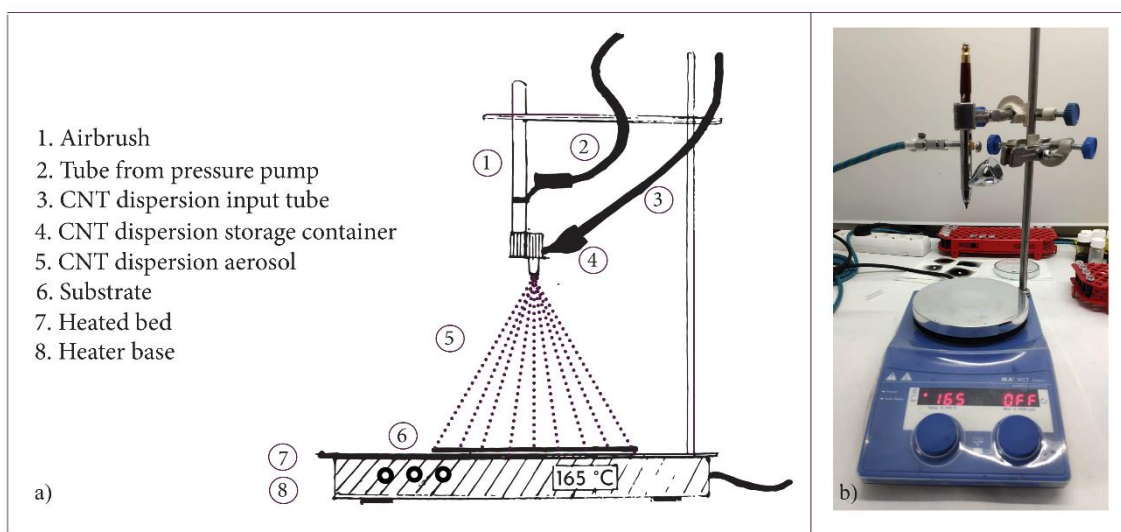


Figure 3. (a) Schematic of Airbrush apparatus. (b) Picture of Airbrush apparatus

The airbrush deposition apparatus is shown in 3 above. To establish uniform and homogeneous thin-film spray depositions, the spray pressure as well as spray volume for each spray had to be adjusted accordingly.

During the airbrush deposition for every BI2 IDE sensor substrate, a multimeter was used to monitor the thin-film deposition thickness. An output resistance in the range of $1\text{k}\Omega$ - $5\text{k}\Omega$ across the main output leads of the BI2 IDE sensor substrate indicated that the desired deposition layer thickness had been achieved. Exceeding the required deposition thickness resulted in resistance readings below $1\text{k}\Omega$.

It was, however, difficult to achieve the aforementioned resistance range for deposited MWCNT-COOH thin film on the BI2 IDE sensor platform of line/gap $100\mu\text{m}/100\mu\text{m}$. This is probably because the electrical conductivity of MWCNT-COOH was too low (at the used dispersion ratio) for use with an IDE of line/gap $100\mu\text{m}/100\mu\text{m}$. It is for this reason that a BI2 IDE sensor platform of line/gap $50\mu\text{m}/50\mu\text{m}$ was used for successful deposition of the MWCNT-COOH thin film.

3.2.3 Measurement of sensor parameters

3.2.3.1 Measurement set-up

During measurement, all samples under test were placed in the climatic chamber, Vötsch VCV³ 7060-5, with controlled temperature and constant relative humidity (RH) value of 40%. The measurements' part was done in two identical cycles. The first measurement cycle involved five BI2 IDE sensor substrate samples deposited with unfunctionalized SWCNT and another five deposited with MWCNT-COOH. Measurement of the SWCNT-COOH and unfunctionalized MWCNT BI2 IDE sensor substrate samples was done thereafter as the second measurement cycle. Each of the two measurement cycles ran for 24 hours.

In order to conduct the tests, the prepared samples were placed in a 10-position contact box, inside the climatic chamber. The 10-position contact box can be connected to cables that provide a connection between the prepared IDE samples under test and circuitry external to the climatic chamber. Through these cables, the prepared IDE samples were connected to a ten-channel multiplexer. A RLC meter, Keysight 4980, set at 0.25V frequency of 1kHz was connected to the multiplexer output to ensure precise impedance measurement values for each of the prepared IDE samples under test. 0.25V was chosen as RLC operating voltage to measure the organic thin layer deposition

impedance because it was voltage high enough to ensure an accurate reading and not too high to damage the properties of the organic thin layer material under test. The measurands from every sample under test were then logged onto a computer.

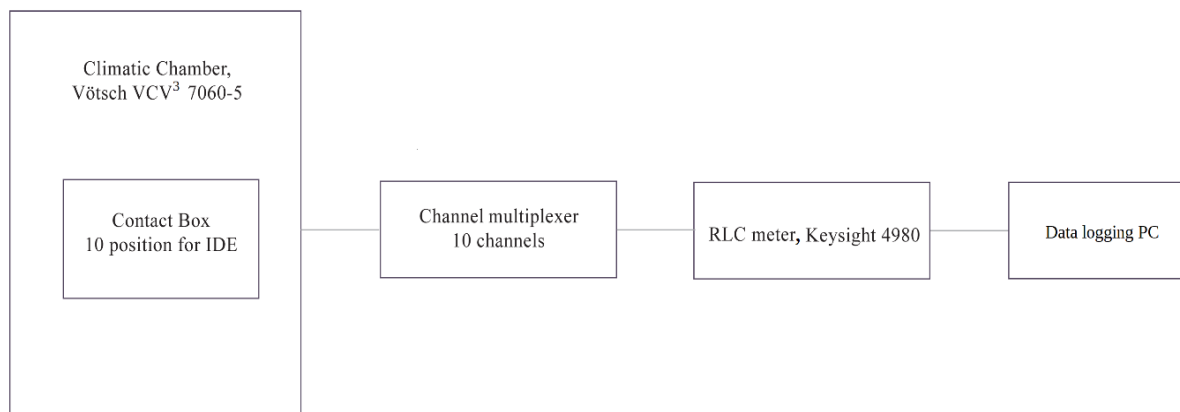


Figure 4. Measurement, experiment set-up.

Table 3. Multiplexor channel numbers during measurement.

Channel number	First measurement cycle	Second measurement cycle
1 to 5	SWCNT	SWCNT-COOH
6 to 10	MWCNT-COOH	MWCNT

3.2.3.2 Climatic chamber temperature profile

A climatic chamber temperature profile with a step-size of 10°C operating in the range 10°C - 80°C was chosen. The step-size temperature change was carried out every 20 minutes meaning that a given temperature was held constant in the chamber for ideally 20 minutes. To rise from the minimum temperature value, 10°C, to the maximum value, 80°C, took 140 minutes. Seven more steps of 10°C were taken to cool down to the minimum temperature value of 10°C over an additional 140 minutes. This means that the time period of the climatic chamber temperature profile was 280 mins. Five such time periods ($T_1 - T_5$) were set to run over a period of 24 hours in each of the two measurement cycles. The figure 5 below, shows the set temperature profile for one time period and five time periods (entire length for each one of the two measurement cycles).

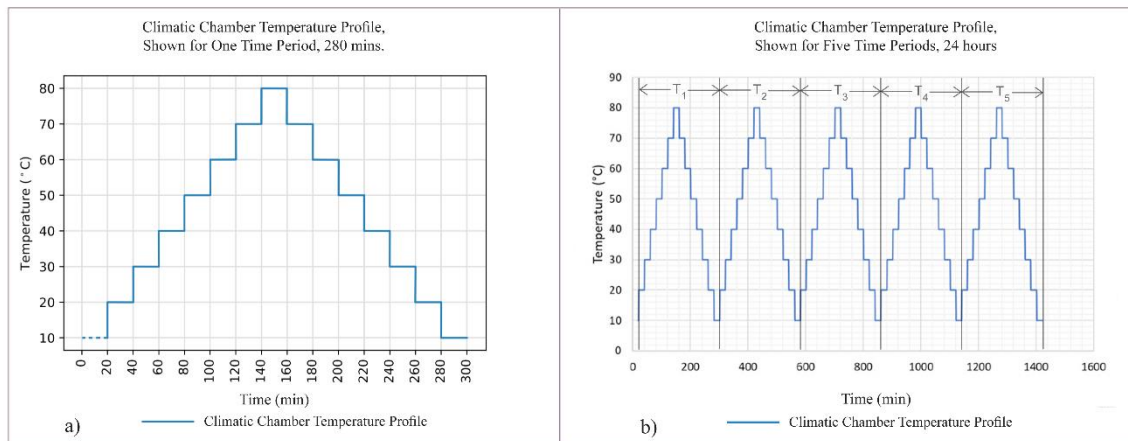


Figure 5. Graphs of the pre-set climatic chamber temperature profile shown, (a) for one time-period (T_1), (b) for five time-periods ($T_1 - T_5$).

The sampling frequency for the climatic chamber temperature profile was set at 1 temperature data point per second. This data, for the entire length of each one of the two measurement cycles, was recorded and logged onto the computer. Two separate climatic chamber temperature profile files were obtained, one from each of the two measurement cycles.

3.2.3.3 Measurement channels

Impedance, of the CNT materials under test, was measured and recorded for each of the ten channels in both measurement cycles. Data from each channel was written to an individual file and stored on the data-logging computer.

Data analysis

To analyse the data from these measurements first required the synchronisation of the data recorded from the climate chamber with the data points recorded from the measurement channels. This was necessary because climatic chamber sampling frequency was different to measurement channels sampling frequency. To achieve data synchronisation a small macro was written in Vi-Improved, Vim, programmed to synchronise the data points to one data point every second in both climatic chamber files and measurement channel data output files.

With climatic chamber and measurement channels' data points were synchronised, graphs of the resistance versus climatic chamber temperature were plotted, for all measurement channels. These graphs are shown in figures i. to xx. in the appendix. By visually inspecting the graphs, it was observed that all the four materials tested displayed a negative coefficient of resistance. Furthermore, the graphs helped with determining which measurement channels contained distorted data readings and which ones did not. Table 4, below indicates which channels had good data, partially good data and which ones had completely distorted data.

Table 4. Overview of the results from the measurement channels.

	1st measurement	2nd measurement
	(material)	(material)
channel 1	(SWCNT)	(SWCNT-COOH)
channel 2	(SWCNT)	(SWCNT-COOH)
channel 3	(SWCNT)	(SWCNT-COOH)
channel 4	(SWCNT)	(SWCNT-COOH)
channel 5	(SWCNT)	(SWCNT-COOH)
channel 6	(MWCNT-COOH)	(MWCNT)
channel 7	(MWCNT-COOH)	(MWCNT)
channel 8	(MWCNT-COOH)	(MWCNT)
channel 9	(MWCNT-COOH)	(MWCNT)
channel 10	(MWCNT-COOH)	(MWCNT)

good measurement	
partially good measurement	
bad measurement (total distortion)	

The channels with totally distorted data measurement were discarded from any further data processing. From the channels with partially good measurements, undistorted portions were considered for further data processing in addition to all the data from the channels with good measurement. Measured data points from each channel were divided into 5 portions based on the climatic chamber time periods, ($T_1 - T_5$) as shown in figure 5b. All data measurement points obtained in the portion T_1 (the first 300 minutes of measurement) were discarded. This was done to ensure that all measurements considered were conducted strictly under the RH and temperature conditions as set in the climatic chamber without the potential influence of ambient room RH and temperature conditions that maybe present at the beginning of measurement. To this effect only the climatic chamber time portions T_2 to T_5 were considered in all of the measurements.

The next step involved calculation of the average resistance of the materials under test, at every corresponding step temperature of the climatic chamber temperature profile for each measurement channel. These average resistance values were then used as representative resistance values at corresponding step temperatures of the climatic chamber temperature profile. Results of these calculations are shown in the (a) part of the tables i. to xx. in the appendix, for all 20 channels.

Each of the calculated average resistance values was then calculated as a percentage ($\%R_{T_n}$) of the average resistance value at 10°C in each local temperature profile time-period (T_n). Results of these calculations are shown in the (b) part of the tables i. to xx. in the appendix, for all 20 channels.

$$\%R_{T_n} = \frac{(\text{Average } R \text{ value at each temperature step in } T_n)}{(\text{Average } R \text{ value at } 10^\circ\text{C in } T_n)} * 100$$

Next, the difference, $\%R_{T_n} - \%R_{T_{n-1}}$, between adjacent temperature steps was calculated, in each of the local temperature profile time-periods (T_n). Results of these calculations are shown in the (c) part of the tables i. to xx. in the appendix, for all 20 channels.

Finally, an average value of the differences in percent values for each one of the four CNT materials used was calculated. The results of these calculations are shown in tables 4 to 7 and graphs 6 to 9.

Table 4. Average relative percent change values for the material SWCNT.

Average %Δ Values for SWCNT Material.										
Climatic Chamber temperature profile period, T	T1		T2		T3		T4		T5	
Relative time of measurement (min)	21 - 160	161 - 300	301 - 440	441 - 580	581 - 720	721 - 860	861 - 1000	1001 - 1140	1141 - 1280	1281 - 1420
Chamber temperature profile trend	Rise	Fall	Rise	Fall	Rise	Fall	Rise	Fall	Rise	Fall
%Δ in R between 20°C and 30°C					-3.17					
%Δ in R between 30°C and 40°C				-2.63		-3.11		-3.32		-3.38
%Δ in R between 40°C and 50°C				-2.16		-2.84		-3.14		-2.71
%Δ in R between 50°C and 60°C				-1.21		-2.63		-2.91		-2.10
%Δ in R between 60°C and 70°C				-0.30		-1.95		-2.47		-1.35
%Δ in R between 70°C and 80°C				1.33		-0.70		-1.67		-0.84
%Δ in R between 80°C and 70°C					5.18		3.74		3.20	2.77
%Δ in R between 70°C and 60°C					3.83		3.25		3.10	2.78
%Δ in R between 60°C and 50°C					3.29		3.14		3.10	2.63
%Δ in R between 50°C and 40°C					3.20		3.15		3.14	2.39
%Δ in R between 40°C and 30°C					3.28		3.06		1.94	2.25
%Δ in R between 30°C and 20°C					3.42		3.42		1.70	2.09
%Δ in R between 20°C and 10°C					3.43		3.61		1.91	

Relative Change of Resistance with Respect to Change in Temperature
Material: SWCNT

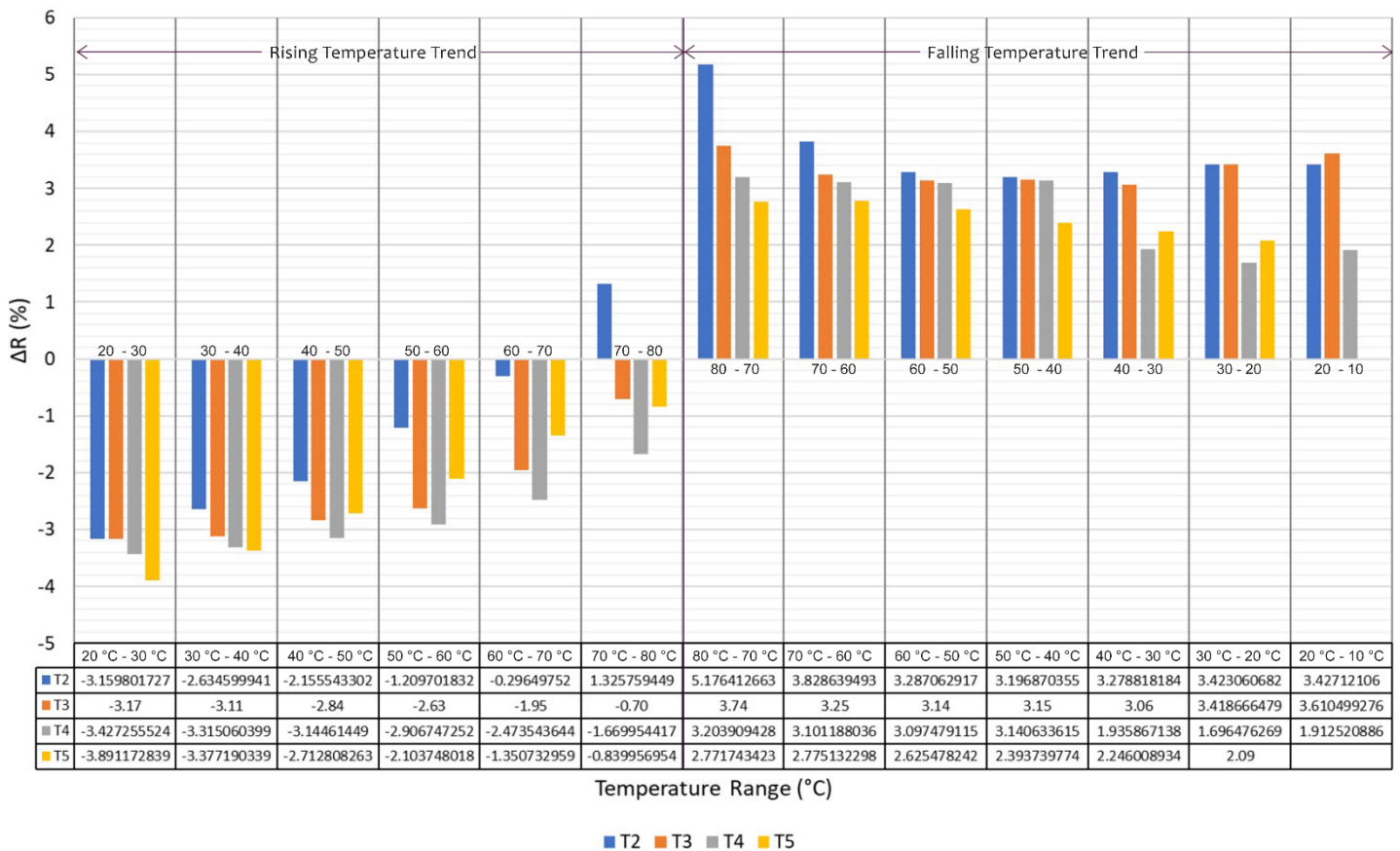


Figure 6. Graph depicting the average relative percent change of the resistance for the material SWCNT, with temperature change.

Table 5. Average relative percent change values for the material MWCNT-COOH.

Average %Δ Values for MWCNT-COOH Material.										
Climatic Chamber temperature profile period, T	T1		T2		T3		T4		T5	
Relative time of measurement (min)	21 - 160	161 - 300	301 - 440	441 - 580	581 - 720	721 - 860	861 - 1000	1001 - 1140	1141 - 1280	1281 - 1420
Chamber temperature profile trend	Rise	Fall	Rise	Fall	Rise	Fall	Rise	Fall	Rise	Fall
%Δ in R between 20°C and 30°C			-3.04		-2.60		-2.58		-2.09	
%Δ in R between 30°C and 40°C			-3.28		-2.89		-2.78		-2.32	
%Δ in R between 40°C and 50°C			-3.95		-3.21		-2.96		-2.54	
%Δ in R between 50°C and 60°C			-3.92		-2.75		-1.70		-2.69	
%Δ in R between 60°C and 70°C			-5.25		-4.54		-3.59		-2.92	
%Δ in R between 70°C and 80°C			-9.49		-6.47		-4.04		-4.26	
%Δ in R between 80°C and 70°C				-3.21		-2.42		-3.48		-1.27
%Δ in R between 70°C and 60°C				3.16		3.11		2.29		1.94
%Δ in R between 60°C and 50°C				2.27		1.49		1.91		2.17
%Δ in R between 50°C and 40°C				3.30		2.61		2.43		2.39
%Δ in R between 40°C and 30°C				3.47		2.51		2.70		2.39
%Δ in R between 30°C and 20°C				3.04		2.86		2.70		2.24
%Δ in R between 20°C and 10°C				2.33		2.85		2.50		

Relative Change of Resistance with Respect to Change in Temperature
Material: MWCNT-COOH

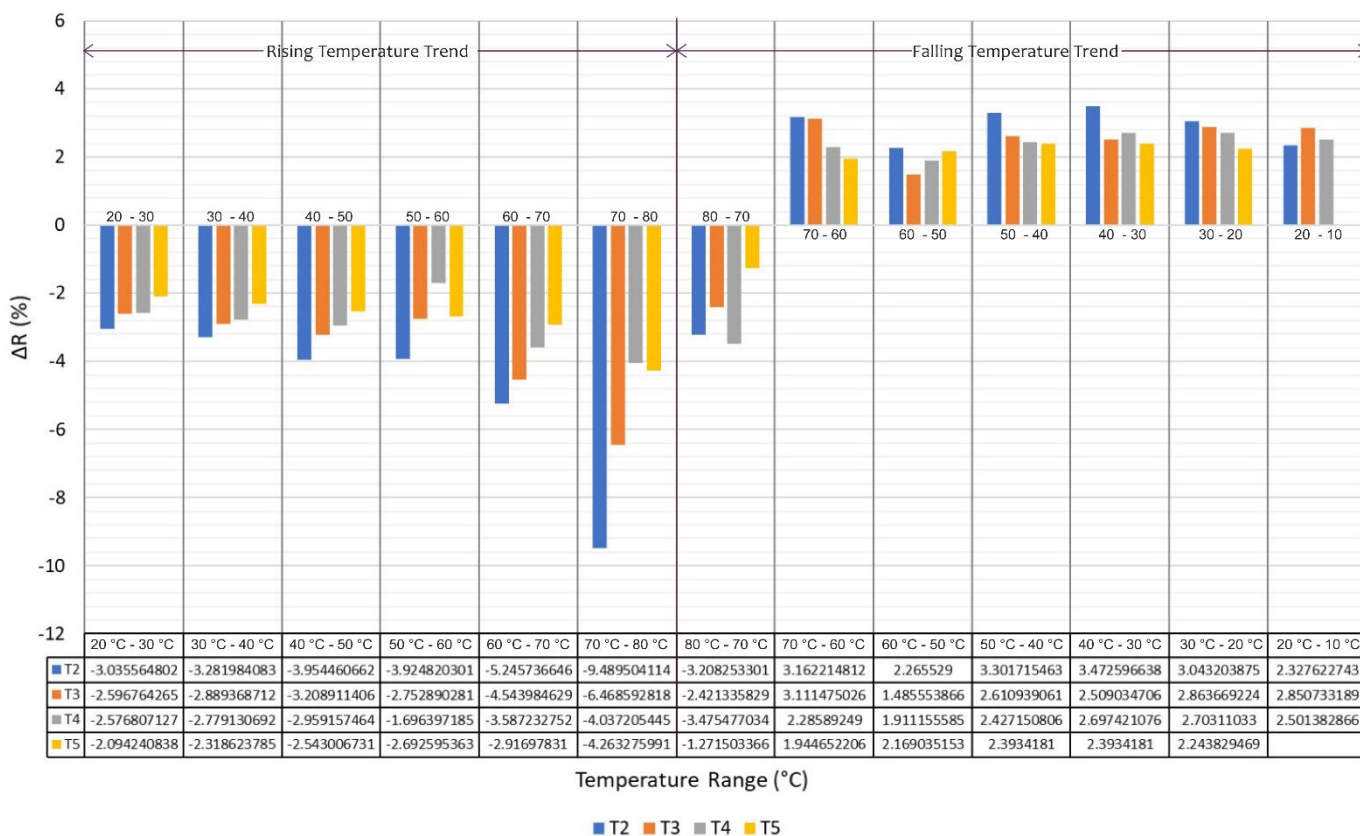


Figure 7. Graph depicting the average relative percent change of the resistance for the material MWCNT-COOH, with temperature change.

Table 6. Average relative percent change values for the material SWCNT-COOH.

Average %Δ Values for SWCNT-COOH Material.										
Climatic Chamber temperature profile period, T	T1		T2		T3		T4		T5	
Relative time of measurement (min)	21 - 160	161 - 300	301 - 440	441 - 580	581 - 720	721 - 860	861 - 1000	1001 - 1140	1141 - 1280	1281 - 1420
Chamber temperature profile trend	Rise	Fall	Rise	Fall	Rise	Fall	Rise	Fall	Rise	Fall
%Δ in R between 20°C and 30°C			-2.67		-2.54		-2.59		-2.97	
%Δ in R between 30°C and 40°C			-2.29		-2.47		-2.74		-2.79	
%Δ in R between 40°C and 50°C			-1.68		-2.33		-2.56		-2.55	
%Δ in R between 50°C and 60°C			-1.03		-2.32		-2.59		-2.35	
%Δ in R between 60°C and 70°C			-0.34		-2.10		-2.40		-1.74	
%Δ in R between 70°C and 80°C			-0.01		-1.58		-2.24		-1.19	
%Δ in R between 80°C and 70°C				2.66		1.67		1.48		1.86
%Δ in R between 70°C and 60°C				2.76		2.54		2.48		2.39
%Δ in R between 60°C and 50°C				2.73		2.70		2.33		2.26
%Δ in R between 50°C and 40°C				2.68		2.62		2.12		2.08
%Δ in R between 40°C and 30°C				2.55		2.75		2.01		1.82
%Δ in R between 30°C and 20°C				2.74		2.80		1.93		1.62
%Δ in R between 20°C and 10°C				2.89		2.83		1.96		

Relative Change of Resistance with Respect to Change in Temperature
Material: SWCNT-COOH

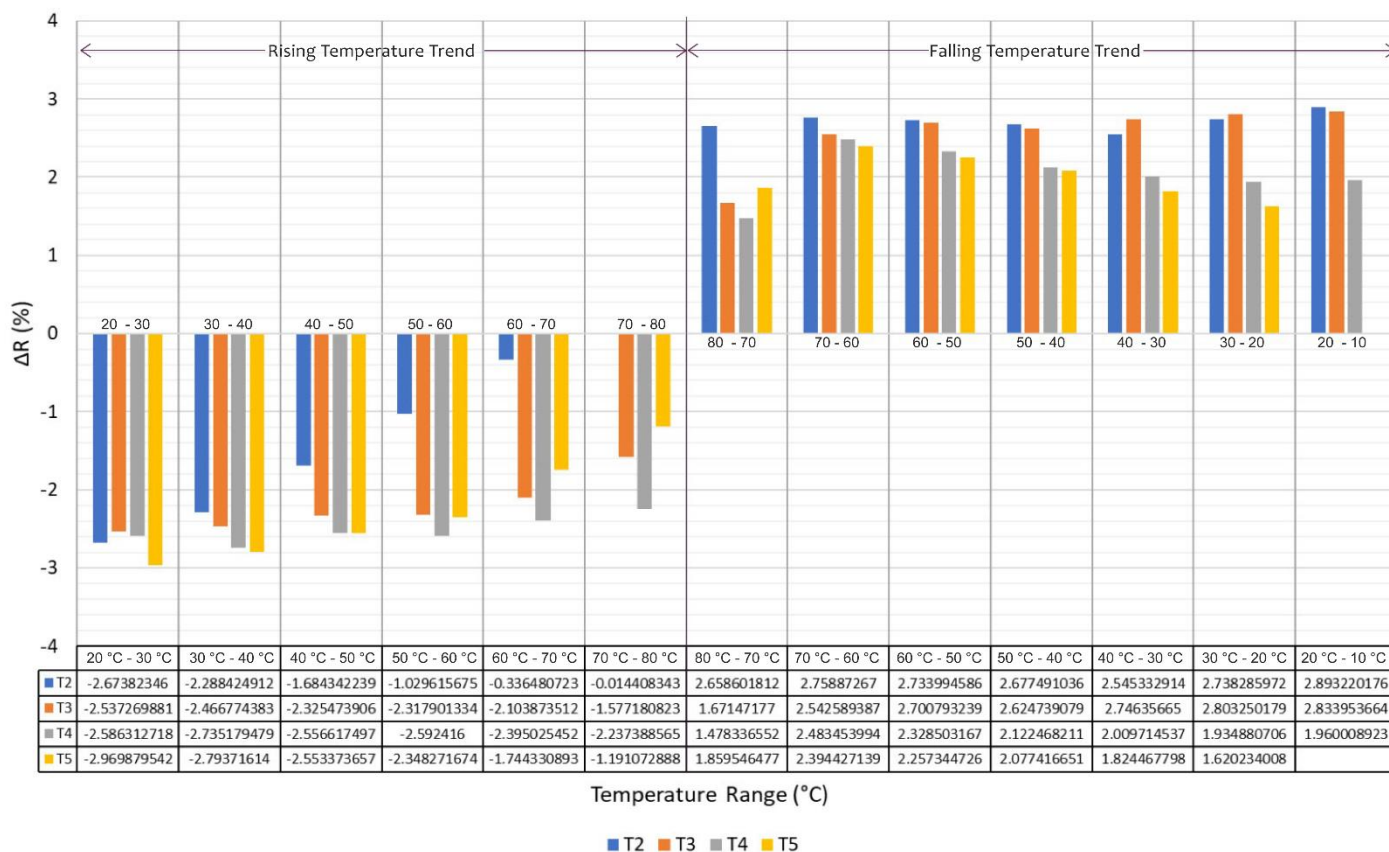


Figure 8. Graph depicting the average relative percent change of the resistance for the material SWCNT-COOH, with temperature change.

Table 7. Average relative percent change values for the material MWCNT.

Average %Δ Values for MWCNT Material.										
Climatic Chamber temperature profile period, T	T1		T2		T3		T4		T5	
Relative time of measurement (min)	21 - 160	161 - 300	301 - 440	441 - 580	581 - 720	721 - 860	861 - 1000	1001 - 1140	1141 - 1280	1281 - 1420
Chamber temperature profile trend	Rise	Fall	Rise	Fall	Rise	Fall	Rise	Fall	Rise	Fall
%Δ in R between 20°C and 30°C			-1.22		-0.92		-0.98		-1.03	
%Δ in R between 30°C and 40°C			-1.25		-1.09		-1.12		-1.15	
%Δ in R between 40°C and 50°C			-1.09		-1.17		-1.18		-1.25	
%Δ in R between 50°C and 60°C			-0.98		-1.21		-1.15		-1.26	
%Δ in R between 60°C and 70°C			-0.92		-1.17		-1.17		-1.08	
%Δ in R between 70°C and 80°C			-1.45		-1.53		-1.49		-1.25	
%Δ in R between 80°C and 70°C				-0.54		-0.53		-0.50		-0.16
%Δ in R between 70°C and 60°C				0.76		0.82		0.83		0.85
%Δ in R between 60°C and 50°C				1.08		1.07		1.01		1.00
%Δ in R between 50°C and 40°C				1.13		1.15		1.08		1.04
%Δ in R between 40°C and 30°C				1.09		1.21		1.09		1.09
%Δ in R between 30°C and 20°C				1.22		1.26		1.01		1.03
%Δ in R between 20°C and 10°C				1.30		1.26		1.12		

Relative Change of Resistance with Respect to Change in Temperature.
Material: MWCNT

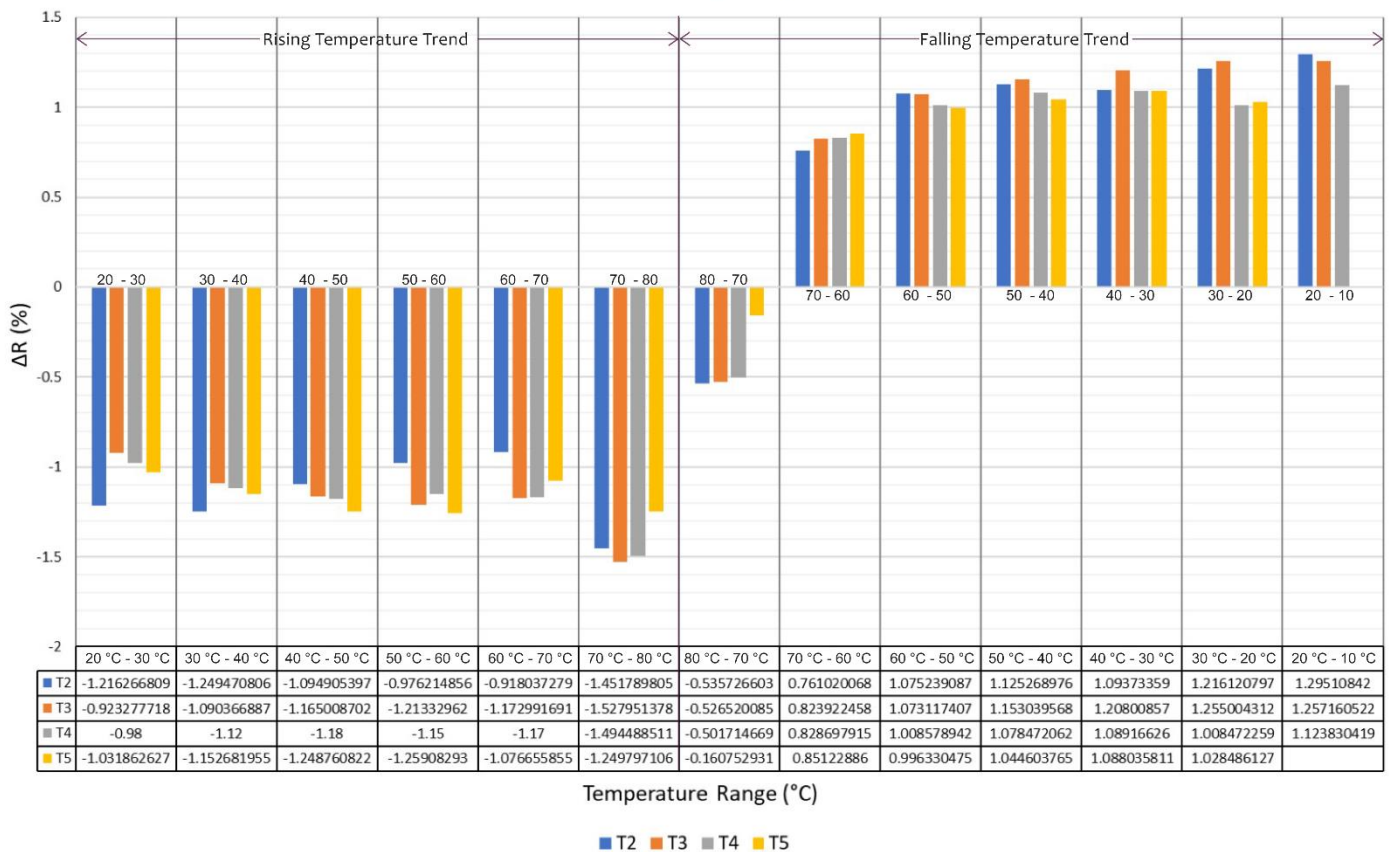


Figure 9. Graph depicting the average relative percent change of the resistance for the material MWCNT.

Discussion

From the graphs in the index, figure i. to xx., it can be seen that the resistance of all the CNT carbon materials used show increasing trends with reduction in temperature and show decreasing trends with rising temperature. It was also observed that sensor substrates deposited with the same material all registered different resistance values when measured at the same temperature points. This was mainly due to the fact that it was impractical to deposit, onto any two substrates a thin film of equal thickness. It is mainly because of this reason that the method of relative percent change in the resistance values for the materials under test was selected. This method also serves well as a metric upon which temperature dependence comparisons can be made among different materials.

By comparing the graphs in figures 6-9 it can be observed that MWCNT-COOH showed the greatest temperature sensitivity to temperature change among the materials measured. It displayed a maximum relative sensitivity of almost as high as 9.48% for the rising temperature between 70°C and 80°C. For rising temperature trends, it displayed relative sensitivity in the range roughly of 2.5% to 4%. For falling temperature trends sensitivity was between 2% to 3%. The second most sensitive material is SWCNT recording maximum sensitivity of a about 5%. For rising temperature trends sensitivities were mostly between 1% and 4%, whereas for rising trends sensitivity was between 1.5% and 5.1%. SWCNT displayed roughly between 1% and 3% for rising and falling temperature trends. The lowest relative sensitivity was displayed by MWCNT. The maximum sensitivity recorded was 1.5% during a temperature rise from 70°C and 80°C.

Materials like MWCOOH with high sensitivity are suitable for use in applications like temperature sensors whereas those with low sensitivity are more suitable for use in applications such as chemical sensing where more stable temperature dependency is required.

It was observed, however, from the graphs of MWCNT-COOH and MWCNT that between the falling temperatures trend from 80°C to 70°C, negative relative percentage

change in resistance was recorded. This behaviour may most likely be attributed to slow reaction of CNTs as a transition is made from increasing to decreasing temperature.

Conclusion

The presented work is focused on carbon nanotubes and verification of their temperature dependence. In the first part of this work, an overview of some of the properties of some CNMs are mentioned with a particular emphasis on CNTs. Some of the production methods of CNTs are outlined. Possibilities of functionalisation are also mentioned. The remarkable properties of carbon together with the ability to functionalize CNMs hold great promise for their continued use in electronics e.g., in the development of cheaper and greener energy conversion and storage technologies, such as solar technology. Sensors like gas sensors, temperature and humidity sensors, biosensors etc greatly benefiting from advancements in carbon technology. Carbon technology will most likely play a major role in the emergence of smart cities.

An overview of some deposition technologies suitable for CNMs was carried out in part two of the thesis. The methods presented all have advantages and disadvantages. The main areas of research and development in this field include the quest to improve or develop deposition techniques that are able to deposit thin layers to a high precision accuracy, are scalable and produce layers that are durable. The cost is also another factor of great concern.

Airbrush spray deposition technology was used for all depositions in the experiment part of this thesis. Using this method, it was impractical to conduct repeatable depositions of equal thickness. Nevertheless, this method is cheap and served the purpose the experiment well.

The aim of the practice part of this thesis was to verify the temperature dependence of selected carbon nanomaterials. The comparison was achieved by means of calculating the relative percent changes in the temperature dependent resistance values of the materials under test. It was established that of the given materials, MWCNT-COOH

displayed the most sensitivity to changes in temperature and that MWCNT displayed the least sensitivity.

References

- [1] P. S. Karthik, A. L. Himaja, and S. P. Singh, "Carbon-allotropes: Synthesis methods, applications and future perspectives," *Carbon Letters*, vol. 15, no. 4. pp. 219–237, 2014, doi: 10.5714/CL.2014.15.4.219.
- [2] U. Kamran, Y.-J. Heo, J. W. Lee, and S.-J. Park, "Functionalized carbon materials for electronic devices: A review," *Micromachines*, vol. 10, no. 4, 2019, doi: 10.3390/mi10040234.
- [3] S. Nasir, M. Z. M. Z. Hussein, Z. Zainal, and N. A. N. A. Yusof, "Carbon-based nanomaterials/allotropes: A glimpse of their synthesis, properties and some applications," *Materials (Basel)*, vol. 11, no. 2, p. 295, 2018, doi: 10.3390/ma11020295.
- [4] M. C. Roco, "Environmentally responsible development of nanotechnology," *Environ. Sci. Technol.*, vol. 39, no. 5, pp. 106A-112A, 2005, [Online]. Available: https://scholar.google.com/scholar?hl=en&as_sdt=2005&cites=8055011134892914671&scipsc=&q=Environmentally+responsible+development+of+nanotechnology+cite&btnG=.
- [5] S. H. Hajiabadi, H. Aghaei, M. Kalateh-Aghamohammadi, and M. Shorgasthi, "An overview on the significance of carbon-based nanomaterials in upstream oil and gas industry," *Journal of Petroleum Science and Engineering*, vol. 186. Elsevier B.V., p. 106783, Mar. 01, 2020, doi: 10.1016/j.petrol.2019.106783.
- [6] Y. Yang, X. Yang, Y. Yang, and Q. Yuan, "Aptamer-functionalized carbon nanomaterials electrochemical sensors for detecting cancer relevant biomolecules," *Carbon*, vol. 129. Elsevier Ltd, pp. 380–395, Apr. 01, 2018, doi: 10.1016/j.carbon.2017.12.013.
- [7] L. Dai, "Chapter 1 - From conventional technology to carbon nanotechnology: The fourth industrial revolution and the discoveries of C60, carbon nanotube and nanodiamond," L. B. T.-C. N. Dai, Ed. Amsterdam: Elsevier, 2006, pp. 3–11.

- [8] S. Hanna Varghese *et al.*, “Sensors based on carbon nanotubes and their applications: a review,” *Curr. Nanosci.*, vol. 6, no. 4, pp. 331–346, 2010.
- [9] “Richard P. Feynman - Biographical.” <https://www.nobelprize.org/prizes/physics/1965/feynman/biographical/> (accessed May 09, 2021).
- [10] J. E. Hulla, S. C. Sahu, and A. W. Hayes, “Nanotechnology: History and future,” *Hum. Exp. Toxicol.*, vol. 34, no. 12, pp. 1318–1321, Nov. 2015, doi: 10.1177/0960327115603588.
- [11] R. G. R. G. Mendes *et al.*, “Carbon nanostructures as a multi-functional platform for sensing applications,” *Chemosensors*, vol. 6, no. 4, 2018, doi: 10.3390/chemosensors6040060.
- [12] T. E. Saraswati, U. H. Setiawan, M. R. Ihsan, I. Isnaeni, and Y. Herbani, “The Study of the Optical Properties of C60 Fullerene in Different Organic Solvents,” *Open Chem.*, vol. 17, no. 1, pp. 1198–1212, 2019.
- [13] H. W. Kroto, J. R. Heath, S. C. O’Brien, R. F. Curl, and R. E. Smalley, “C60: Buckminsterfullerene,” *Nature*, vol. 318, no. 6042, pp. 162–163, 1985, doi: 10.1038/318162a0.
- [14] S. Iijima, “Helical microtubules of graphitic carbon,” *Nature*, vol. 354, no. 6348, pp. 56–58, 1991.
- [15] V. D. N. Bezzon *et al.*, “Carbon Nanostructure-based Sensors: A Brief Review on Recent Advances,” *Adv. Mater. Sci. Eng.*, vol. 2019, 2019, doi: 10.1155/2019/4293073.
- [16] K. S. Novoselov *et al.*, “Electric field effect in atomically thin carbon films,” *Science (80-.)*, vol. 306, no. 5696, pp. 666–669, 2004.
- [17] J. Sengupta, “Carbon nanotube fabrication at industrial scale: Opportunities and

- challenges,” *Handb. Nanomater. Ind. Appl.*, pp. 172–194, 2018.
- [18] E. H. L. Falcao and F. Wudl, “Carbon allotropes: beyond graphite and diamond,” *J. Chem. Technol. Biotechnol. Int. Res. Process. Environ. Clean Technol.*, vol. 82, no. 6, pp. 524–531, 2007.
- [19] A. Streitwieser, C. H. Heathcock, E. M. Kosower, and P. J. Corfield, *Introduction to organic chemistry*, no. 547 STR. Macmillan New York, 1992.
- [20] A. Hirsch, “The era of carbon allotropes,” *Nat. Mater.*, vol. 9, no. 11, pp. 868–871, 2010.
- [21] F. R. Baptista, S. A. Belhout, S. Giordani, and S. J. Quinn, “Recent developments in carbon nanomaterial sensors,” *Chem. Soc. Rev.*, vol. 44, no. 13, pp. 4433–4453, 2015.
- [22] E. A. Belenkov and V. A. Greshnyakov, “Classification schemes for carbon phases and nanostructures,” *New Carbon Mater.*, vol. 28, no. 4, pp. 273–282, 2013, doi: [https://doi.org/10.1016/S1872-5805\(13\)60081-5](https://doi.org/10.1016/S1872-5805(13)60081-5).
- [23] Y. Chen, Y. Xie, X. Yan, M. L. Cohen, and S. Zhang, “Topological carbon materials: A new perspective,” *Physics Reports*, vol. 868. Elsevier B.V., pp. 1–32, Jul. 03, 2020, doi: [10.1016/j.physrep.2020.05.003](https://doi.org/10.1016/j.physrep.2020.05.003).
- [24] Q. Zhang, J. Huang, W. Qian, Y. Zhang, and F. Wei, “The road for nanomaterials industry: A review of carbon nanotube production, post-treatment, and bulk applications for composites and energy storage,” *Small*, vol. 9, no. 8, pp. 1237–1265, 2013.
- [25] H. Hwang, J. Jeong, Y. Kim, and M. Chang, “Carbon Nanomaterials as Versatile Platforms for Biosensing Applications,” *Micromachines*, vol. 11, p. 814, Aug. 2020, doi: [10.3390/mi11090814](https://doi.org/10.3390/mi11090814).
- [26] V. Georgakilas, J. Perman, J. Tucek, and R. Zboril, “Broad Family of Carbon

- Nanoallotropes: Classification, Chemistry, and Applications of Fullerenes, Carbon Dots, Nanotubes, Graphene, Nanodiamonds, and Combined Superstructures,” *Chem. Rev.*, vol. 115, May 2015, doi: 10.1021/cr500304f.
- [27] F. Xie, M. Yang, M. Jiang, X. J. Huang, W. Q. Liu, and P. H. Xie, “Carbon-based nanomaterials – A promising electrochemical sensor toward persistent toxic substance,” *TrAC - Trends Anal. Chem.*, vol. 119, p. 115624, 2019, doi: 10.1016/j.trac.2019.115624.
- [28] C. S. Jon, L. Y. Meng, and D. Li, “Recent review on carbon nanomaterials functionalized with ionic liquids in sample pretreatment application,” *TrAC - Trends in Analytical Chemistry*, vol. 120. Elsevier B.V., p. 115641, Nov. 01, 2019, doi: 10.1016/j.trac.2019.115641.
- [29] N. Malik, T. Arfin, and A. U. Khan, “Graphene nanomaterials: Chemistry and pharmaceutical perspectives,” in *Nanomaterials for Drug Delivery and Therapy*, Elsevier, 2019, pp. 373–402.
- [30] E. Osawa, “Superaromaticity,” *Kagaku*, vol. 25, pp. 854–863, 1970.
- [31] A. A. Taherpour and F. Mousavi, “Carbon nanomaterials for electroanalysis in pharmaceutical applications,” in *Fullerenes, Graphenes and Nanotubes: A Pharmaceutical Approach*, Elsevier, 2018, pp. 169–225.
- [32] L. Becker, J. L. Bada, R. E. Winans, J. E. Hunt, T. E. Bunch, and B. M. French, “Fullerenes in the 1.85-billion-year-old Sudbury impact structure,” *Science (80-.)*, vol. 265, no. 5172, pp. 642–645, 1994.
- [33] S. Pizzarello *et al.*, “The organic content of the Tagish Lake meteorite,” *Science (80-.)*, vol. 293, no. 5538, pp. 2236–2239, 2001.
- [34] W. Zhenxia *et al.*, “Fullerenes in the fossil of dinosaur egg,” *Fuller. Sci. Technol.*, vol. 6, no. 4, pp. 715–720, 1998.

- [35] D. Heymann, L. P. F. Chibante, R. R. Brooks, W. S. Wolbach, and R. E. Smalley, "Fullerenes in the Cretaceous-Tertiary boundary layer," *Science* (80-.), vol. 265, no. 5172, pp. 645–647, 1994.
- [36] P. R. Buseck, "Geological fullerenes: Review and analysis," *Earth Planet. Sci. Lett.*, vol. 203, no. 3–4, pp. 781–792, Nov. 2002, doi: 10.1016/S0012-821X(02)00819-1.
- [37] D. Felder-Flesch, "(Endo) Fullerenes: From Production to Isolation," in *Fullerenes*, 2011, pp. 3–11.
- [38] W. Krätschmer, L. D. Lamb, K. Fostiropoulos, and D. R. Huffman, "Solid C 60: a new form of carbon," *Nature*, vol. 347, no. 6291, pp. 354–358, 1990.
- [39] R. E. Haufler *et al.*, "Efficient production of C60 (buckminsterfullerene), C60H36, and the solvated buckide ion," *J. Phys. Chem.*, vol. 94, no. 24, pp. 8634–8636, Nov. 1990, doi: 10.1021/j100387a005.
- [40] A. Nimibofa, E. A. Newton, A. Y. Cyprain, and W. Donbebe, "Fullerenes: synthesis and applications," *J Mater Sci*, vol. 7, pp. 22–33, 2018.
- [41] D. Jariwala, V. K. Sangwan, L. J. Lauhon, T. J. Marks, and M. C. Hersam, "Carbon nanomaterials for electronics, optoelectronics, photovoltaics, and sensing," *Chem. Soc. Rev.*, vol. 42, no. 7, pp. 2824–2860, 2013, doi: 10.1039/c2cs35335k.
- [42] M. Mojica, J. A. Alonso, and F. Méndez, "Synthesis of fullerenes," *J. Phys. Org. Chem.*, vol. 26, no. 7, pp. 526–539, 2013.
- [43] R. S. Ruoff and A. L. Ruoff, "The bulk modulus of C60 molecules and crystals: a molecular mechanics approach," *Appl. Phys. Lett.*, vol. 59, no. 13, pp. 1553–1555, 1991.
- [44] E. Castro, A. H. Garcia, G. Zavala, and L. Echevoyen, "Fullerenes in biology and medicine," *J. Mater. Chem. B*, vol. 5, no. 32, pp. 6523–6535, 2017.

- [45] S. Thakral and R. M. Mehta, "Fullerenes: An introduction and overview of their biological properties," *Indian J. Pharm. Sci.*, vol. 68, no. 1, p. 13, 2006, doi: 10.1002/chin.200637226.
- [46] G. T. Hermanson, "Buckyballs, Fullerenes, and Carbon Nanotubes," in *Bioconjugate Techniques*, Elsevier, 2013, pp. 741–755.
- [47] S. Afreen, K. Muthoosamy, S. Manickam, and U. Hashim, "Functionalized fullerene (C60) as a potential nanomediator in the fabrication of highly sensitive biosensors," *Biosens. Bioelectron.*, vol. 63, pp. 354–364, 2015.
- [48] N. Furuuchi, R. G. Shrestha, Y. Yamashita, T. Hirao, K. Ariga, and L. K. Shrestha, "Self-assembled fullerene crystals as excellent aromatic vapor sensors," *Sensors (Switzerland)*, vol. 19, no. 2, pp. 1–12, 2019, doi: 10.3390/s19020267.
- [49] S. Iijima and T. Ichihashi, "Single-shell carbon nanotubes of 1-nm diameter," *Nature*, vol. 363, no. 6430, pp. 603–605, 1993.
- [50] S. H. K. S. H. K. Yap, K. K. K. K. Chan, S. C. S. C. Tjin, and K. T. K.-T. Yong, "Carbon allotrope-based optical fibers for environmental and biological sensing: A review," *Sensors (Switzerland)*, vol. 20, no. 7, 2020, doi: 10.3390/s20072046.
- [51] M. J. Yee *et al.*, "Carbon nanomaterials based films for strain sensing application—A review," *Nano-Structures and Nano-Objects*, vol. 18. Elsevier B.V., p. 100312, Apr. 01, 2019, doi: 10.1016/j.nanoso.2019.100312.
- [52] S. Tiwari, V. Kumar, A. Huczko, R. Oraon, A. De Adhikari, and G. Nayak, "Magical Allotropes of Carbon: Prospects and Applications," *Crit. Rev. Solid State Mater. Sci.*, vol. 41, Nov. 2015, doi: 10.1080/10408436.2015.1127206.
- [53] S. Kruss, A. J. Hilmer, J. Zhang, N. F. Reuel, B. Mu, and M. S. Strano, "Carbon nanotubes as optical biomedical sensors," *Advanced Drug Delivery Reviews*, vol. 65, no. 15. Elsevier, pp. 1933–1950, Dec. 01, 2013, doi: 10.1016/j.addr.2013.07.015.

- [54] R. Kour, S. Arya, S.-J. Young, V. Gupta, P. Bandhoria, and A. Khosla, "Review—Recent Advances in Carbon Nanomaterials as Electrochemical Biosensors," *J. Electrochem. Soc.*, vol. 167, no. 3, p. 37555, 2020, doi: 10.1149/1945-7111/ab6bc4.
- [55] B. Abdallah, A. M. A. Elhissi, W. Ahmed, and M. Najlah, "Carbon nanotubes drug delivery system for cancer treatment," in *Advances in Medical and Surgical Engineering*, Elsevier, 2020, pp. 313–332.
- [56] H. Kim *et al.*, "Tensile properties of millimeter-long multi-walled carbon nanotubes," *Sci. Rep.*, vol. 7, no. 1, pp. 1–7, 2017.
- [57] X. L. Xie, Y. W. Mai, and X. P. Zhou, "Dispersion and alignment of carbon nanotubes in polymer matrix: A review," *Materials Science and Engineering R: Reports*, vol. 49, no. 4. Elsevier Ltd, pp. 89–112, May 19, 2005, doi: 10.1016/j.mser.2005.04.002.
- [58] A. E. M. A. Mohamed and M. A. Mohamed, "Carbon nanotubes: Synthesis, characterization, and applications," in *Carbon Nanomaterials for Agri-food and Environmental Applications*, Elsevier, 2019, pp. 21–32.
- [59] J. T. W. Yeow and N. Sinha, "Carbon nanotube and fullerene sensors," in *Sensors Based on Nanostructured Materials*, Springer, 2009, pp. 11–28.
- [60] M. Azizi-Lalabadi, H. Hashemi, J. Feng, and S. M. Jafari, "Carbon nanomaterials against pathogens; the antimicrobial activity of carbon nanotubes, graphene/graphene oxide, fullerenes, and their nanocomposites," *Advances in Colloid and Interface Science*, vol. 284. Elsevier B.V., p. 102250, Oct. 01, 2020, doi: 10.1016/j.cis.2020.102250.
- [61] C. E. Baddour and C. Briens, "Carbon nanotube synthesis: a review," *Int. J. Chem. React. Eng.*, vol. 3, no. 1, 2005.
- [62] N. Rajesh Jesudoss Hynes *et al.*, "Synthesis, properties, and characterization of carbon nanotube-reinforced metal matrix composites," in *Nanocarbon and its*

- Composites: Preparation, Properties and Applications*, Elsevier, 2018, pp. 805–830.
- [63] T. Guo, P. Nikolaev, A. Thess, D. T. Colbert, and R. E. Smalley, “Catalytic growth of single-walled nanotubes by laser vaporization,” *Chem. Phys. Lett.*, vol. 243, no. 1–2, pp. 49–54, Sep. 1995, doi: 10.1016/0009-2614(95)00825-O.
- [64] H. Dai, J. H. Hafner, A. G. Rinzler, D. T. Colbert, and R. E. Smalley, “Nanotubes as nanoprobe in scanning probe microscopy,” *Nature*, vol. 384, no. 6605, pp. 147–150, 1996.
- [65] V. Choudhary, B. P. Singh, and R. B. Mathur, “Carbon nanotubes and their composites,” *Synth. Appl. Carbon Nanotub. their Compos.*, no. 9, pp. 193–222, 2013.
- [66] M. Jahanshahi and A. D. Kiadehi, “Fabrication, purification and characterization of carbon nanotubes: Arc-discharge in liquid media (ADLM),” *Synth. Appl. Carbon Nanotub. Their Compos.*, pp. 55–76, 2013.
- [67] M. José-Yacamán, M. Miki-Yoshida, L. Rendon, and J. G. Santiesteban, “Catalytic growth of carbon microtubules with fullerene structure,” *Appl. Phys. Lett.*, vol. 62, no. 6, pp. 657–659, 1993.
- [68] E. Joselevich, H. Dai, J. Liu, K. Hata, and A. H. Windle, “Carbon nanotube synthesis and organization,” *Carbon Nanotub.*, pp. 101–165, 2007.
- [69] S. Zhang, Z. Li, C. Yang, Y. Xu, and J. Zhou, “Application of image stitching method in corrosion morphology analysis,” *J. Electron. Imaging*, vol. 28, no. 1, p. 13045, 2019.
- [70] M. Patila, N. Chalmpes, E. Dounousi, H. Stamatis, and D. Gournis, “Use of functionalized carbon nanotubes for the development of robust nanobiocatalysts,” in *Methods in Enzymology*, vol. 630, Academic Press Inc., 2020, pp. 263–301.
- [71] N. Maheshwari *et al.*, “Functionalized Carbon Nanotubes for Protein, Peptide, and

- Gene Delivery,” in *Biomaterials and Bionanotechnology*, Elsevier, 2019, pp. 613–637.
- [72] S. Beg *et al.*, “Emergence in the functionalized carbon nanotubes as smart nanocarriers for drug delivery applications,” in *Fullerenes, Graphenes and Nanotubes: A Pharmaceutical Approach*, Elsevier, 2018, pp. 105–133.
- [73] J. Stulik and A. Hamacek, “Carbon Nanotubes Ammonia Sensor Printed by Aerosol Jet System.”
- [74] M. M. Velázquez, T. Alejo, D. López-Díaz, B. Martín-García, and M. D. Merchán, “Langmuir-Blodgett Methodology: A Versatile Technique to Build 2D Material Films,” in *Two-dimensional Materials - Synthesis, Characterization and Potential Applications*, InTech, 2016.
- [75] M. S. Kim, L. Ma, Z. Choudhury, S. S. Moganty, S. Wei, and L. A. Archer, “Fabricating multifunctional nanoparticle membranes by a fast layer-by-layer Langmuir–Blodgett process: Application in lithium–sulfur batteries,” *J. Mater. Chem. A*, vol. 4, no. 38, pp. 14709–14719, 2016.
- [76] E. B. Aydin, M. Aydin, and M. K. Sezginurk, “Immobilization Techniques of Nanomaterials,” in *New Developments in Nanosensors for Pharmaceutical Analysis*, Elsevier, 2019, pp. 47–78.
- [77] “Depositing Monolayers & Thin Films of Nanoparticles – nanoComposix.” <https://nanocomposix.com/pages/depositing-monolayers-and-thin-films-of-nanoparticles#target> (accessed May 16, 2021).
- [78] M. N. Norizan *et al.*, “Carbon nanotubes: functionalisation and their application in chemical sensors,” *RSC Adv.*, vol. 10, no. 71, pp. 43704–43732, 2020.
- [79] A. R. Boccaccini, J. Cho, J. A. Roether, B. J. C. Thomas, E. Jane Minay, and M. S. P. Shaffer, “Electrophoretic deposition of carbon nanotubes,” *Carbon*, vol. 44, no. 15. Pergamon, pp. 3149–3160, Dec. 01, 2006, doi: 10.1016/j.carbon.2006.06.021.

- [80] M. Atiq Ur Rehman, Q. Chen, A. Braem, M. S. P. Shaffer, and A. R. Boccaccini, "Electrophoretic deposition of carbon nanotubes: recent progress and remaining challenges," *Int. Mater. Rev.*, pp. 1–30, 2020.
- [81] A. Sarkar and D. Hah, "Electrophoretic deposition of carbon nanotubes on silicon substrates," *J. Electron. Mater.*, vol. 41, no. 11, pp. 3130–3138, 2012.
- [82] I. A. Neacșu, A. I. Nicoară, O. R. Vasile, and B. Ș. Vasile, "Inorganic micro- and nanostructured implants for tissue engineering," in *Nanobiomaterials in Hard Tissue Engineering: Applications of Nanobiomaterials*, Elsevier Inc., 2016, pp. 271–295.
- [83] K. Kakaei, M. D. Esrafil, and A. Ehsani, "Graphene and Anticorrosive Properties," in *Interface Science and Technology*, vol. 27, Elsevier B.V., 2019, pp. 303–337.
- [84] Q. Zheng, Z. Li, J. Yang, and J. K. Kim, "Graphene oxide-based transparent conductive films," *Progress in Materials Science*, vol. 64, Elsevier Ltd, pp. 200–247, Jul. 01, 2014, doi: 10.1016/j.pmatsci.2014.03.004.
- [85] D. Lončarević and Ž. Čupić, "The perspective of using nanocatalysts in the environmental requirements and energy needs of industry," in *Industrial Applications of Nanomaterials*, Elsevier, 2019, pp. 91–122.
- [86] J. R. Creighton and P. Ho, "Introduction to chemical vapor deposition (CVD)," *Chem. Vap. Depos.*, vol. 2, pp. 1–22, 2001.
- [87] L. Sun *et al.*, "Chemical vapour deposition," *Nat. Rev. Methods Prim.*, vol. 1, no. 1, pp. 1–20, 2021.
- [88] T. Wang *et al.*, "A review on graphene-based gas/vapor sensors with unique properties and potential applications," *Nano-Micro Lett.*, vol. 8, no. 2, pp. 95–119, 2016.
- [89] A. Sanginario, B. Miccoli, and D. Demarchi, "Carbon Nanotubes as an Effective Opportunity for Cancer Diagnosis and Treatment," *Biosensors*, vol. 7, no. 1, 2017,

doi: 10.3390/bios7010009.

- [90] S. T. R. Naqvi *et al.*, “Modification strategies for improving the solubility/dispersion of carbon nanotubes,” *Journal of Molecular Liquids*, vol. 297. Elsevier B.V., p. 111919, Jan. 01, 2020, doi: 10.1016/j.molliq.2019.111919.
- [91] B. Kharisov, O. Kharissova, and U. Ortiz Mendez, “Methods for Dispersion of Carbon Nanotubes in Water and Common Solvents,” *MRS Proc.*, vol. 1700, pp. 109–114, Jan. 2014, doi: 10.1557/opl.2014.605.
- [92] A. Montazeri and M. Chitsazzadeh, “Effect of sonication parameters on the mechanical properties of multi-walled carbon nanotube/epoxy composites,” *Mater. Des.*, vol. 56, pp. 500–508, Apr. 2014, doi: 10.1016/J.MATDES.2013.11.013.
- [93] L. Vaisman, H. D. Wagner, and G. Marom, “The role of surfactants in dispersion of carbon nanotubes,” *Adv. Colloid Interface Sci.*, vol. 128, pp. 37–46, 2006.
- [94] A. Mamishev, K. Sundara-Rajan, F. Yang, Y. Du, and M. Zahn, “Interdigital sensors and transducers,” *Proc. IEEE*, vol. 92, pp. 808–845, Jun. 2004, doi: 10.1109/JPROC.2004.826603.

Appendix.

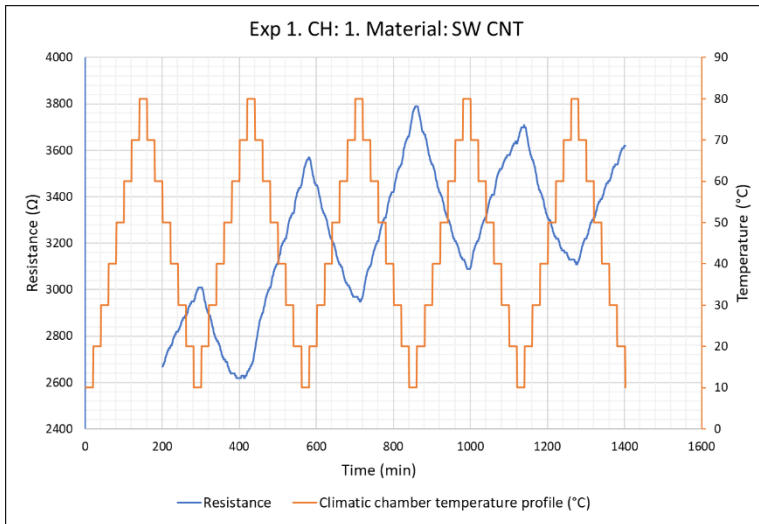


Figure i. Resistance of deposited thin film material as a function of temperature.

Measurement error Outside measurement range

Table i (a). Average R value at each temperature step.

1st measurement cycle. CH: 1. Material: SW.											
Climatic Chamber temperature profile period, T	T1		T2		T3		T4		T5		
Relative time of measurement (min)	21 - 160	161 - 300	301 - 440	441 - 580	581 - 720	721 - 860	861 - 1000	1001 - 1140	1141 - 1280	1281 - 1420	
Chamber temperature profile trend	Rise	Fall	Rise	Fall	Rise	Fall	Rise	Fall	Rise	Fall	
Average R at 80°C (Ω)			2.69E+03		2.96E+03		3.09E+03		3.12E+03		
Average R at 70°C (Ω)			2.63E+03	2.87E+03	2.98E+03	3.08E+03	3.15E+03	3.19E+03	3.14E+03	3.21E+03	
Average R at 60°C (Ω)			2.62E+03	2.99E+03	3.05E+03	3.19E+03	3.24E+03	3.29E+03	3.19E+03	3.29E+03	
Average R at 50°C (Ω)			2.66E+03	3.10E+03	3.14E+03	3.30E+03	3.34E+03	3.40E+03	3.26E+03	3.38E+03	
Average R at 40°C (Ω)			2.73E+03	3.21E+03	3.24E+03	3.41E+03	3.45E+03	3.51E+03	3.35E+03	3.46E+03	
Average R at 30°C (Ω)			2.82E+03	3.32E+03	3.36E+03	3.52E+03	3.57E+03	3.57E+03	3.46E+03	3.53E+03	
Average R at 20°C (Ω)			2.93E+03	3.43E+03	3.47E+03	3.64E+03	3.70E+03	3.63E+03	3.60E+03	3.61E+03	
Average R at 10°C (Ω)				3.55E+03		3.78E+03		3.70E+03			

Table i (b). Percent of average R value at each temperature step WRT average R value at 10°C in each T.

1st measurement cycle. CH: 1. Material: SW.											
Climatic Chamber temperature profile period, T	T1		T2		T3		T4		T5		
Relative time of measurement (min)	21 - 160	161 - 300	301 - 440	441 - 580	581 - 720	721 - 860	861 - 1000	1001 - 1140	1141 - 1280	1281 - 1420	
Chamber temperature profile trend	Rise	Fall	Rise	Fall	Rise	Fall	Rise	Fall	Rise	Fall	
% of average R at 80°C WRT R at 10°C in each T			75.85		78.29		83.62		86.49		
% of average R at 70°C WRT R at 10°C in each T			74.03	80.82	78.87	81.64	85.22	86.40	87.14	88.91	
% of average R at 60°C WRT R at 10°C in each T			73.88	84.25	80.65	84.48	87.53	89.11	88.38	91.30	
% of average R at 50°C WRT R at 10°C in each T			74.80	87.27	83.13	87.32	90.36	91.98	90.29	93.67	
% of average R at 40°C WRT R at 10°C in each T			76.80	90.29	85.87	90.30	93.39	94.89	92.89	95.86	
% of average R at 30°C WRT R at 10°C in each T			79.33	93.42	88.90	93.24	96.61	96.63	96.09	97.98	
% of average R at 20°C WRT R at 10°C in each T			82.43	96.65	91.99	96.49	100.02	98.18	99.82	100.00	
% of average R at 10°C WRT R at 10°C in each T				100.00		100.00		100.00			

Table i (c). Change in R percentage value from a given temperature step to the next temperature step.

1st measurement cycle. CH: 1. Material: SW.											
Climatic Chamber temperature profile period, T	T1		T2		T3		T4		T5		
Relative time of measurement (min)	21 - 160	161 - 300	301 - 440	441 - 580	581 - 720	721 - 860	861 - 1000	1001 - 1140	1141 - 1280	1281 - 1420	
Chamber temperature profile trend	Rise	Fall	Rise	Fall	Rise	Fall	Rise	Fall	Rise	Fall	
%Δ in R between 20°C - 30°C			-3.10		-3.08		-3.42		-3.73		
%Δ in R between 30°C - 40°C			-2.54		-3.03		-3.22		-3.20		
%Δ in R between 40°C - 50°C			-2.00		-2.74		-3.02		-2.60		
%Δ in R between 50°C - 60°C			-0.92		-2.48		-2.83		-1.92		
%Δ in R between 60°C - 70°C			0.15		-1.78		-2.31		-1.24		
%Δ in R between 70°C - 80°C			1.82		-0.58		-1.60		-0.66		
%Δ in R between 70°C - 60°C				3.43		2.84		2.70		2.40	
%Δ in R between 60°C - 50°C				3.02		2.84		2.88		2.37	
%Δ in R between 50°C - 40°C				3.02		2.98		2.90		2.19	
%Δ in R between 40°C - 30°C				3.12		2.94		1.75		2.12	
%Δ in R between 30°C - 20°C				3.23		3.25		1.55		2.02	
%Δ in R between 20°C - 10°C				3.35		3.51		1.82			

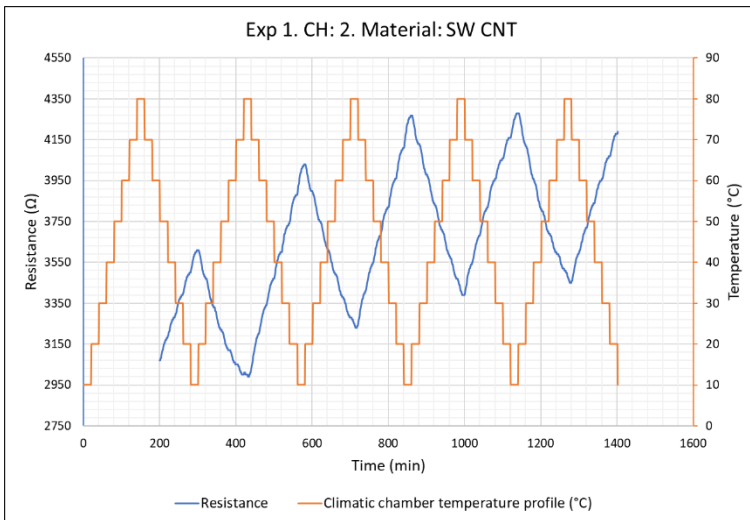


Figure ii. Resistance of deposited thin film material as a function of temperature.

Measurement error
 Outside measurement range

Table ii (a). Average R value at each temperature step.

1st measurement cycle. CH: 2. Material: SW.										
Climatic Chamber temperature profile period, T	T1		T2		T3		T4		T5	
Relative time of measurement (min)	21 - 160	161 - 300	301 - 440	441 - 580	581 - 720	721 - 860	861 - 1000	1001 - 1140	1141 - 1280	1281 - 1420
Chamber temperature profile trend	Rise	Fall	Rise	Fall	Rise	Fall	Rise	Fall	Rise	Fall
Average R at 80°C (Ω)			3.00E+03		3.24E+03		3.40E+03		3.46E+03	
Average R at 70°C (Ω)			3.01E+03	3.16E+03	3.31E+03	3.38E+03	3.50E+03	3.52E+03	3.54E+03	3.57E+03
Average R at 60°C (Ω)			3.07E+03	3.31E+03	3.41E+03	3.52E+03	3.62E+03	3.66E+03	3.63E+03	3.70E+03
Average R at 50°C (Ω)			3.15E+03	3.45E+03	3.53E+03	3.66E+03	3.75E+03	3.80E+03	3.73E+03	3.82E+03
Average R at 40°C (Ω)			3.26E+03	3.58E+03	3.66E+03	3.80E+03	3.88E+03	3.94E+03	3.86E+03	3.94E+03
Average R at 30°C (Ω)			3.38E+03	3.72E+03	3.79E+03	3.94E+03	4.02E+03	4.04E+03	4.01E+03	4.05E+03
Average R at 20°C (Ω)			3.51E+03	3.86E+03	3.93E+03	4.09E+03	4.16E+03	4.15E+03	4.17E+03	4.17E+03
Average R at 10°C (Ω)				4.01E+03		4.25E+03		4.27E+03		

Table ii (b). Percent of average R value at each temperature step WRT average R value at 10°C in each T.

1st measurement cycle. CH: 2. Material: SW.										
Climatic Chamber temperature profile period, T	T1		T2		T3		T4		T5	
Relative time of measurement (min)	21 - 160	161 - 300	301 - 440	441 - 580	581 - 720	721 - 860	861 - 1000	1001 - 1140	1141 - 1280	1281 - 1420
Chamber temperature profile trend	Rise	Fall	Rise	Fall	Rise	Fall	Rise	Fall	Rise	Fall
% of average R at 80°C WRT R at 10°C in each T			74.80		76.25		79.67		83.16	
% of average R at 70°C WRT R at 10°C in each T			75.16	78.95	77.81	79.50	82.01	82.52	85.01	85.64
% of average R at 60°C WRT R at 10°C in each T			76.64	82.67	80.27	82.86	84.83	85.81	87.04	88.70
% of average R at 50°C WRT R at 10°C in each T			78.63	86.07	83.12	86.18	87.81	89.05	89.61	91.69
% of average R at 40°C WRT R at 10°C in each T			81.27	89.41	86.07	89.47	90.98	92.26	92.58	94.52
% of average R at 30°C WRT R at 10°C in each T			84.24	92.79	89.28	92.75	94.20	94.78	96.14	97.29
% of average R at 20°C WRT R at 10°C in each T			87.62	96.39	92.42	96.28	97.53	97.29	99.98	100.00
% of average R at 10°C WRT R at 10°C in each T				100.00		100.00		100.00		

Table ii (c). Change in R percentage value from a given temperature step to the next temperature step.

1st measurement cycle. CH: 2. Material: SW.										
Climatic Chamber temperature profile period, T	T1		T2		T3		T4		T5	
Relative time of measurement (min)	21 - 160	161 - 300	301 - 440	441 - 580	581 - 720	721 - 860	861 - 1000	1001 - 1140	1141 - 1280	1281 - 1420
Chamber temperature profile trend	Rise	Fall	Rise	Fall	Rise	Fall	Rise	Fall	Rise	Fall
%Δ in R between 20°C - 30°C			-3.38		-3.15		-3.32		-3.84	
%Δ in R between 30°C - 40°C			-2.97		-3.21		-3.22		-3.56	
%Δ in R between 40°C - 50°C			-2.63		-2.95		-3.18		-2.97	
%Δ in R between 50°C - 60°C			-2.00		-2.85		-2.98		-2.57	
%Δ in R between 60°C - 70°C			-1.47		-2.46		-2.81		-2.03	
%Δ in R between 70°C - 80°C			-0.36		-1.56		-2.34		-1.85	
%Δ in R between 70°C - 60°C				3.72		3.36		3.28		3.05
%Δ in R between 60°C - 50°C				3.40		3.32		3.24		2.99
%Δ in R between 50°C - 40°C				3.33		3.30		3.22		2.84
%Δ in R between 40°C - 30°C				3.38		3.27		2.51		2.77
%Δ in R between 30°C - 20°C				3.61		3.53		2.51		2.71
%Δ in R between 20°C - 10°C				3.61		3.72		2.71		

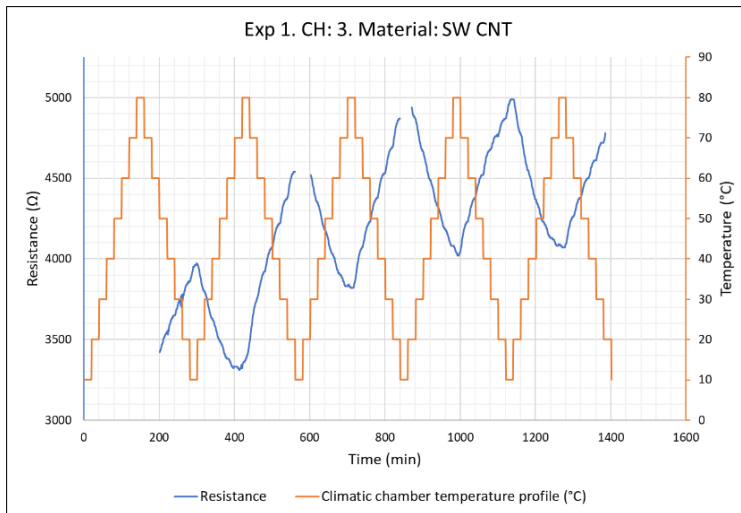


Figure iii. Resistance of deposited thin film material as a function of temperature.

Measurement error
 Outside measurement range

Table iii (a). Average R value at each temperature step.

1st measurement cycle. CH: 3. Material: SW.											
Climatic Chamber temperature profile period, T	T1		T2		T3		T4		T5		
Relative time of measurement (min)	21 - 160	161 - 300	301 - 440	441 - 580	581 - 720	721 - 860	861 - 1000	1001 - 1140	1141 - 1280	1281 - 1420	
Chamber temperature profile trend	Rise	Fall	Rise	Fall	Rise	Fall	Rise	Fall	Rise	Fall	
Average R at 80°C (Ω)			3.44E+03		3.84E+03		4.03E+03		4.08E+03		
Average R at 70°C (Ω)			3.33E+03	3.73E+03	3.83E+03	4.06E+03	4.09E+03	4.22E+03	4.09E+03	4.25E+03	
Average R at 60°C (Ω)			3.33E+03	3.91E+03	3.91E+03	4.22E+03	4.20E+03	4.37E+03	4.14E+03	4.37E+03	
Average R at 50°C (Ω)			3.39E+03	4.06E+03	4.05E+03	4.37E+03	4.34E+03	4.52E+03	4.25E+03	4.49E+03	
Average R at 40°C (Ω)			3.51E+03	4.21E+03	4.20E+03	4.53E+03	4.51E+03	4.67E+03	4.39E+03	4.61E+03	
Average R at 30°C (Ω)			3.65E+03	4.37E+03	4.37E+03	4.69E+03	4.69E+03	4.76E+03	4.58E+03	4.72E+03	
Average R at 20°C (Ω)			3.81E+03	4.53E+03		4.86E+03	4.89E+03	4.87E+03	4.80E+03		
Average R at 10°C (Ω)							4.99E+03				

Table iii (b). Percent of average R value at each temperature step WRT average R value at 10°C in each T.

1st measurement cycle. CH: 3. Material: SW.											
Climatic Chamber temperature profile period, T	T1		T2		T3		T4		T5		
Relative time of measurement (min)	21 - 160	161 - 300	301 - 440	441 - 580	581 - 720	721 - 860	861 - 1000	1001 - 1140	1141 - 1280	1281 - 1420	
Chamber temperature profile trend	Rise	Fall	Rise	Fall	Rise	Fall	Rise	Fall	Rise	Fall	
% of average R at 80°C WRT R at 10°C in each T							80.86				
% of average R at 70°C WRT R at 10°C in each T							81.92	84.69			
% of average R at 60°C WRT R at 10°C in each T							84.14	87.68			
% of average R at 50°C WRT R at 10°C in each T							87.08	90.52			
% of average R at 40°C WRT R at 10°C in each T							90.40	93.62			
% of average R at 30°C WRT R at 10°C in each T							94.00	95.50			
% of average R at 20°C WRT R at 10°C in each T							97.98	97.54			
% of average R at 10°C WRT R at 10°C in each T								100.00			

Table iii (c). Change in R percentage value from a given temperature step to the next

1st measurement cycle. CH: 3. Material: SW.											
Climatic Chamber temperature profile period, T	T1		T2		T3		T4		T5		
Relative time of measurement (min)	21 - 160	161 - 300	301 - 440	441 - 580	581 - 720	721 - 860	861 - 1000	1001 - 1140	1141 - 1280	1281 - 1420	
Chamber temperature profile trend	Rise	Fall	Rise	Fall	Rise	Fall	Rise	Fall	Rise	Fall	
%Δ in R between 20°C - 30°C							-3.97				
%Δ in R between 30°C - 40°C							-3.61				
%Δ in R between 40°C - 50°C							-3.32				
%Δ in R between 50°C - 60°C							-2.93				
%Δ in R between 60°C - 70°C							-2.22				
%Δ in R between 70°C - 80°C							-1.06				
%Δ in R between 70°C - 60°C								2.99			
%Δ in R between 60°C - 50°C								2.84			
%Δ in R between 50°C - 40°C								3.10			
%Δ in R between 40°C - 30°C								1.88			
%Δ in R between 30°C - 20°C								2.04			
%Δ in R between 20°C - 10°C								2.46			

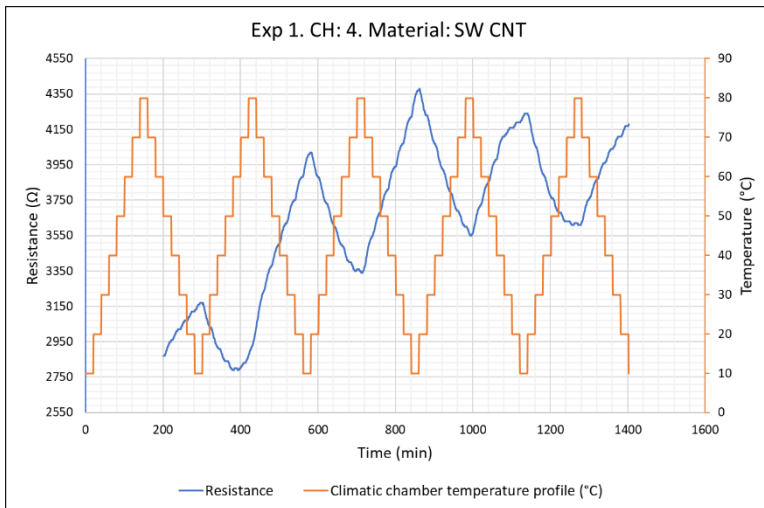


Figure iv. Resistance of deposited thin film material as a function of temperature.

Measurement error
 Outside measurement range

Table iv (a). Average R value at each temperature step.

First measurement cycle. CH: 4. Material: SW.										
Climatic Chamber temperature profile period, T	T1		T2		T3		T4		T5	
Relative time of measurement (min)	21 - 160	161 - 300	301 - 440	441 - 580	581 - 720	721 - 860	861 - 1000	1001 - 1140	1141 - 1280	1281 - 1420
Chamber temperature profile trend	Rise	Fall	Rise	Fall	Rise	Fall	Rise	Fall	Rise	Fall
Average R at 80°C (Ω)			2.96E+03		3.35E+03		3.56E+03		3.61E+03	
Average R at 70°C (Ω)			2.84E+03	3.20E+03	3.36E+03	3.52E+03	3.62E+03	3.70E+03	3.62E+03	3.73E+03
Average R at 60°C (Ω)			2.80E+03	3.35E+03	3.42E+03	3.66E+03	3.71E+03	3.83E+03	3.64E+03	3.84E+03
Average R at 50°C (Ω)			2.81E+03	3.48E+03	3.53E+03	3.79E+03	3.84E+03	3.96E+03	3.71E+03	3.95E+03
Average R at 40°C (Ω)			2.87E+03	3.61E+03	3.65E+03	3.92E+03	3.97E+03	4.10E+03	3.81E+03	4.03E+03
Average R at 30°C (Ω)			2.95E+03	3.73E+03	3.77E+03	4.05E+03	4.11E+03	4.15E+03	3.94E+03	4.10E+03
Average R at 20°C (Ω)			3.07E+03	3.87E+03	3.91E+03	4.20E+03	4.26E+03	4.19E+03	4.11E+03	4.16E+03
Average R at 10°C (Ω)				4.00E+03		4.35E+03		4.24E+03		

Table iv (b). Percent of average R value at each temperature step WRT average R value at 10°C in each T.

First measurement cycle. CH: 4. Material: SW.										
Climatic Chamber temperature profile period, T	T1		T2		T3		T4		T5	
Relative time of measurement (min)	21 - 160	161 - 300	301 - 440	441 - 580	581 - 720	721 - 860	861 - 1000	1001 - 1140	1141 - 1280	1281 - 1420
Chamber temperature profile trend	Rise	Fall	Rise	Fall	Rise	Fall	Rise	Fall	Rise	Fall
Average R at 80°C (Ω)			2.96E+03		3.35E+03		3.56E+03		3.61E+03	
Average R at 70°C (Ω)			2.84E+03	3.20E+03	3.36E+03	3.52E+03	3.62E+03	3.70E+03	3.62E+03	3.73E+03
Average R at 60°C (Ω)			2.80E+03	3.35E+03	3.42E+03	3.66E+03	3.71E+03	3.83E+03	3.64E+03	3.84E+03
Average R at 50°C (Ω)			2.81E+03	3.48E+03	3.53E+03	3.79E+03	3.84E+03	3.96E+03	3.71E+03	3.95E+03
Average R at 40°C (Ω)			2.87E+03	3.61E+03	3.65E+03	3.92E+03	3.97E+03	4.10E+03	3.81E+03	4.03E+03
Average R at 30°C (Ω)			2.95E+03	3.73E+03	3.77E+03	4.05E+03	4.11E+03	4.15E+03	3.94E+03	4.10E+03
Average R at 20°C (Ω)			3.07E+03	3.87E+03	3.91E+03	4.20E+03	4.26E+03	4.19E+03	4.11E+03	4.16E+03
Average R at 10°C (Ω)				4.00E+03		4.35E+03		4.24E+03		

Table iv (c). Change in R percentage value from a given temperature step to the next

1st measurement cycle. CH: 4. Material: SW.										
Climatic Chamber temperature profile period, T	T1		T2		T3		T4		T5	
Relative time of measurement (min)	21 - 160	161 - 300	301 - 440	441 - 580	581 - 720	721 - 860	861 - 1000	1001 - 1140	1141 - 1280	1281 - 1420
Chamber temperature profile trend	Rise	Fall	Rise	Fall	Rise	Fall	Rise	Fall	Rise	Fall
%Δ in R between 20°C - 30°C			-2.93		-3.24		-3.50		-4.02	
%Δ in R between 30°C - 40°C			-2.16		-2.94		-3.43		-3.17	
%Δ in R between 40°C - 50°C			-1.48		-2.69		-3.13		-2.42	
%Δ in R between 50°C - 60°C			-0.30		-2.38		-2.85		-1.64	
%Δ in R between 60°C - 70°C			1.14		-1.55		-2.28		-0.65	
%Δ in R between 70°C - 80°C			3.05		-0.21		-1.46		-0.09	
%Δ in R between 70°C - 60°C				3.93		3.17		3.11		2.66
%Δ in R between 60°C - 50°C				3.25		3.09		3.07		2.42
%Δ in R between 50°C - 40°C				3.09		3.09		3.20		2.05
%Δ in R between 40°C - 30°C				3.18		2.97		1.37		1.75
%Δ in R between 30°C - 20°C				3.32		3.36		0.82		1.46
%Δ in R between 20°C - 10°C				3.30		3.53		1.12		

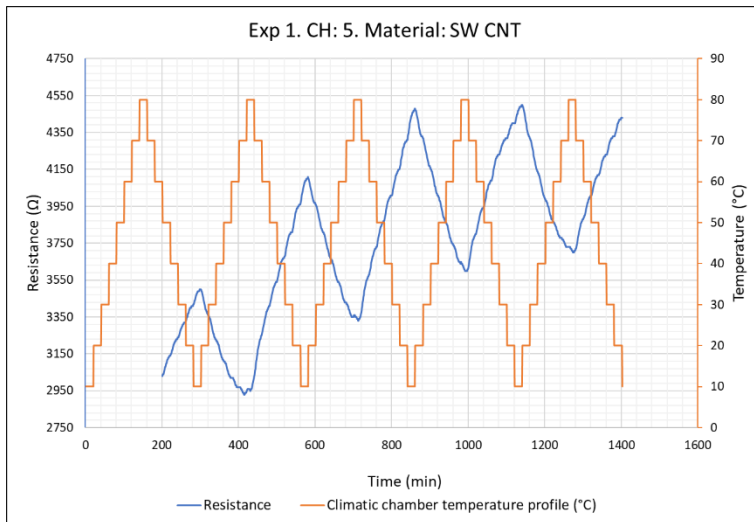


Figure v. Resistance of deposited thin film material as a function of temperature.

Measurement error
 Outside measurement range

Table v (a). Average R value at each temperature step.

First measurement cycle. CH: 5. Material: SW.										
Climatic Chamber temperature profile period, T	T1		T2		T3		T4		T5	
Relative time of measurement (min)	21 - 160	161 - 300	301 - 440	441 - 580	581 - 720	721 - 860	861 - 1000	1001 - 1140	1141 - 1280	1281 - 1420
Chamber temperature profile trend	Rise	Fall	Rise	Fall	Rise	Fall	Rise	Fall	Rise	Fall
Average R at 80°C (Ω)			2.97E+03		3.34E+03		3.60E+03		3.71E+03	
Average R at 70°C (Ω)			2.94E+03	3.21E+03	3.36E+03	3.54E+03	3.66E+03	3.78E+03	3.74E+03	3.85E+03
Average R at 60°C (Ω)			2.98E+03	3.38E+03	3.45E+03	3.70E+03	3.77E+03	3.92E+03	3.81E+03	3.98E+03
Average R at 50°C (Ω)			3.05E+03	3.52E+03	3.58E+03	3.85E+03	3.91E+03	4.07E+03	3.91E+03	4.10E+03
Average R at 40°C (Ω)			3.15E+03	3.66E+03	3.71E+03	3.99E+03	4.05E+03	4.21E+03	4.03E+03	4.21E+03
Average R at 30°C (Ω)			3.27E+03	3.80E+03	3.85E+03	4.13E+03	4.20E+03	4.31E+03	4.19E+03	4.32E+03
Average R at 20°C (Ω)			3.40E+03	3.94E+03	4.00E+03	4.29E+03	4.36E+03	4.39E+03	4.37E+03	4.41E+03
Average R at 10°C (Ω)				4.08E+03		4.45E+03		4.48E+03		

Table v (b). Percent of average R value at each temperature step WRT average R value at 10°C in each T.

1st measurement cycle. CH: 5. Material: SW.										
Climatic Chamber temperature profile period, T	T1		T2		T3		T4		T5	
Relative time of measurement (min)	21 - 160	161 - 300	301 - 440	441 - 580	581 - 720	721 - 860	861 - 1000	1001 - 1140	1141 - 1280	1281 - 1420
Chamber temperature profile trend	Rise	Fall	Rise	Fall	Rise	Fall	Rise	Fall	Rise	Fall
% of average R at 80°C WRT R at 10°C in each T			72.79		75.07		80.39		84.01	
% of average R at 70°C WRT R at 10°C in each T			71.99	78.53	75.52	79.56	81.67	84.22	84.78	87.29
% of average R at 60°C WRT R at 10°C in each T			72.99	82.77	77.54	83.17	84.16	87.53	86.26	90.28
% of average R at 50°C WRT R at 10°C in each T			74.62	86.24	80.33	86.48	87.12	90.73	88.55	93.00
% of average R at 40°C WRT R at 10°C in each T			77.13	89.58	83.30	89.73	90.37	93.98	91.41	95.49
% of average R at 30°C WRT R at 10°C in each T			80.00	93.01	86.56	92.79	93.75	96.09	94.99	97.84
% of average R at 20°C WRT R at 10°C in each T			83.23	96.55	89.77	96.32	97.22	97.99	98.97	100.00
% of average R at 10°C WRT R at 10°C in each T				100.00		100.00		100.00		

Table v (c). Change in R percentage value from a given temperature step to the next

1st measurement cycle. CH: 5. Material: SW.										
Climatic Chamber temperature profile period, T	T1		T2		T3		T4		T5	
Relative time of measurement (min)	21 - 160	161 - 300	301 - 440	441 - 580	581 - 720	721 - 860	861 - 1000	1001 - 1140	1141 - 1280	1281 - 1420
Chamber temperature profile trend	Rise	Fall	Rise	Fall	Rise	Fall	Rise	Fall	Rise	Fall
%Δ in R between 20°C - 30°C			-3.23		-3.21		-3.47		-3.98	
%Δ in R between 30°C - 40°C			-2.87		-3.27		-3.39		-3.58	
%Δ in R between 40°C - 50°C			-2.52		-2.96		-3.24		-2.86	
%Δ in R between 50°C - 60°C			-1.63		-2.80		-2.96		-2.29	
%Δ in R between 60°C - 70°C			-1.00		-2.02		-2.49		-1.48	
%Δ in R between 70°C - 80°C			0.80		-0.45		-1.28		-0.76	
%Δ in R between 70°C - 60°C				4.23		3.61		3.31		2.99
%Δ in R between 60°C - 50°C				3.47		3.31		3.20		2.72
%Δ in R between 50°C - 40°C				3.34		3.25		3.24		2.49
%Δ in R between 40°C - 30°C				3.43		3.06		2.11		2.35
%Δ in R between 30°C - 20°C				3.54		3.53		1.91		2.16
%Δ in R between 20°C - 10°C				3.45		3.68		2.01		

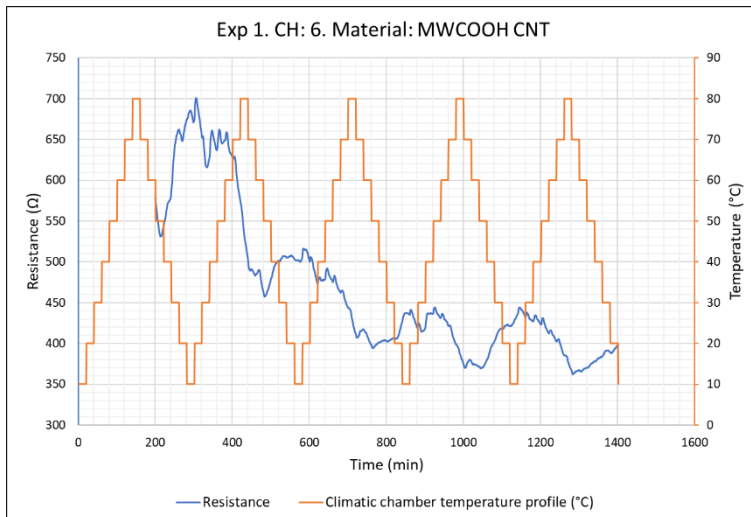


Figure vi. Resistance of deposited thin film material as a function of temperature.

Measurement error
 Outside measurement range

Table vi (a). Average R value at each temperature step.

First measurement cycle. CH: 6. Material: SW.										
Climatic Chamber temperature profile period, T	T1		T2		T3		T4		T5	
Relative time of measurement (min)	21 - 160	161 - 300	301 - 440	441 - 580	581 - 720	721 - 860	861 - 1000	1001 - 1140	1141 - 1280	1281 - 1420
Chamber temperature profile trend	Rise	Fall	Rise	Fall	Rise	Fall	Rise	Fall	Rise	Fall
Average R at 80°C (Ω)			5.23E+02		4.23E+02		3.83E+02		3.74E+02	
Average R at 70°C (Ω)			5.96E+02	4.88E+02	4.51E+02	4.15E+02	4.07E+02	3.78E+02	3.95E+02	3.66E+02
Average R at 60°C (Ω)			6.36E+02	4.79E+02	4.69E+02	4.05E+02	4.28E+02	3.73E+02	4.09E+02	3.69E+02
Average R at 50°C (Ω)			6.48E+02	4.68E+02	4.81E+02	3.98E+02	4.35E+02	3.73E+02	4.20E+02	3.76E+02
Average R at 40°C (Ω)			6.47E+02	4.98E+02	4.77E+02	4.03E+02	4.36E+02	3.97E+02	4.28E+02	3.82E+02
Average R at 30°C (Ω)			6.19E+02	5.07E+02	4.87E+02	4.05E+02	4.15E+02	4.16E+02	4.30E+02	3.91E+02
Average R at 20°C (Ω)			6.78E+02	5.07E+02	5.11E+02	4.15E+02	4.27E+02	4.22E+02	4.38E+02	3.94E+02
Average R at 10°C (Ω)				5.01E+02		4.37E+02		4.29E+02		

Table vi (b). Percent of average R value at each temperature step WRT average R value at 10°C in each T.

1st measurement cycle. CH: 6. Material: SW.										
Climatic Chamber temperature profile period, T	T1		T2		T3		T4		T5	
Relative time of measurement (min)	21 - 160	161 - 300	301 - 440	441 - 580	581 - 720	721 - 860	861 - 1000	1001 - 1140	1141 - 1280	1281 - 1420
Chamber temperature profile trend	Rise	Fall	Rise	Fall	Rise	Fall	Rise	Fall	Rise	Fall
% of average R at 80°C WRT R at 10°C in each T			104.44		96.84		89.12		95.06	
% of average R at 70°C WRT R at 10°C in each T			118.97	97.30	103.37	94.96	94.77	88.06	100.21	92.84
% of average R at 60°C WRT R at 10°C in each T			126.85	95.57	107.33	92.63	99.64	86.87	103.81	93.61
% of average R at 50°C WRT R at 10°C in each T			129.26	93.43	110.24	91.24	101.38	86.98	106.56	95.36
% of average R at 40°C WRT R at 10°C in each T			129.04	99.38	109.33	92.36	101.63	92.44	108.70	97.07
% of average R at 30°C WRT R at 10°C in each T			123.58	101.07	111.45	92.78	96.76	96.97	109.07	99.24
% of average R at 20°C WRT R at 10°C in each T			135.21	101.11	117.01	94.92	99.47	98.31	111.33	100.00
% of average R at 10°C WRT R at 10°C in each T				100.00		100.00		100.00		

Table vi (c). Change in R percentage value from a given temperature step to the next

1st measurement cycle. CH: 6. Material: SW.										
Climatic Chamber temperature profile period, T	T1		T2		T3		T4		T5	
Relative time of measurement (min)	21 - 160	161 - 300	301 - 440	441 - 580	581 - 720	721 - 860	861 - 1000	1001 - 1140	1141 - 1280	1281 - 1420
Chamber temperature profile trend	Rise	Fall	Rise	Fall	Rise	Fall	Rise	Fall	Rise	Fall
%Δ in R between 20°C - 30°C			-11.63		-5.56		-2.71		-2.26	
%Δ in R between 30°C - 40°C			5.46		-2.12		4.87		-0.37	
%Δ in R between 40°C - 50°C			0.22		0.92		-0.25		-2.15	
%Δ in R between 50°C - 60°C			-2.41		-2.91		-1.74		-2.75	
%Δ in R between 60°C - 70°C			-7.87		-3.96		-4.87		-3.60	
%Δ in R between 70°C - 80°C			-14.53		-6.54		-5.65		-5.15	
%Δ in R between 70°C - 60°C				-1.72		-2.33		-1.19		0.76
%Δ in R between 60°C - 50°C				-2.14		-1.39		0.11		1.75
%Δ in R between 50°C - 40°C				5.95		1.12		5.46		1.71
%Δ in R between 40°C - 30°C				1.69		0.42		4.53		2.17
%Δ in R between 30°C - 20°C				0.04		2.14		1.33		0.76
%Δ in R between 20°C - 10°C				-1.11		5.08		1.69		

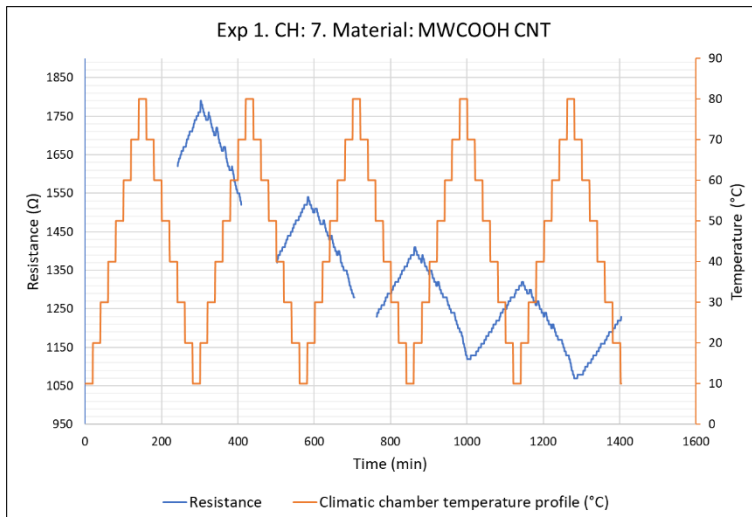


Figure vii. Resistance of deposited thin film material as a function of temperature.

Measurement error
 Outside measurement range

Table vii (a). Average R value at each temperature step.

First measurement cycle. CH: 7. Material: .										
Climatic Chamber temperature profile period, T	T1		T2		T3		T4		T5	
Relative time of measurement (min)	21 - 160	161 - 300	301 - 440	441 - 580	581 - 720	721 - 860	861 - 1000	1001 - 1140	1141 - 1280	1281 - 1420
Chamber temperature profile trend	Rise	Fall	Rise	Fall	Rise	Fall	Rise	Fall	Rise	Fall
Average R at 80°C (Ω)							1.15E+03		1.10E+03	
Average R at 70°C (Ω)			1.52E+03		1.31E+03		1.21E+03	1.13E+03	1.15E+03	1.08E+03
Average R at 60°C (Ω)			1.57E+03		1.36E+03		1.25E+03	1.15E+03	1.18E+03	1.10E+03
Average R at 50°C (Ω)			1.63E+03		1.41E+03	1.25E+03	1.29E+03	1.18E+03	1.22E+03	1.13E+03
Average R at 40°C (Ω)			1.68E+03	1.40E+03	1.45E+03	1.29E+03	1.32E+03	1.21E+03	1.25E+03	1.16E+03
Average R at 30°C (Ω)			1.72E+03	1.44E+03	1.48E+03	1.32E+03	1.36E+03	1.25E+03	1.27E+03	1.19E+03
Average R at 20°C (Ω)			1.75E+03	1.48E+03	1.51E+03	1.35E+03	1.38E+03	1.28E+03	1.30E+03	1.22E+03
Average R at 10°C (Ω)				1.52E+03		1.39E+03		1.30E+03		

Table vii (b). Percent of average R value at each temperature step WRT average R value at 10°C in each T.

1st measurement cycle. CH: 7. Material: SW.										
Climatic Chamber temperature profile period, T	T1		T2		T3		T4		T5	
Relative time of measurement (min)	21 - 160	161 - 300	301 - 440	441 - 580	581 - 720	721 - 860	861 - 1000	1001 - 1140	1141 - 1280	1281 - 1420
Chamber temperature profile trend	Rise	Fall	Rise	Fall	Rise	Fall	Rise	Fall	Rise	Fall
% of average R at 80°C WRT R at 10°C in each T							88.01		90.13	
% of average R at 70°C WRT R at 10°C in each T			100.30		94.56	0.00	92.89	86.61	94.39	88.86
% of average R at 60°C WRT R at 10°C in each T			103.78		98.23	0.00	96.16	88.35	97.31	90.80
% of average R at 50°C WRT R at 10°C in each T			107.32		101.44	90.43	98.95	90.66	100.00	92.97
% of average R at 40°C WRT R at 10°C in each T			110.68	92.44	104.33	92.85	101.60	93.10	102.54	95.36
% of average R at 30°C WRT R at 10°C in each T			113.32	94.96	106.82	95.02	104.04	95.54	104.86	97.76
% of average R at 20°C WRT R at 10°C in each T			115.60	97.48	108.98	97.57	106.21	97.84	106.96	100.00
% of average R at 10°C WRT R at 10°C in each T				100.00		100.00		100.00		

Table vii (c). Change in R percentage value from a given temperature step to the next

1st measurement cycle. CH: 7. Material: SW.										
Climatic Chamber temperature profile period, T	T1		T2		T3		T4		T5	
Relative time of measurement (min)	21 - 160	161 - 300	301 - 440	441 - 580	581 - 720	721 - 860	861 - 1000	1001 - 1140	1141 - 1280	1281 - 1420
Chamber temperature profile trend	Rise	Fall	Rise	Fall	Rise	Fall	Rise	Fall	Rise	Fall
%Δ in R between 20°C - 30°C			-2.28		-2.16		-2.16		-2.09	
%Δ in R between 30°C - 40°C			-2.64		-2.49		-2.44		-2.32	
%Δ in R between 40°C - 50°C			-3.36		-2.89		-2.65		-2.54	
%Δ in R between 50°C - 60°C			-3.54		-3.21		-2.79		-2.69	
%Δ in R between 60°C - 70°C			-3.48		-3.67		-3.28		-2.92	
%Δ in R between 70°C - 80°C			-100.30		-94.56		-4.88		-4.26	
%Δ in R between 70°C - 60°C				0.00		0.00		1.74		1.94
%Δ in R between 60°C - 50°C				0.00		90.43		2.30		2.17
%Δ in R between 50°C - 40°C				92.44		2.43		2.44		2.39
%Δ in R between 40°C - 30°C				2.52		2.16		2.44		2.39
%Δ in R between 30°C - 20°C				2.52		2.56		2.30		2.24
%Δ in R between 20°C - 10°C				2.52		2.43		2.16		

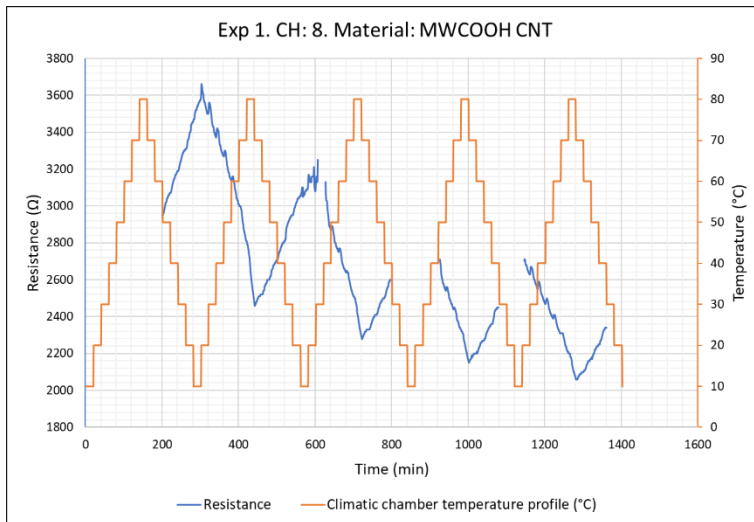


Figure viii. Resistance of deposited thin film material as a function of temperature.

Measurement error
 Outside measurement range

Table viii (a). Average R value at each temperature step.

First measurement cycle. CH: 8. Material: .										
Climatic Chamber temperature profile period, T	T1		T2		T3		T4		T5	
Relative time of measurement (min)	21 - 160	161 - 300	301 - 440	441 - 580	581 - 720	721 - 860	861 - 1000	1001 - 1140	1141 - 1280	1281 - 1420
Chamber temperature profile trend	Rise	Fall	Rise	Fall	Rise	Fall	Rise	Fall	Rise	Fall
Average R at 80°C (Ω)			2.60E+03		2.37E+03		2.22E+03		2.12E+03	
Average R at 70°C (Ω)			2.88E+03	2.51E+03	2.55E+03	2.32E+03	2.37E+03	2.19E+03	2.25E+03	2.09E+03
Average R at 60°C (Ω)			3.06E+03	2.59E+03	2.67E+03	2.40E+03	2.48E+03	2.26E+03	2.34E+03	2.16E+03
Average R at 50°C (Ω)			3.19E+03	2.69E+03	2.79E+03	2.49E+03	2.59E+03	2.34E+03	2.43E+03	2.23E+03
Average R at 40°C (Ω)			3.31E+03	2.79E+03	2.95E+03	2.59E+03		2.44E+03	2.51E+03	2.32E+03
Average R at 30°C (Ω)			3.43E+03	2.93E+03					2.59E+03	
Average R at 20°C (Ω)			3.54E+03	3.03E+03	3.15E+03				2.66E+03	
Average R at 10°C (Ω)				3.07E+03						

Table viii (b). Percent of average R value at each temperature step WRT average R value at 10°C in each T.

1st measurement cycle. CH: 8. Material: SW.										
Climatic Chamber temperature profile period, T	T1		T2		T3		T4		T5	
Relative time of measurement (min)	21 - 160	161 - 300	301 - 440	441 - 580	581 - 720	721 - 860	861 - 1000	1001 - 1140	1141 - 1280	1281 - 1420
Chamber temperature profile trend	Rise	Fall	Rise	Fall	Rise	Fall	Rise	Fall	Rise	Fall
% of average R at 80°C WRT R at 10°C in each T			84.51							
% of average R at 70°C WRT R at 10°C in each T			93.55	81.61						
% of average R at 60°C WRT R at 10°C in each T			99.53	84.18						
% of average R at 50°C WRT R at 10°C in each T			103.61	87.34						
% of average R at 40°C WRT R at 10°C in each T			107.78	90.72						
% of average R at 30°C WRT R at 10°C in each T			111.44	95.33						
% of average R at 20°C WRT R at 10°C in each T			115.08	98.61						
% of average R at 10°C WRT R at 10°C in each T				100.00						

Table viii (c). Change in R percentage value from a given temperature step to the next

1st measurement cycle. CH: 8. Material: SW.										
Climatic Chamber temperature profile period, T	T1		T2		T3		T4		T5	
Relative time of measurement (min)	21 - 160	161 - 300	301 - 440	441 - 580	581 - 720	721 - 860	861 - 1000	1001 - 1140	1141 - 1280	1281 - 1420
Chamber temperature profile trend	Rise	Fall	Rise	Fall	Rise	Fall	Rise	Fall	Rise	Fall
%Δ in R between 20°C - 30°C			-3.64							
%Δ in R between 30°C - 40°C			-3.67							
%Δ in R between 40°C - 50°C			-4.17							
%Δ in R between 50°C - 60°C			-4.08							
%Δ in R between 60°C - 70°C			-5.97							
%Δ in R between 70°C - 80°C			-9.05							
%Δ in R between 70°C - 60°C				2.57						
%Δ in R between 60°C - 50°C				3.16						
%Δ in R between 50°C - 40°C				3.37						
%Δ in R between 40°C - 30°C				4.61						
%Δ in R between 30°C - 20°C				3.28						
%Δ in R between 20°C - 10°C				1.39						

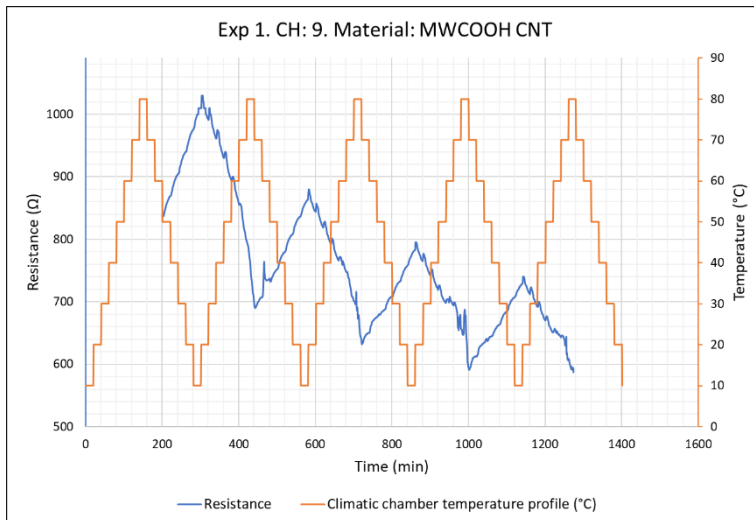


Figure ix. Resistance of deposited thin film material as a function of temperature.

Measurement error
 Outside measurement range

Table ix (a). Average R value at each temperature step.

First measurement cycle. CH: 9. Material: .										
Climatic Chamber temperature profile period, T	T1		T2		T3		T4		T5	
Relative time of measurement (min)	21 - 160	161 - 300	301 - 440	441 - 580	581 - 720	721 - 860	861 - 1000	1001 - 1140	1141 - 1280	1281 - 1420
Chamber temperature profile trend	Rise	Fall	Rise	Fall	Rise	Fall	Rise	Fall	Rise	Fall
Average R at 80°C (Ω)			7.33E+02		6.66E+02		6.50E+02		5.92E+02	
Average R at 70°C (Ω)			8.18E+02	7.03E+02	7.17E+02	6.47E+02	6.73E+02	6.10E+02	6.31E+02	
Average R at 60°C (Ω)			8.72E+02	7.35E+02	7.59E+02	6.72E+02	7.01E+02	6.30E+02	6.49E+02	
Average R at 50°C (Ω)			9.08E+02	7.47E+02	7.76E+02	6.83E+02	7.06E+02	6.41E+02	6.59E+02	
Average R at 40°C (Ω)			9.45E+02	7.75E+02	8.04E+02	7.05E+02	7.29E+02	6.59E+02	6.80E+02	
Average R at 30°C (Ω)			9.75E+02	8.03E+02	8.29E+02	7.27E+02	7.52E+02	6.80E+02	7.01E+02	
Average R at 20°C (Ω)			1.00E+03	8.31E+02	8.53E+02	7.52E+02	7.74E+02	7.03E+02	7.21E+02	
Average R at 10°C (Ω)				8.58E+02		7.77E+02		7.23E+02		

Table ix (b). Percent of average R value at each temperature step WRT average R value at 10°C in each T.

1st measurement cycle. CH: 9. Material: SW.										
Climatic Chamber temperature profile period, T	T1		T2		T3		T4		T5	
Relative time of measurement (min)	21 - 160	161 - 300	301 - 440	441 - 580	581 - 720	721 - 860	861 - 1000	1001 - 1140	1141 - 1280	1281 - 1420
Chamber temperature profile trend	Rise	Fall	Rise	Fall	Rise	Fall	Rise	Fall	Rise	Fall
% of average R at 80°C WRT R at 10°C in each T			85.48		85.73		89.89			
% of average R at 70°C WRT R at 10°C in each T			95.41	81.96	92.20	83.31	93.09	84.34		
% of average R at 60°C WRT R at 10°C in each T			101.70	85.71	97.61	86.42	96.98	87.17		
% of average R at 50°C WRT R at 10°C in each T			105.85	87.08	99.91	87.91	97.59	88.69		
% of average R at 40°C WRT R at 10°C in each T			110.19	90.31	103.44	90.70	100.85	91.10		
% of average R at 30°C WRT R at 10°C in each T			113.73	93.60	106.73	93.55	103.97	94.05		
% of average R at 20°C WRT R at 10°C in each T			116.92	96.93	109.76	96.72	106.96	97.16		
% of average R at 10°C WRT R at 10°C in each T				100.00		100.00		100.00		

Table ix (c). Change in R percentage value from a given temperature step to the next

1st measurement cycle. CH: 9. Material: SW.										
Climatic Chamber temperature profile period, T	T1		T2		T3		T4		T5	
Relative time of measurement (min)	21 - 160	161 - 300	301 - 440	441 - 580	581 - 720	721 - 860	861 - 1000	1001 - 1140	1141 - 1280	1281 - 1420
Chamber temperature profile trend	Rise	Fall	Rise	Fall	Rise	Fall	Rise	Fall	Rise	Fall
%Δ in R between 20°C - 30°C			-3.19		-3.03		-2.99			
%Δ in R between 30°C - 40°C			-3.54		-3.29		-3.12			
%Δ in R between 40°C - 50°C			-4.33		-3.53		-3.27			
%Δ in R between 50°C - 60°C			-4.15		-2.29		-0.60			
%Δ in R between 60°C - 70°C			-6.29		-5.42		-3.90			
%Δ in R between 70°C - 80°C			-9.93		-6.47		-3.19			
%Δ in R between 70°C - 60°C				3.75		3.11		2.83		
%Δ in R between 60°C - 50°C				1.37		1.49		1.52		
%Δ in R between 50°C - 40°C				3.23		2.80		2.41		
%Δ in R between 40°C - 30°C				3.29		2.85		2.95		
%Δ in R between 30°C - 20°C				3.33		3.17		3.10		
%Δ in R between 20°C - 10°C				3.07		3.28		2.84		

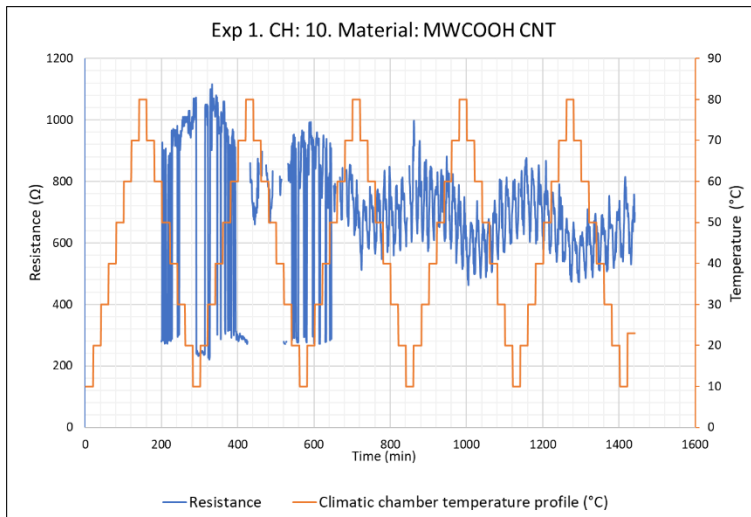


Figure x. Resistance of deposited thin film material as a function of temperature.

Measurement error
 Outside measurement range

Table x (a). Average R value at each temperature step.

First measurement cycle. CH: 10. Material: .										
Climatic Chamber temperature profile period, T	T1		T2		T3		T4		T5	
Relative time of measurement (min)	21 - 160	161 - 300	301 - 440	441 - 580	581 - 720	721 - 860	861 - 1000	1001 - 1140	1141 - 1280	1281 - 1420
Chamber temperature profile trend	Rise	Fall	Rise	Fall	Rise	Fall	Rise	Fall	Rise	Fall
Average R at 80°C (Ω)			8.02E+02		7.08E+02		6.24E+02		5.39E+02	
Average R at 70°C (Ω)			2.91E+02	7.79E+02	7.76E+02	6.99E+02	6.53E+02	6.25E+02	5.89E+02	5.38E+02
Average R at 60°C (Ω)			5.85E+02	8.20E+02	7.61E+02	6.95E+02	7.23E+02	5.74E+02	6.23E+02	5.79E+02
Average R at 50°C (Ω)			7.79E+02	7.73E+02	7.77E+02	6.64E+02	7.50E+02	5.91E+02	6.83E+02	5.93E+02
Average R at 40°C (Ω)			9.18E+02	6.71E+02	7.07E+02	6.79E+02	7.07E+02	6.79E+02	7.53E+02	6.21E+02
Average R at 30°C (Ω)			1.05E+03	8.43E+02	7.72E+02	6.74E+02	7.47E+02	6.75E+02	7.77E+02	6.37E+02
Average R at 20°C (Ω)			5.99E+02	4.74E+02	8.72E+02	7.49E+02	7.60E+02	6.62E+02	7.85E+02	6.51E+02
Average R at 10°C (Ω)				8.12E+02		7.27E+02		6.82E+02		

Table x (b). Percent of average R value at each temperature step WRT average R value at 10°C in each T.

1st measurement cycle. CH: 10. Material: SW.										
Climatic Chamber temperature profile period, T	T1		T2		T3		T4		T5	
Relative time of measurement (min)	21 - 160	161 - 300	301 - 440	441 - 580	581 - 720	721 - 860	861 - 1000	1001 - 1140	1141 - 1280	1281 - 1420
Chamber temperature profile trend	Rise	Fall	Rise	Fall	Rise	Fall	Rise	Fall	Rise	Fall
% of average R at 80°C WRT R at 10°C in each T			98.78		97.41		91.54		82.85	
% of average R at 70°C WRT R at 10°C in each T			35.79	95.99	106.79	96.16	95.79	91.62	90.45	82.67
% of average R at 60°C WRT R at 10°C in each T			72.07	100.96	104.67	95.61	106.02	84.14	95.66	88.90
% of average R at 50°C WRT R at 10°C in each T			95.96	95.26	106.85	91.40	109.97	86.70	104.90	91.15
% of average R at 40°C WRT R at 10°C in each T			113.06	82.60	97.30	93.47	103.74	99.62	115.64	95.42
% of average R at 30°C WRT R at 10°C in each T			129.11	103.88	106.26	92.71	109.62	99.02	119.43	97.92
% of average R at 20°C WRT R at 10°C in each T			73.83	58.32	119.98	102.99	111.45	97.17	120.56	100.00
% of average R at 10°C WRT R at 10°C in each T				100.00		100.00		100.00		

Table x (c). Change in R percentage value from a given temperature step to the next

1st measurement cycle. CH: 10. Material: SW.										
Climatic Chamber temperature profile period, T	T1		T2		T3		T4		T5	
Relative time of measurement (min)	21 - 160	161 - 300	301 - 440	441 - 580	581 - 720	721 - 860	861 - 1000	1001 - 1140	1141 - 1280	1281 - 1420
Chamber temperature profile trend	Rise	Fall	Rise	Fall	Rise	Fall	Rise	Fall	Rise	Fall
%Δ in R between 20°C - 30°C			55.28		-13.72		-1.83		-1.13	
%Δ in R between 30°C - 40°C			-16.06		-8.95		-5.88		-3.79	
%Δ in R between 40°C - 50°C			-17.10		9.54		6.22		-10.74	
%Δ in R between 50°C - 60°C			-23.88		-2.18		-3.95		-9.25	
%Δ in R between 60°C - 70°C			-36.29		2.12		-10.23		-5.21	
%Δ in R between 70°C - 80°C			62.99		-9.38		-4.25		-7.60	
%Δ in R between 70°C - 60°C				4.97		-0.55		-7.48		6.23
%Δ in R between 60°C - 50°C				-5.70		-4.22		2.56		2.25
%Δ in R between 50°C - 40°C				-12.66		2.08		12.92		4.27
%Δ in R between 40°C - 30°C				21.28		-0.76		-0.60		2.50
%Δ in R between 30°C - 20°C				-45.56		10.28		-1.85		2.08
%Δ in R between 20°C - 10°C				41.68		-2.99		2.83		

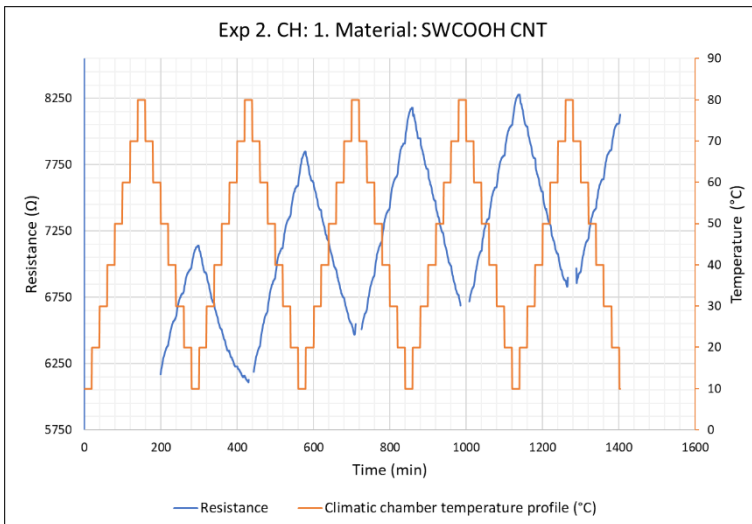


Figure xi. Resistance of deposited thin film material as a function of temperature.

Measurement error
 Outside measurement range

Table xi (a). Average R value at each temperature step.

2nd measurement cycle. CH: 1. Material: SWCOOH.										
Climatic Chamber temperature profile period, T	T1		T2		T3		T4		T5	
Relative time of measurement (min)	21 - 160	161 - 300	301 - 440	441 - 580	581 - 720	721 - 860	861 - 1000	1001 - 1140	1141 - 1280	1281 - 1420
Chamber temperature profile trend	Rise	Fall	Rise	Fall	Rise	Fall	Rise	Fall	Rise	Fall
Average R at 80°C (Ω)			6.12E+03		6.52E+03					
Average R at 70°C (Ω)			6.17E+03	6.33E+03	6.59E+03	6.61E+03	6.81E+03	6.79E+03	6.91E+03	6.91E+03
Average R at 60°C (Ω)			6.25E+03	6.60E+03	6.79E+03	6.87E+03	7.04E+03	7.06E+03	7.12E+03	7.16E+03
Average R at 50°C (Ω)			6.37E+03	6.86E+03	7.01E+03	7.14E+03	7.28E+03	7.32E+03	7.35E+03	7.40E+03
Average R at 40°C (Ω)			6.55E+03	7.10E+03	7.22E+03	7.39E+03	7.52E+03	7.56E+03	7.59E+03	7.63E+03
Average R at 30°C (Ω)			6.75E+03	7.33E+03	7.44E+03	7.64E+03	7.75E+03	7.80E+03	7.84E+03	7.84E+03
Average R at 20°C (Ω)			6.97E+03	7.57E+03	7.65E+03	7.90E+03	7.97E+03	8.03E+03	8.08E+03	8.05E+03
Average R at 10°C (Ω)				7.82E+03		8.16E+03		8.26E+03		

Table xi (b). Percent of average R value at each temperature step WRT average R value at 10°C in each T.

2nd measurement cycle. CH: 1. Material: SWCOOH.										
Climatic Chamber temperature profile period, T	T1		T2		T3		T4		T5	
Relative time of measurement (min)	21 - 160	161 - 300	301 - 440	441 - 580	581 - 720	721 - 860	861 - 1000	1001 - 1140	1141 - 1280	1281 - 1420
Chamber temperature profile trend	Rise	Fall	Rise	Fall	Rise	Fall	Rise	Fall	Rise	Fall
% of average R at 80°C WRT R at 10°C in each T			78.24		79.97		0.00		0.00	
% of average R at 70°C WRT R at 10°C in each T			78.82	80.96	80.81	81.02	82.43	82.18	85.83	85.83
% of average R at 60°C WRT R at 10°C in each T			79.85	84.36	83.20	84.26	85.17	85.48	88.46	88.89
% of average R at 50°C WRT R at 10°C in each T			81.48	87.68	85.88	87.51	88.11	88.60	91.33	91.84
% of average R at 40°C WRT R at 10°C in each T			83.73	90.76	88.54	90.62	90.98	91.54	94.28	94.70
% of average R at 30°C WRT R at 10°C in each T			86.32	93.75	91.26	93.69	93.83	94.42	97.34	97.42
% of average R at 20°C WRT R at 10°C in each T			89.04	96.79	93.81	96.82	96.50	97.16	100.29	100.00
% of average R at 10°C WRT R at 10°C in each T				100.00		100.00		100.00		

Table xi (c). Change in R percentage value from a given temperature step to the next

2nd measurement cycle. CH: 1. Material: SWCOOH.										
Climatic Chamber temperature profile period, T	T1		T2		T3		T4		T5	
Relative time of measurement (min)	21 - 160	161 - 300	301 - 440	441 - 580	581 - 720	721 - 860	861 - 1000	1001 - 1140	1141 - 1280	1281 - 1420
Chamber temperature profile trend	Rise	Fall	Rise	Fall	Rise	Fall	Rise	Fall	Rise	Fall
%Δ in R between 20°C - 30°C			-2.72		-2.55		-2.67		-2.94	
%Δ in R between 30°C - 40°C			-2.60		-2.72		-2.84		-3.07	
%Δ in R between 40°C - 50°C			-2.25		-2.66		-2.87		-2.94	
%Δ in R between 50°C - 60°C			-1.62		-2.67		-2.94		-2.87	
%Δ in R between 60°C - 70°C			-1.04		-2.39		-2.75		-2.63	
%Δ in R between 70°C - 80°C			-0.58		-0.84					
%Δ in R between 70°C - 60°C				3.40		3.24		3.29		3.06
%Δ in R between 60°C - 50°C				3.31		3.25		3.12		2.96
%Δ in R between 50°C - 40°C				3.08		3.11		2.94		2.86
%Δ in R between 40°C - 30°C				2.99		3.06		2.88		2.72
%Δ in R between 30°C - 20°C				3.04		3.13		2.74		2.58
%Δ in R between 20°C - 10°C				3.21		3.18		2.84		

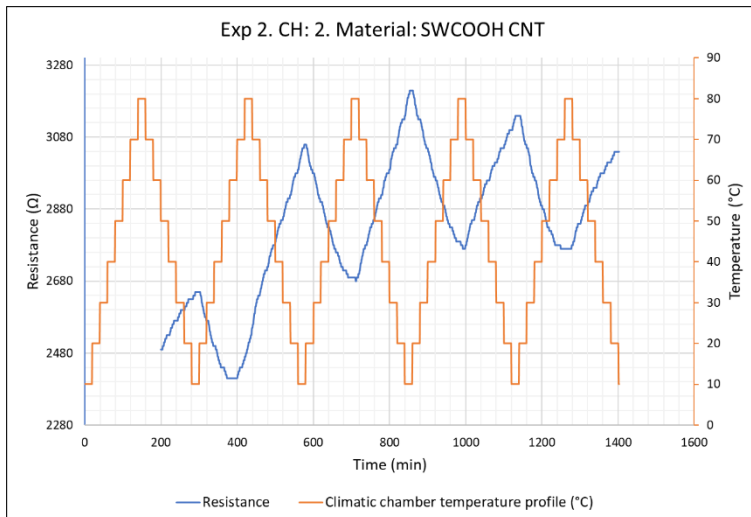


Figure xii. Resistance of deposited thin film material as a function of temperature.

Measurement error
 Outside measurement range

Table xii (a). Average R value at each temperature step.

2nd measurement cycle. CH: 2. Material: SWCOOH.										
Climatic Chamber temperature profile period, T	T1		T2		T3		T4		T5	
Relative time of measurement (min)	21 - 160	161 - 300	301 - 440	441 - 580	581 - 720	721 - 860	861 - 1000	1001 - 1140	1141 - 1280	1281 - 1420
Chamber temperature profile trend	Rise	Fall	Rise	Fall	Rise	Fall	Rise	Fall	Rise	Fall
Average R at 80°C (Ω)			2.52E+03		2.69E+03		2.77E+03		2.77E+03	
Average R at 70°C (Ω)			2.45E+03	2.63E+03	2.69E+03	2.77E+03	2.80E+03	2.84E+03	2.77E+03	2.83E+03
Average R at 60°C (Ω)			2.41E+03	2.71E+03	2.72E+03	2.84E+03	2.85E+03	2.90E+03	2.79E+03	2.89E+03
Average R at 50°C (Ω)			2.42E+03	2.77E+03	2.78E+03	2.91E+03	2.91E+03	2.95E+03	2.84E+03	2.93E+03
Average R at 40°C (Ω)			2.46E+03	2.84E+03	2.85E+03	2.98E+03	2.99E+03	3.00E+03	2.91E+03	2.98E+03
Average R at 30°C (Ω)			2.52E+03	2.91E+03	2.92E+03	3.05E+03	3.06E+03	3.05E+03	2.99E+03	3.01E+03
Average R at 20°C (Ω)			2.59E+03	2.98E+03	3.00E+03	3.13E+03	3.14E+03	3.10E+03	3.08E+03	3.04E+03
Average R at 10°C (Ω)				3.05E+03		3.21E+03		3.14E+03		

Table xii (b). Percent of average R value at each temperature step WRT average R value at 10°C in each T.

2nd measurement cycle. CH: 2. Material: SWCOOH.										
Climatic Chamber temperature profile period, T	T1		T2		T3		T4		T5	
Relative time of measurement (min)	21 - 160	161 - 300	301 - 440	441 - 580	581 - 720	721 - 860	861 - 1000	1001 - 1140	1141 - 1280	1281 - 1420
Chamber temperature profile trend	Rise	Fall	Rise	Fall	Rise	Fall	Rise	Fall	Rise	Fall
% of average R at 80°C WRT R at 10°C in each T			82.56		83.90		88.36		91.18	
% of average R at 70°C WRT R at 10°C in each T			80.20	86.20	83.99	86.40	89.14	90.44	91.15	93.22
% of average R at 60°C WRT R at 10°C in each T			78.99	88.66	84.99	88.55	90.67	92.35	91.71	94.93
% of average R at 50°C WRT R at 10°C in each T			79.15	90.92	86.74	90.73	92.80	94.07	93.42	96.51
% of average R at 40°C WRT R at 10°C in each T			80.47	93.15	88.83	92.89	95.09	95.64	95.65	97.92
% of average R at 30°C WRT R at 10°C in each T			82.50	95.25	91.11	95.16	97.58	97.10	98.29	98.98
% of average R at 20°C WRT R at 10°C in each T			84.96	97.54	93.48	97.55	100.06	98.60	101.18	100.00
% of average R at 10°C WRT R at 10°C in each T				100.00		100.00		100.00		

Table xii (c). Change in R percentage value from a given temperature step to the next

2nd measurement cycle. CH: 2. Material: SWCOOH.										
Climatic Chamber temperature profile period, T	T1		T2		T3		T4		T5	
Relative time of measurement (min)	21 - 160	161 - 300	301 - 440	441 - 580	581 - 720	721 - 860	861 - 1000	1001 - 1140	1141 - 1280	1281 - 1420
Chamber temperature profile trend	Rise	Fall	Rise	Fall	Rise	Fall	Rise	Fall	Rise	Fall
%Δ in R between 20°C - 30°C			-2.46		-2.37		-2.48		-2.90	
%Δ in R between 30°C - 40°C			-2.03		-2.28		-2.48		-2.63	
%Δ in R between 40°C - 50°C			-1.31		-2.09		-2.29		-2.24	
%Δ in R between 50°C - 60°C			-0.16		-1.75		-2.13		-1.71	
%Δ in R between 60°C - 70°C			1.21		-1.00		-1.53		-0.56	
%Δ in R between 70°C - 80°C			2.36		-0.09		-0.78		0.03	
%Δ in R between 70°C - 60°C				2.46		2.15		1.91		1.71
%Δ in R between 60°C - 50°C				2.26		2.18		1.72		1.58
%Δ in R between 50°C - 40°C				2.23		2.15		1.56		1.41
%Δ in R between 40°C - 30°C				2.10		2.28		1.47		1.05
%Δ in R between 30°C - 20°C				2.29		2.38		1.50		1.02
%Δ in R between 20°C - 10°C				2.46		2.45		1.40		

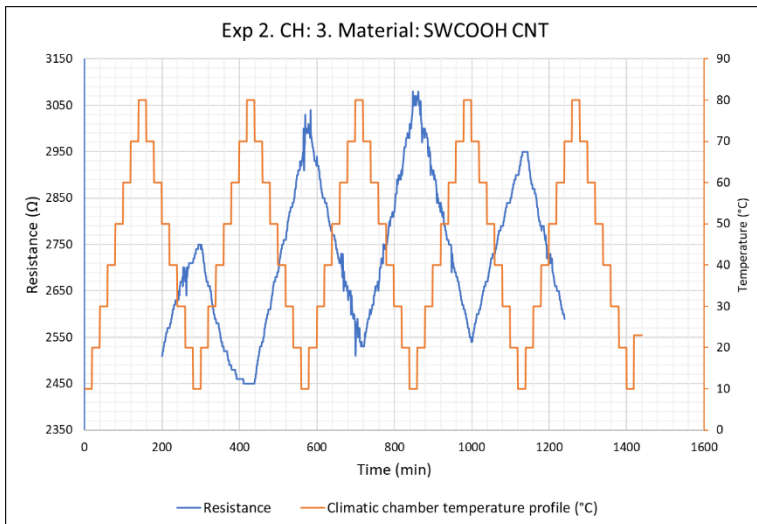


Figure xiii. Resistance of deposited thin film material as a function of temperature.

Measurement error
 Outside measurement range

Table xiii (a). Average R value at each temperature step.

2nd measurement cycle. CH: 3. Material: SWCOOH.										
Climatic Chamber temperature profile period, T	T1		T2		T3		T4		T5	
Relative time of measurement (min)	21 - 160	161 - 300	301 - 440	441 - 580	581 - 720	721 - 860	861 - 1000	1001 - 1140	1141 - 1280	1281 - 1420
Chamber temperature profile trend	Rise	Fall	Rise	Fall	Rise	Fall	Rise	Fall	Rise	Fall
Average R at 80°C (Ω)			2.45E+03		2.54E+03		2.56E+03			
Average R at 70°C (Ω)			2.45E+03	2.53E+03	2.60E+03	2.59E+03	2.63E+03	2.59E+03		
Average R at 60°C (Ω)			2.47E+03	2.60E+03	2.67E+03	2.66E+03	2.70E+03	2.66E+03	2.61E+03	
Average R at 50°C (Ω)			2.50E+03	2.68E+03	2.73E+03	2.74E+03	2.78E+03	2.72E+03	2.67E+03	
Average R at 40°C (Ω)			2.54E+03	2.75E+03	2.79E+03	2.81E+03	2.85E+03	2.78E+03	2.74E+03	
Average R at 30°C (Ω)			2.61E+03	2.83E+03	2.86E+03	2.90E+03	2.93E+03	2.84E+03	2.81E+03	
Average R at 20°C (Ω)			2.68E+03	2.91E+03	2.94E+03	2.98E+03	3.00E+03	2.89E+03	2.89E+03	
Average R at 10°C (Ω)				3.00E+03		3.06E+03		2.95E+03		

Table xiii (b). Percent of average R value at each temperature step WRT average R value at 10°C in each T.

2nd measurement cycle. CH: 3. Material: SWCOOH.										
Climatic Chamber temperature profile period, T	T1		T2		T3		T4		T5	
Relative time of measurement (min)	21 - 160	161 - 300	301 - 440	441 - 580	581 - 720	721 - 860	861 - 1000	1001 - 1140	1141 - 1280	1281 - 1420
Chamber temperature profile trend	Rise	Fall	Rise	Fall	Rise	Fall	Rise	Fall	Rise	Fall
% of average R at 80°C WRT R at 10°C in each T			81.72		83.07		86.81			
% of average R at 70°C WRT R at 10°C in each T			81.79	84.22	85.09	84.67	89.28	87.99		
% of average R at 60°C WRT R at 10°C in each T			82.22	86.76	87.12	86.89	91.72	90.23		
% of average R at 50°C WRT R at 10°C in each T			83.29	89.29	89.24	89.44	94.13	92.40		
% of average R at 40°C WRT R at 10°C in each T			84.82	91.86	91.30	91.83	96.51	94.40		
% of average R at 30°C WRT R at 10°C in each T			86.92	94.36	93.59	94.64	99.32	96.27		
% of average R at 20°C WRT R at 10°C in each T			89.49	97.07	96.14	97.39	101.63	98.17		
% of average R at 10°C WRT R at 10°C in each T				100.00		100.00		100.00		

Table xiii (c). Change in R percentage value from a given temperature step to the next

2nd measurement cycle. CH: 3. Material: SWCOOH.										
Climatic Chamber temperature profile period, T	T1		T2		T3		T4		T5	
Relative time of measurement (min)	21 - 160	161 - 300	301 - 440	441 - 580	581 - 720	721 - 860	861 - 1000	1001 - 1140	1141 - 1280	1281 - 1420
Chamber temperature profile trend	Rise	Fall	Rise	Fall	Rise	Fall	Rise	Fall	Rise	Fall
%Δ in R between 20°C - 30°C			-2.57		-2.55		-2.31			
%Δ in R between 30°C - 40°C			-2.10		-2.29		-2.82			
%Δ in R between 40°C - 50°C			-1.53		-2.06		-2.37			
%Δ in R between 50°C - 60°C			-1.07		-2.12		-2.41			
%Δ in R between 60°C - 70°C			-0.43		-2.03		-2.44			
%Δ in R between 70°C - 80°C			-0.07		-2.03		-2.47			
%Δ in R between 70°C - 60°C				2.54		2.22		2.24		
%Δ in R between 60°C - 50°C				2.54		2.55		2.17		
%Δ in R between 50°C - 40°C				2.57		2.39		2.00		
%Δ in R between 40°C - 30°C				2.50				1.87		
%Δ in R between 30°C - 20°C				2.71				1.90		
%Δ in R between 20°C - 10°C				2.93				1.83		

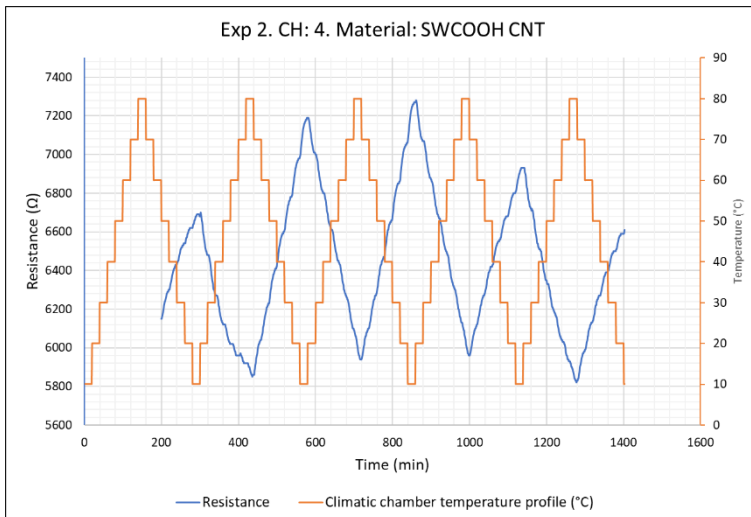


Figure xiv. Resistance of deposited thin film material as a function of temperature.

Measurement error
 Outside measurement range

Table xiv (a). Average R value at each temperature step.

2nd measurement cycle. CH: 4. Material: SWCOOH.										
Climatic Chamber temperature profile period, T	T1		T2		T3		T4		T5	
Relative time of measurement (min)	21 - 160	161 - 300	301 - 440	441 - 580	581 - 720	721 - 860	861 - 1000	1001 - 1140	1141 - 1280	1281 - 1420
Chamber temperature profile trend	Rise	Fall	Rise	Fall	Rise	Fall	Rise	Fall	Rise	Fall
Average R at 80°C (Ω)			5.87E+03		5.97E+03		6.00E+03		5.85E+03	
Average R at 70°C (Ω)			5.93E+03	6.02E+03	6.14E+03	6.08E+03	6.18E+03	6.09E+03	5.96E+03	5.96E+03
Average R at 60°C (Ω)			5.97E+03	6.20E+03	6.32E+03	6.25E+03	6.36E+03	6.25E+03	6.08E+03	6.11E+03
Average R at 50°C (Ω)			6.05E+03	6.39E+03	6.50E+03	6.45E+03	6.55E+03	6.41E+03	6.23E+03	6.25E+03
Average R at 40°C (Ω)			6.17E+03	6.58E+03	6.67E+03	6.64E+03	6.73E+03	6.54E+03	6.40E+03	6.38E+03
Average R at 30°C (Ω)			6.34E+03	6.76E+03	6.85E+03	6.84E+03	6.92E+03	6.67E+03	6.58E+03	6.49E+03
Average R at 20°C (Ω)			6.53E+03	6.96E+03	7.04E+03	7.04E+03	7.11E+03	6.79E+03	6.77E+03	6.59E+03
Average R at 10°C (Ω)				7.17E+03		7.26E+03		6.92E+03		

Table xiv (b). Percent of average R value at each temperature step WRT average R value at 10°C in each T.

2nd measurement cycle. CH: 4. Material: SWCOOH.										
Climatic Chamber temperature profile period, T	T1		T2		T3		T4		T5	
Relative time of measurement (min)	21 - 160	161 - 300	301 - 440	441 - 580	581 - 720	721 - 860	861 - 1000	1001 - 1140	1141 - 1280	1281 - 1420
Chamber temperature profile trend	Rise	Fall	Rise	Fall	Rise	Fall	Rise	Fall	Rise	Fall
% of average R at 80°C WRT R at 10°C in each T			81.89		82.21		86.64		88.76	
% of average R at 70°C WRT R at 10°C in each T			82.73	83.91	84.59	83.77	89.35	87.95	90.46	90.46
% of average R at 60°C WRT R at 10°C in each T			83.31	86.48	87.05	86.19	91.92	90.30	92.31	92.80
% of average R at 50°C WRT R at 10°C in each T			84.42	89.16	89.53	88.86	94.64	92.56	94.66	94.95
% of average R at 40°C WRT R at 10°C in each T			86.06	91.81	91.95	91.52	97.24	94.54	97.17	96.90
% of average R at 30°C WRT R at 10°C in each T			88.41	94.36	94.45	94.27	99.97	96.39	99.89	98.60
% of average R at 20°C WRT R at 10°C in each T			91.16	97.13	97.02	97.09	102.69	98.14	102.83	100.00
% of average R at 10°C WRT R at 10°C in each T				100.00		100.00		100.00		

Table xiv (c). Change in R percentage value from a given temperature step to the next

2nd measurement cycle. CH: 4. Material: SWCOOH.										
Climatic Chamber temperature profile period, T	T1		T2		T3		T4		T5	
Relative time of measurement (min)	21 - 160	161 - 300	301 - 440	441 - 580	581 - 720	721 - 860	861 - 1000	1001 - 1140	1141 - 1280	1281 - 1420
Chamber temperature profile trend	Rise	Fall	Rise	Fall	Rise	Fall	Rise	Fall	Rise	Fall
%Δ in R between 20°C - 30°C			-2.75		-2.58		-2.72		-2.95	
%Δ in R between 30°C - 40°C			-2.34		-2.49		-2.73		-2.72	
%Δ in R between 40°C - 50°C			-1.65		-2.43		-2.60		-2.51	
%Δ in R between 50°C - 60°C			-1.10		-2.48		-2.72		-2.35	
%Δ in R between 60°C - 70°C			-0.59		-2.45		-2.57		-1.85	
%Δ in R between 70°C - 80°C			-0.84		-2.38		-2.71		-1.70	
%Δ in R between 70°C - 60°C				2.57		2.43		2.36		2.34
%Δ in R between 60°C - 50°C				2.68		2.67		2.25		2.16
%Δ in R between 50°C - 40°C				2.65		2.66		1.98		1.94
%Δ in R between 40°C - 30°C				2.55		2.74		1.85		1.70
%Δ in R between 30°C - 20°C				2.76		2.82		1.75		1.40
%Δ in R between 20°C - 10°C				2.87		2.91		1.86		

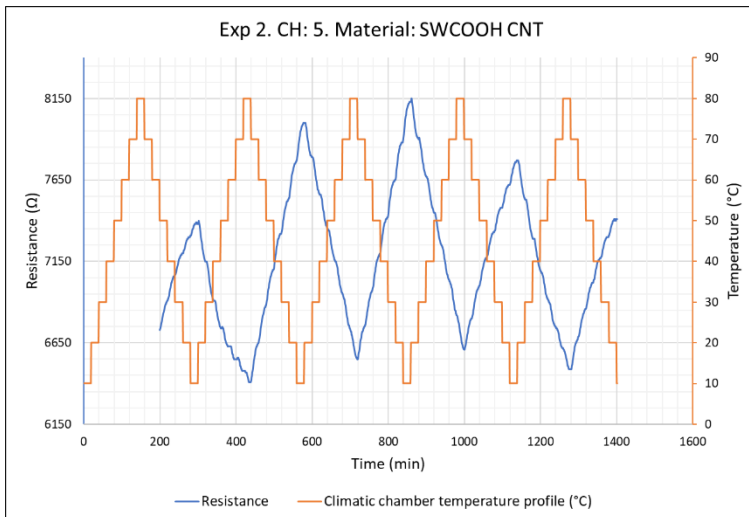


Figure xv. Resistance of deposited thin film material as a function of temperature.

Measurement error
 Outside measurement range

Table xv (a). Average R value at each temperature step.

2nd measurement cycle. CH: 5. Material: SWCOOH.										
Climatic Chamber temperature profile period, T	T1		T2		T3		T4		T5	
Relative time of measurement (min)	21 - 160	161 - 300	301 - 440	441 - 580	581 - 720	721 - 860	861 - 1000	1001 - 1140	1141 - 1280	1281 - 1420
Chamber temperature profile trend	Rise	Fall	Rise	Fall	Rise	Fall	Rise	Fall	Rise	Fall
Average R at 80°C (Ω)			6.43E+03		6.59E+03		6.66E+03		6.51E+03	
Average R at 70°C (Ω)			6.50E+03	6.62E+03	6.80E+03	6.72E+03	6.89E+03	6.76E+03	6.65E+03	6.65E+03
Average R at 60°C (Ω)			6.57E+03	6.84E+03	7.01E+03	6.94E+03	7.10E+03	6.96E+03	6.79E+03	6.83E+03
Average R at 50°C (Ω)			6.66E+03	7.07E+03	7.22E+03	7.17E+03	7.31E+03	7.15E+03	6.98E+03	7.00E+03
Average R at 40°C (Ω)			6.80E+03	7.30E+03	7.41E+03	7.40E+03	7.52E+03	7.31E+03	7.16E+03	7.16E+03
Average R at 30°C (Ω)			6.99E+03	7.51E+03	7.62E+03	7.63E+03	7.73E+03	7.47E+03	7.37E+03	7.29E+03
Average R at 20°C (Ω)			7.22E+03	7.74E+03	7.83E+03	7.87E+03	7.95E+03	7.61E+03	7.60E+03	7.40E+03
Average R at 10°C (Ω)				7.98E+03		8.11E+03		7.75E+03		

Table xv (b). Percent of average R value at each temperature step WRT average R value at 10°C in each T.

2nd measurement cycle. CH: 5. Material: SWCOOH.										
Climatic Chamber temperature profile period, T	T1		T2		T3		T4		T5	
Relative time of measurement (min)	21 - 160	161 - 300	301 - 440	441 - 580	581 - 720	721 - 860	861 - 1000	1001 - 1140	1141 - 1280	1281 - 1420
Chamber temperature profile trend	Rise	Fall	Rise	Fall	Rise	Fall	Rise	Fall	Rise	Fall
% of average R at 80°C WRT R at 10°C in each T			80.55		81.24		85.90		87.96	
% of average R at 70°C WRT R at 10°C in each T			81.51	82.96	83.78	82.89	88.89	87.24	89.86	89.80
% of average R at 60°C WRT R at 10°C in each T			82.35	85.79	86.43	85.56	91.57	89.86	91.80	92.27
% of average R at 50°C WRT R at 10°C in each T			83.54	88.68	88.99	88.41	94.34	92.23	94.26	94.61
% of average R at 40°C WRT R at 10°C in each T			85.22	91.54	91.38	91.22	96.98	94.36	96.78	96.70
% of average R at 30°C WRT R at 10°C in each T			87.59	94.12	93.93	94.06	99.78	96.35	99.54	98.53
% of average R at 20°C WRT R at 10°C in each T			90.46	97.00	96.57	96.99	102.53	98.14	102.64	100.00
% of average R at 10°C WRT R at 10°C in each T				100.00		100.00		100.00		

Table xv (c). Change in R percentage value from a given temperature step to the next

2nd measurement cycle. CH: 5. Material: SWCOOH.										
Climatic Chamber temperature profile period, T	T1		T2		T3		T4		T5	
Relative time of measurement (min)	21 - 160	161 - 300	301 - 440	441 - 580	581 - 720	721 - 860	861 - 1000	1001 - 1140	1141 - 1280	1281 - 1420
Chamber temperature profile trend	Rise	Fall	Rise	Fall	Rise	Fall	Rise	Fall	Rise	Fall
%Δ in R between 20°C - 30°C			-2.87		-2.64		-2.75		-3.09	
%Δ in R between 30°C - 40°C			-2.37		-2.55		-2.80		-2.76	
%Δ in R between 40°C - 50°C			-1.68		-2.39		-2.65		-2.53	
%Δ in R between 50°C - 60°C			-1.19		-2.56		-2.76		-2.46	
%Δ in R between 60°C - 70°C			-0.84		-2.65		-2.68		-1.93	
%Δ in R between 70°C - 80°C			-0.95		-2.54		-2.99		-1.91	
%Δ in R between 70°C - 60°C				2.83		2.68		2.62		2.47
%Δ in R between 60°C - 50°C				2.88		2.85		2.37		2.34
%Δ in R between 50°C - 40°C				2.86		2.81		2.13		2.09
%Δ in R between 40°C - 30°C				2.58		2.84		1.99		1.82
%Δ in R between 30°C - 20°C				2.88		2.94		1.79		1.47
%Δ in R between 20°C - 10°C				3.00		3.01		1.86		

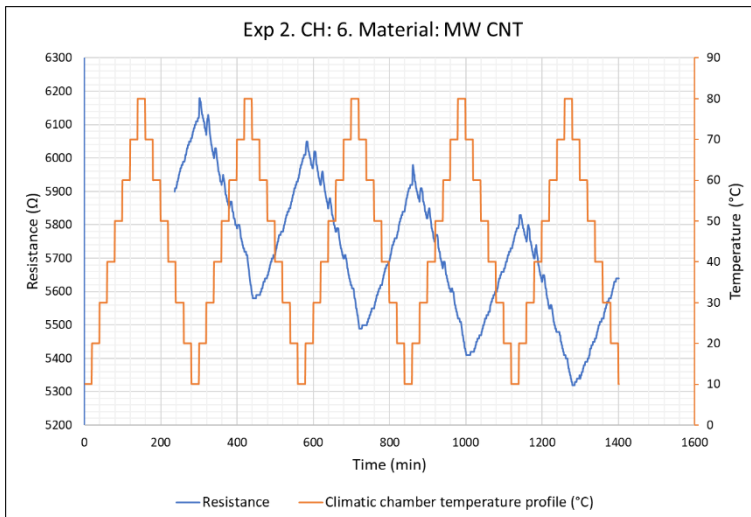


Figure xvi. Resistance of deposited thin film material as a function of temperature.

Measurement error
 Outside measurement range

Table xvi (a). Average R value at each temperature step.

2nd measurement cycle. CH: 6. Material: MW										
Climatic Chamber temperature profile period, T	T1		T2		T3		T4		T5	
Relative time of measurement (min)	21 - 160	161 - 300	301 - 440	441 - 580	581 - 720	721 - 860	861 - 1000	1001 - 1140	1141 - 1280	1281 - 1420
Chamber temperature profile trend	Rise	Fall	Rise	Fall	Rise	Fall	Rise	Fall	Rise	Fall
Average R at 80°C (Ω)			5.65E+03		5.55E+03		5.46E+03		5.36E+03	
Average R at 70°C (Ω)			5.75E+03	5.59E+03	5.65E+03	5.50E+03	5.56E+03	5.42E+03	5.44E+03	5.34E+03
Average R at 60°C (Ω)			5.82E+03	5.63E+03	5.73E+03	5.54E+03	5.63E+03	5.46E+03	5.50E+03	5.38E+03
Average R at 50°C (Ω)			5.88E+03	5.70E+03	5.81E+03	5.61E+03	5.71E+03	5.52E+03	5.59E+03	5.44E+03
Average R at 40°C (Ω)			5.96E+03	5.77E+03	5.89E+03	5.68E+03	5.78E+03	5.59E+03	5.67E+03	5.51E+03
Average R at 30°C (Ω)			6.04E+03	5.84E+03	5.95E+03	5.75E+03	5.85E+03	5.65E+03	5.73E+03	5.57E+03
Average R at 20°C (Ω)			6.11E+03	5.92E+03	5.99E+03	5.83E+03	5.90E+03	5.71E+03	5.78E+03	5.63E+03
Average R at 10°C (Ω)				6.00E+03		5.91E+03		5.78E+03		

Table xvi (b). Percent of average R value at each temperature step WRT average R value at 10°C in each T.

1st measurement cycle. CH: 6. Material: SW.										
Climatic Chamber temperature profile period, T	T1		T2		T3		T4		T5	
Relative time of measurement (min)	21 - 160	161 - 300	301 - 440	441 - 580	581 - 720	721 - 860	861 - 1000	1001 - 1140	1141 - 1280	1281 - 1420
Chamber temperature profile trend	Rise	Fall	Rise	Fall	Rise	Fall	Rise	Fall	Rise	Fall
% of average R at 80°C WRT R at 10°C in each T			94.16		93.89		94.43		95.05	
% of average R at 70°C WRT R at 10°C in each T			95.90	93.18	95.60	93.03	96.09	93.65	96.47	94.73
% of average R at 60°C WRT R at 10°C in each T			97.02	93.95	96.94	93.76	97.35	94.43	97.66	95.57
% of average R at 50°C WRT R at 10°C in each T			98.07	95.05	98.33	94.84	98.69	95.49	99.17	96.63
% of average R at 40°C WRT R at 10°C in each T			99.32	96.23	99.59	96.06	99.93	96.61	100.61	97.79
% of average R at 30°C WRT R at 10°C in each T			100.75	97.33	100.71	97.31	101.11	97.75	101.76	98.89
% of average R at 20°C WRT R at 10°C in each T			101.85	98.63	101.39	98.64	101.95	98.81	102.60	100.00
% of average R at 10°C WRT R at 10°C in each T				100.00		100.00		100.00		

Table xvi (c). Change in R percentage value from a given temperature step to the next

1st measurement cycle. CH: 6. Material: SW.										
Climatic Chamber temperature profile period, T	T1		T2		T3		T4		T5	
Relative time of measurement (min)	21 - 160	161 - 300	301 - 440	441 - 580	581 - 720	721 - 860	861 - 1000	1001 - 1140	1141 - 1280	1281 - 1420
Chamber temperature profile trend	Rise	Fall	Rise	Fall	Rise	Fall	Rise	Fall	Rise	Fall
%Δ in R between 20°C - 30°C			-1.10		-0.68		-0.85		-0.83	
%Δ in R between 30°C - 40°C			-1.43		-1.12		-1.18		-1.15	
%Δ in R between 40°C - 50°C			-1.25		-1.27		-1.25		-1.44	
%Δ in R between 50°C - 60°C			-1.05		-1.39		-1.33		-1.51	
%Δ in R between 60°C - 70°C			-1.12		-1.34		-1.26		-1.19	
%Δ in R between 70°C - 80°C			-1.73		-1.71		-1.66		-1.42	
%Δ in R between 70°C - 60°C				0.77		0.73		0.78		0.83
%Δ in R between 60°C - 50°C				1.10		1.08		1.05		1.07
%Δ in R between 50°C - 40°C				1.18		1.22		1.12		1.15
%Δ in R between 40°C - 30°C				1.10		1.25		1.14		1.10
%Δ in R between 30°C - 20°C				1.30		1.33		1.05		1.11
%Δ in R between 20°C - 10°C				1.37		1.36		1.19		

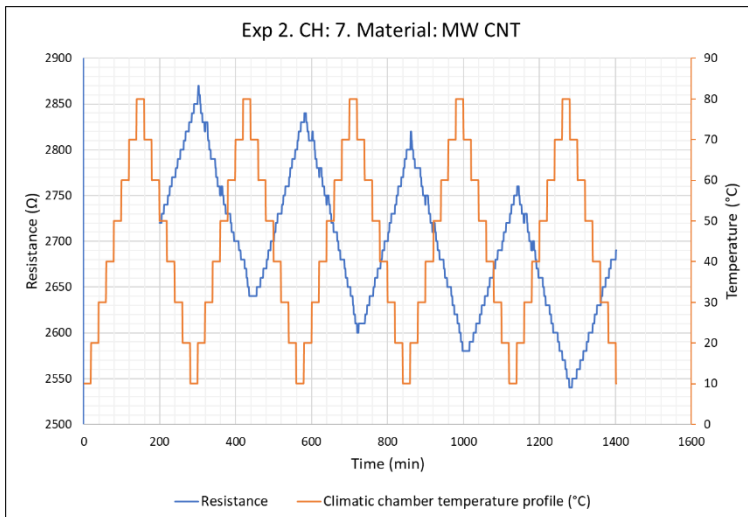


Figure xvii. Resistance of deposited thin film material as a function of temperature.

Measurement error
 Outside measurement range

Table xvii (a). Average R value at each temperature step.

2nd measurement cycle. CH: 7. Material: MW										
Climatic Chamber temperature profile period, T	T1		T2		T3		T4		T5	
Relative time of measurement (min)	21 - 160	161 - 300	301 - 440	441 - 580	581 - 720	721 - 860	861 - 1000	1001 - 1140	1141 - 1280	1281 - 1420
Chamber temperature profile trend	Rise	Fall	Rise	Fall	Rise	Fall	Rise	Fall	Rise	Fall
Average R at 80°C (Ω)			2.65E+03		2.62E+03		2.59E+03		2.55E+03	
Average R at 70°C (Ω)			2.69E+03	2.64E+03	2.66E+03	2.61E+03	2.63E+03	2.58E+03	2.58E+03	2.55E+03
Average R at 60°C (Ω)			2.71E+03	2.67E+03	2.69E+03	2.64E+03	2.66E+03	2.61E+03	2.61E+03	2.57E+03
Average R at 50°C (Ω)			2.74E+03	2.70E+03	2.72E+03	2.67E+03	2.69E+03	2.63E+03	2.64E+03	2.60E+03
Average R at 40°C (Ω)			2.76E+03	2.73E+03	2.76E+03	2.70E+03	2.72E+03	2.66E+03	2.67E+03	2.63E+03
Average R at 30°C (Ω)			2.80E+03	2.76E+03	2.79E+03	2.73E+03	2.75E+03	2.69E+03	2.70E+03	2.66E+03
Average R at 20°C (Ω)			2.83E+03	2.79E+03	2.81E+03	2.76E+03	2.78E+03	2.72E+03	2.73E+03	2.68E+03
Average R at 10°C (Ω)				2.83E+03		2.80E+03		2.75E+03		

Table xvii (b). Percent of average R value at each temperature step WRT average R value at 10°C in each T.

2nd measurement cycle. CH: 7. Material: MW										
Climatic Chamber temperature profile period, T	T1		T2		T3		T4		T5	
Relative time of measurement (min)	21 - 160	161 - 300	301 - 440	441 - 580	581 - 720	721 - 860	861 - 1000	1001 - 1140	1141 - 1280	1281 - 1420
Chamber temperature profile trend	Rise	Fall	Rise	Fall	Rise	Fall	Rise	Fall	Rise	Fall
% of average R at 80°C WRT R at 10°C in each T			93.74		93.53		94.35		95.22	
% of average R at 70°C WRT R at 10°C in each T			94.98	93.49	94.93	93.25	95.74	94.06	96.38	95.19
% of average R at 60°C WRT R at 10°C in each T			95.79	94.30	96.07	94.18	96.87	94.90	97.35	96.04
% of average R at 50°C WRT R at 10°C in each T			96.75	95.37	97.25	95.21	98.00	95.88	98.51	97.01
% of average R at 40°C WRT R at 10°C in each T			97.77	96.50	98.43	96.36	99.16	96.87	99.66	98.06
% of average R at 30°C WRT R at 10°C in each T			98.97	97.56	99.54	97.50	100.29	97.92	100.86	99.07
% of average R at 20°C WRT R at 10°C in each T			100.25	98.76	100.54	98.74	101.35	98.94	101.98	100.00
% of average R at 10°C WRT R at 10°C in each T				100.00		100.00		100.00		

Table xvii (c). Change in R percentage value from a given temperature step to the next

2nd measurement cycle. CH: 7. Material: MW										
Climatic Chamber temperature profile period, T	T1		T2		T3		T4		T5	
Relative time of measurement (min)	21 - 160	161 - 300	301 - 440	441 - 580	581 - 720	721 - 860	861 - 1000	1001 - 1140	1141 - 1280	1281 - 1420
Chamber temperature profile trend	Rise	Fall	Rise	Fall	Rise	Fall	Rise	Fall	Rise	Fall
%Δ in R between 20°C - 30°C			-1.27		-1.00		-1.06		-1.12	
%Δ in R between 30°C - 40°C			-1.20		-1.11		-1.13		-1.19	
%Δ in R between 40°C - 50°C			-1.03		-1.18		-1.17		-1.16	
%Δ in R between 50°C - 60°C			-0.96		-1.18		-1.13		-1.16	
%Δ in R between 60°C - 70°C			-0.81		-1.14		-1.13		-0.97	
%Δ in R between 70°C - 80°C			-1.24		-1.39		-1.39		-1.16	
%Δ in R between 70°C - 60°C				0.81		0.93		0.84		0.86
%Δ in R between 60°C - 50°C				1.06		1.04		0.98		0.97
%Δ in R between 50°C - 40°C				1.13		1.14		0.98		1.04
%Δ in R between 40°C - 30°C				1.06		1.14		1.06		1.01
%Δ in R between 30°C - 20°C				1.20		1.24		1.02		0.93
%Δ in R between 20°C - 10°C				1.24		1.26		1.06		

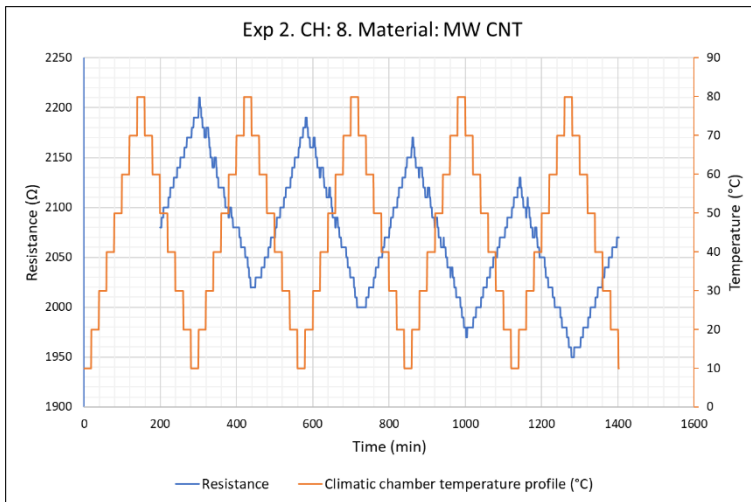


Figure xviii. Resistance of deposited thin film material as a function of temperature.

Measurement error
 Outside measurement range

Table xviii (a). Average R value at each temperature step.

2nd measurement cycle. CH: 8. Material: MW										
Climatic Chamber temperature profile period, T	T1		T2		T3		T4		T5	
Relative time of measurement (min)	21 - 160	161 - 300	301 - 440	441 - 580	581 - 720	721 - 860	861 - 1000	1001 - 1140	1141 - 1280	1281 - 1420
Chamber temperature profile trend	Rise	Fall	Rise	Fall	Rise	Fall	Rise	Fall	Rise	Fall
Average R at 80°C (Ω)			2.03E+03		2.01E+03		1.99E+03		1.96E+03	
Average R at 70°C (Ω)			2.06E+03	2.03E+03	2.04E+03	2.00E+03	2.02E+03	1.98E+03	1.98E+03	1.96E+03
Average R at 60°C (Ω)			2.08E+03	2.05E+03	2.07E+03	2.02E+03	2.04E+03	2.00E+03	2.01E+03	1.98E+03
Average R at 50°C (Ω)			2.10E+03	2.07E+03	2.09E+03	2.05E+03	2.07E+03	2.02E+03	2.03E+03	2.00E+03
Average R at 40°C (Ω)			2.12E+03	2.09E+03	2.12E+03	2.07E+03	2.09E+03	2.05E+03	2.06E+03	2.02E+03
Average R at 30°C (Ω)			2.15E+03	2.12E+03	2.14E+03	2.10E+03	2.12E+03	2.07E+03	2.08E+03	2.04E+03
Average R at 20°C (Ω)			2.18E+03	2.15E+03	2.16E+03	2.12E+03	2.14E+03	2.09E+03	2.10E+03	2.06E+03
Average R at 10°C (Ω)				2.17E+03		2.15E+03		2.11E+03		

Table xviii (b). Percent of average R value at each temperature step WRT average R value at 10°C in each T.

2nd measurement cycle. CH: 8. Material: MW										
Climatic Chamber temperature profile period, T	T1		T2		T3		T4		T5	
Relative time of measurement (min)	21 - 160	161 - 300	301 - 440	441 - 580	581 - 720	721 - 860	861 - 1000	1001 - 1140	1141 - 1280	1281 - 1420
Chamber temperature profile trend	Rise	Fall	Rise	Fall	Rise	Fall	Rise	Fall	Rise	Fall
% of average R at 80°C WRT R at 10°C in each T			93.51		93.44		94.14		95.07	
% of average R at 70°C WRT R at 10°C in each T			94.89	93.33	94.98	93.02	95.60	93.75	96.18	95.02
% of average R at 60°C WRT R at 10°C in each T			95.77	94.07	96.14	93.95	96.78	94.70	97.20	95.99
% of average R at 50°C WRT R at 10°C in each T			96.69	95.17	97.35	95.16	97.92	95.74	98.41	96.96
% of average R at 40°C WRT R at 10°C in each T			97.70	96.32	98.51	96.28	99.15	96.88	99.63	97.93
% of average R at 30°C WRT R at 10°C in each T			98.94	97.47	99.63	97.58	100.24	97.96	100.79	99.04
% of average R at 20°C WRT R at 10°C in each T			100.23	98.71	100.65	98.82	101.33	98.91	101.95	100.00
% of average R at 10°C WRT R at 10°C in each T				100.00		100.00		100.00		

Table xviii (c). Change in R percentage value from a given temperature step to the next

2nd measurement cycle. CH: 8. Material: MW										
Climatic Chamber temperature profile period, T	T1		T2		T3		T4		T5	
Relative time of measurement (min)	21 - 160	161 - 300	301 - 440	441 - 580	581 - 720	721 - 860	861 - 1000	1001 - 1140	1141 - 1280	1281 - 1420
Chamber temperature profile trend	Rise	Fall	Rise	Fall	Rise	Fall	Rise	Fall	Rise	Fall
%Δ in R between 20°C - 30°C			-1.29		-1.02		-1.09		-1.16	
%Δ in R between 30°C - 40°C			-1.24		-1.12		-1.09		-1.16	
%Δ in R between 40°C - 50°C			-1.01		-1.16		-1.23		-1.21	
%Δ in R between 50°C - 60°C			-0.92		-1.21		-1.14		-1.21	
%Δ in R between 60°C - 70°C			-0.87		-1.16		-1.18		-1.02	
%Δ in R between 70°C - 80°C			-1.38		-1.53		-1.46		-1.12	
%Δ in R between 70°C - 60°C				0.74		0.93		0.95		0.97
%Δ in R between 60°C - 50°C				1.10		1.21		1.04		0.97
%Δ in R between 50°C - 40°C				1.15		1.12		1.14		0.97
%Δ in R between 40°C - 30°C				1.15		1.30		1.09		1.12
%Δ in R between 30°C - 20°C				1.24		1.23		0.95		0.96
%Δ in R between 20°C - 10°C				1.29		1.18		1.09		

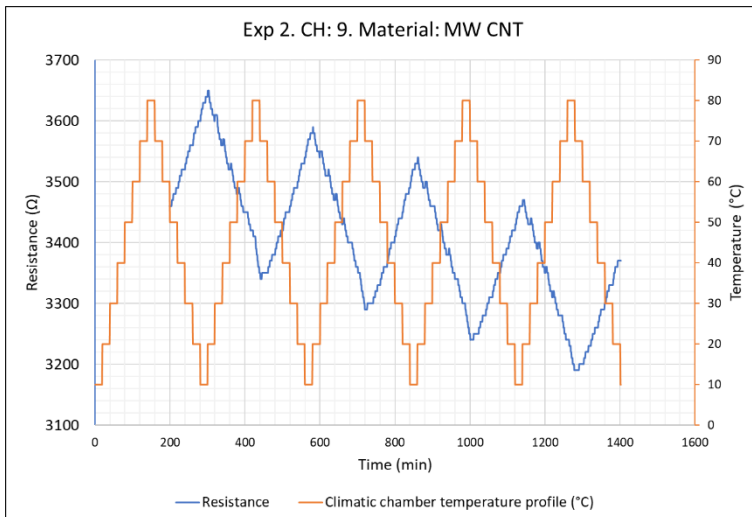


Figure xix. Resistance of deposited thin film material as a function of temperature.

Measurement error
 Outside measurement range

Table xix (a). Average R value at each temperature step.

2nd measurement cycle. CH: 9. Material: MW										
Climatic Chamber temperature profile period, T	T1		T2		T3		T4		T5	
Relative time of measurement (min)	21 - 160	161 - 300	301 - 440	441 - 580	581 - 720	721 - 860	861 - 1000	1001 - 1140	1141 - 1280	1281 - 1420
Chamber temperature profile trend	Rise	Fall	Rise	Fall	Rise	Fall	Rise	Fall	Rise	Fall
Average R at 80°C (Ω)			3.38E+03		3.32E+03		3.27E+03		3.21E+03	
Average R at 70°C (Ω)			3.43E+03	3.35E+03	3.37E+03	3.30E+03	3.32E+03	3.25E+03	3.25E+03	3.20E+03
Average R at 60°C (Ω)			3.46E+03	3.38E+03	3.41E+03	3.33E+03	3.36E+03	3.28E+03	3.29E+03	3.22E+03
Average R at 50°C (Ω)			3.49E+03	3.41E+03	3.45E+03	3.36E+03	3.39E+03	3.31E+03	3.33E+03	3.26E+03
Average R at 40°C (Ω)			3.53E+03	3.45E+03	3.48E+03	3.40E+03	3.43E+03	3.35E+03	3.37E+03	3.29E+03
Average R at 30°C (Ω)			3.57E+03	3.49E+03	3.52E+03	3.44E+03	3.47E+03	3.38E+03	3.40E+03	3.33E+03
Average R at 20°C (Ω)			3.62E+03	3.53E+03	3.55E+03	3.48E+03	3.50E+03	3.42E+03	3.44E+03	3.37E+03
Average R at 10°C (Ω)				3.57E+03		3.53E+03		3.46E+03		

Table xix (b). Percent of average R value at each temperature step WRT average R value at 10°C in each T.

2nd measurement cycle. CH: 9. Material: MW										
Climatic Chamber temperature profile period, T	T1		T2		T3		T4		T5	
Relative time of measurement (min)	21 - 160	161 - 300	301 - 440	441 - 580	581 - 720	721 - 860	861 - 1000	1001 - 1140	1141 - 1280	1281 - 1420
Chamber temperature profile trend	Rise	Fall	Rise	Fall	Rise	Fall	Rise	Fall	Rise	Fall
% of average R at 80°C WRT R at 10°C in each T			94.46		94.16		94.54		95.26	
% of average R at 70°C WRT R at 10°C in each T			95.91	93.73	95.63	93.62	96.01	93.98	96.57	95.02
% of average R at 60°C WRT R at 10°C in each T			96.78	94.46	96.68	94.33	97.11	94.74	97.70	95.77
% of average R at 50°C WRT R at 10°C in each T			97.76	95.50	97.76	95.29	98.12	95.69	98.86	96.75
% of average R at 40°C WRT R at 10°C in each T			98.85	96.53	98.81	96.43	99.19	96.76	100.05	97.76
% of average R at 30°C WRT R at 10°C in each T			99.97	97.59	99.83	97.56	100.26	97.83	101.15	98.89
% of average R at 20°C WRT R at 10°C in each T			101.18	98.71	100.82	98.77	101.19	98.84	102.16	100.00
% of average R at 10°C WRT R at 10°C in each T				100.00		100.00		100.00		

Table xix (c). Change in R percentage value from a given temperature step to the next

2nd measurement cycle. CH: 9. Material: MW										
Climatic Chamber temperature profile period, T	T1		T2		T3		T4		T5	
Relative time of measurement (min)	21 - 160	161 - 300	301 - 440	441 - 580	581 - 720	721 - 860	861 - 1000	1001 - 1140	1141 - 1280	1281 - 1420
Chamber temperature profile trend	Rise	Fall	Rise	Fall	Rise	Fall	Rise	Fall	Rise	Fall
%Δ in R between 20°C - 30°C			-1.20		-0.99		-0.93		-1.01	
%Δ in R between 30°C - 40°C			-1.12		-1.02		-1.07		-1.10	
%Δ in R between 40°C - 50°C			-1.09		-1.05		-1.07		-1.19	
%Δ in R between 50°C - 60°C			-0.98		-1.08		-1.01		-1.16	
%Δ in R between 60°C - 70°C			-0.87		-1.05		-1.10		-1.13	
%Δ in R between 70°C - 80°C			-1.45		-1.48		-1.47		-1.31	
%Δ in R between 70°C - 60°C				0.73		0.71		0.75		0.74
%Δ in R between 60°C - 50°C				1.04		0.96		0.95		0.98
%Δ in R between 50°C - 40°C				1.04		1.13		1.07		1.01
%Δ in R between 40°C - 30°C				1.06		1.13		1.07		1.13
%Δ in R between 30°C - 20°C				1.12		1.21		1.01		1.11
%Δ in R between 20°C - 10°C				1.29		1.23		1.16		

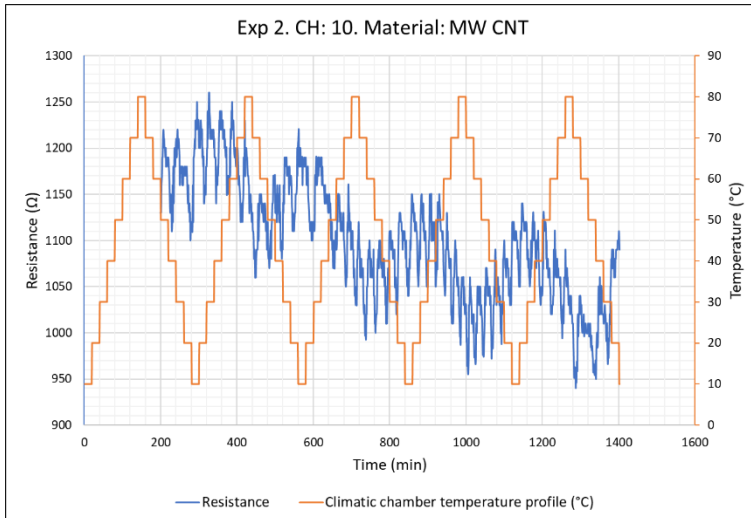


Figure xx. Resistance of deposited thin film material as a function of temperature.

Measurement error
 Outside measurement range

Table xx (a). Average R value at each temperature step.

2nd measurement cycle. CH: 10. Material: MW.										
Climatic Chamber temperature profile period, T	T1		T2		T3		T4		T5	
Relative time of measurement (min)	21 - 160	161 - 300	301 - 440	441 - 580	581 - 720	721 - 860	861 - 1000	1001 - 1140	1141 - 1280	1281 - 1420
Chamber temperature profile trend	Rise	Fall	Rise	Fall	Rise	Fall	Rise	Fall	Rise	Fall
Average resistance at 80°C (Ω)			1.15E+03		1.06E+03		1.04E+03		1.03E+03	
Average resistance at 70°C (Ω)			1.14E+03	1.09E+03	1.13E+03	1.03E+03	1.07E+03	1.03E+03	1.02E+03	1.00E+03
Average resistance at 60°C (Ω)			1.20E+03	1.13E+03	1.12E+03	1.07E+03	1.09E+03	1.04E+03	1.08E+03	1.00E+03
Average resistance at 50°C (Ω)			1.18E+03	1.13E+03	1.09E+03	1.09E+03	1.12E+03	1.05E+03	1.08E+03	9.66E+02
Average resistance at 40°C (Ω)			1.21E+03	1.12E+03	1.15E+03	1.04E+03	1.11E+03	1.03E+03	1.06E+03	1.03E+03
Average resistance at 30°C (Ω)			1.22E+03	1.17E+03	1.18E+03	1.07E+03	1.09E+03	1.03E+03	1.10E+03	9.98E+02
Average resistance at 20°C (Ω)			1.17E+03	1.14E+03	1.11E+03	1.11E+03	1.08E+03	1.05E+03	1.12E+03	1.09E+03
Average resistance at 10°C (Ω)				1.18E+03		1.09E+03		1.09E+03		

Table xx (b). Percent of average R value at each temperature step WRT average R value at 10°C in each T.

2nd measurement cycle. CH: 10. Material: MW.										
Climatic Chamber temperature profile period, T	T1		T2		T3		T4		T5	
Relative time of measurement (min)	21 - 160	161 - 300	301 - 440	441 - 580	581 - 720	721 - 860	861 - 1000	1001 - 1140	1141 - 1280	1281 - 1420
Chamber temperature profile trend	Rise	Fall	Rise	Fall	Rise	Fall	Rise	Fall	Rise	Fall
% of average Res @ 80°C wrt Res @ 10°C in each T			97.46		97.24		95.49		94.73	
% of average Res @ 70°C wrt Res @ 10°C in each T			96.44	92.71	103.40	94.30	98.35	94.51	94.22	91.97
% of average Res @ 60°C wrt Res @ 10°C in each T			102.03	95.34	103.03	98.25	99.91	95.24	98.96	92.19
% of average Res @ 50°C wrt Res @ 10°C in each T			99.92	96.10	100.18	99.72	102.66	96.06	99.24	88.86
% of average Res @ 40°C wrt Res @ 10°C in each T			102.29	94.66	105.33	95.59	101.92	94.74	97.12	95.10
% of average Res @ 30°C wrt Res @ 10°C in each T			103.31	99.41	108.09	97.98	100.09	94.29	101.17	91.76
% of average Res @ 20°C wrt Res @ 10°C in each T			99.32	96.78	102.39	101.85	99.27	95.97	102.83	100.00
% of average Res @ 10°C wrt Res @ 10°C in each T				100.00		100.00		100.00		

Table xx (c). Change in R percentage value from a given temperature step to the next

2nd measurement cycle. CH: 10. Material: MW.										
Climatic Chamber temperature profile period, T	T1		T2		T3		T4		T5	
Relative time of measurement (min)	21 - 160	161 - 300	301 - 440	441 - 580	581 - 720	721 - 860	861 - 1000	1001 - 1140	1141 - 1280	1281 - 1420
Chamber temperature profile trend	Rise	Fall	Rise	Fall	Rise	Fall	Rise	Fall	Rise	Fall
%Δ in resistance between 20°C - 30°C			3.98		5.70		0.82		-1.66	
%Δ in resistance between 30°C - 40°C			-1.02		-2.76		1.83		-4.05	
%Δ in resistance between 40°C - 50°C			-2.37		-5.15		0.73		2.12	
%Δ in resistance between 50°C - 60°C			2.12		2.85		-2.75		-0.28	
%Δ in resistance between 60°C - 70°C			-5.59		0.37		-1.56		-4.75	
%Δ in resistance between 70°C - 80°C			1.02		-6.16		-2.86		0.52	
%Δ in resistance between 70°C - 60°C				2.63		3.95		0.73		0.22
%Δ in resistance between 60°C - 50°C				0.76		1.47		0.82		-3.34
%Δ in resistance between 50°C - 40°C				-1.44		-4.14		-1.32		6.24
%Δ in resistance between 40°C - 30°C				4.75		2.39		-0.45		-3.34
%Δ in resistance between 30°C - 20°C				-2.63		3.88		1.68		8.24
%Δ in resistance between 20°C - 10°C				3.22		-1.85		4.03		

